L-910900-17

Analytical Design and Performance Studies of Nuclear Furnace Tests of Small Nuclear Light Bulb Models

NASA Contract No. SNPC-70

UNITED AIRCRAFT CORPORATION

United Aircraft Research Laboratories

EAST HARTFORD, CONNECTICUT

United Aircraft Research Laboratories

UNITED AIRCRAFT CORPORATION

EAST HARTFORD, CONNECTICUT 06108

L-910900-17

Analytical Design and Performance
Studies of Nuclear Furnace Tests
of Small Nuclear Light Bulb Models

NASA Contract No. SNPC-70

REPORTED BY Thomas S. Latham

Thomas S. Latham

Richard J. Rodgers

Richard J. Rodgers

APPROVED BY James W. Clark

James W. Clark, Chief
Fluid and Systems Dynamics

DATE September 1972

NO. OF PAGES 87

COPY NO. 28

FOREWORD

An exploratory experimental and theoretical investigation of gaseous nuclear rocket technology was conducted by the United Aircraft Research Laboratories under Contract SNPC-70 with the joint AEC-NASA Space Nuclear Systems Office. The Technical Supervisors of the Contract for NASA were Captain C. E. Franklin (USAF) of SNSO for the initial portion of the Contract performance period, and Dr. Karlheinz Thom of SNSO and Mr. Herbert J. Heppler of the NASA Lewis Research Center for the final portions. The following nine reports (including the present report) comprise the required Final Technical Report under the Contract:

1. Roman, W. C. and J. F. Jaminet: Development of RF Plasma Simulations of In-Reactor Tests of Small Models of the Nuclear Light Bulb Fuel Region. United Aircraft Research Laboratories Report L-910900-12, September 1972.

2. Klein, J. F.: Nuclear Light Bulb Propellant Heating Simulation Using a Tungsten-Particle/Argon Aerosol and Radiation from a DC Arc Surrounded by a Segmented Mirror Cavity. United Aircraft Research Laboratories Report L-910900-13, September 1972.

3. Jaminet, J. F.: Development of a Model and Test Equipment for Cold-Flow Tests at 500 Atm of Small Nuclear Light Bulb Configurations. United Aircraft Research Laboratories Report L-910900-14, September 1972.

4. Kendall, J. S. and R. C. Stoeffler: Conceptual Design Studies and Experiments Related to Cavity Exhaust Systems for Nuclear Light Bulb Configurations. United Aircraft Research Laboratories Report L-910900-15, September 1972.

5. Rodgers, R. J. and T. S. Latham: Analytical Design and Performance Studies of the Nuclear Light Bulb Engine. United Aircraft Research Laboratories Report L-910900-16, September 1972.

6. Latham, T. S. and R. J. Rodgers: Analytical Design and Performance Studies of Nuclear Furnace Tests of Small Nuclear Light Bulb Models. United Aircraft Research Laboratories Report L-910900-17, September 1972. (Present Report)

7. Krascella, N. L.: Spectral Absorption Coefficients of Argon and Silicon and Spectral Reflectivity of Aluminum. United Aircraft Research Laboratories Report L-910904-3, September 1972.

8. Palma, G. E.: Measurements of the UV and VUV Transmission of Optical Materials During High-Energy Electron Irradiation. United Aircraft Research Laboratories Report L-990929-3, September 1972.

9. Kendall, J. S.: Investigation of Gaseous Nuclear Rocket Technology -- Summary Technical Report. United Aircraft Research Laboratories Report L-910905-13, September 1972.

Report L-910900-17

Analytical Design and Performance Studies of Nuclear Furnace Tests of Small Nuclear Light Bulb Models

TABLE OF CONTENTS

TABLE OF CONTENTS (Continued)

Report L-910900-17

Analytical Design and Performance Studies of Nuclear Furnace Tests of Small Nuclear Light Bulb Models

SUMMARY

Analytical studies were continued to identify the design and performance characteristics of a small-scale model of a nuclear light bulb unit cell suitable for testing in the Nuclear Furnace reactor. Emphasis was placed on calculating performance characteristics based on detailed radiant heat transfer analyses, on designing the test assembly for ease of insertion, connection, and withdrawal at the reactor test cell, and on determining instrumentation and test effluent handling requirements. In addition, a review of candidate test reactors for future nuclear light bulb in-reactor tests was conducted.

The results of the study indicate that a meaningful series of in-reactor demonstration tests of fuel containment, transparent-wall performance, and propellant heating could be conducted using the Nuclear Furnace reactor. Processing of the effluent from an in-reactor test could be accomplished by flowing the exit gases through the Nuclear Furnace scrubber or by adding a separate scrubber loop to handle the in-reactor test effluent. The test cell design was chosen such that the test capsule could be inserted, connected, and withdrawn from a Nuclear Furnace without transporting the entire system by rail from the test cell to the remote Maintenance-Assembly-Disassembly (MAD) building. With this mode of operation, it is estimated that 10 to 20 test runs could be performed using one Nuclear Furnace core.

Results of detailed radiant heat transfer and performance analyses indicated that thermal radiation fluxes corresponding to black-body radiating temperatures of approximately 5420°K could be sustained in a fissioning uranium plasma in a test configuration having reflecting walls and operating at a pressure of 500 atm. Tests could also be conducted to demonstrate that internally-cooled transparent walls are capable of withstanding both the nuclear radiation and thermal environments anticipated for a nuclear light bulb engine and that seeded propellant can be heated to exhaust temperatures in the range of 3300 to 3700°K.

Simulation tests of models similar in geometry to those anticipated for in-reactor demonstration tests have been performed using the UARL 1.2-MW rf induction heater and dc arc facilities. To date, these tests have included successful injection of gaseous uranium hexafluoride and tungsten particles in argon carrier gas into rf plasmas operating at pressures up to about 40 atm with up to 125 kW of

radiated power. Bulk exit temperatures of 4515°K have been measured in simulated propellant streams heated by dc arc discharges. In addition, a fiberglass pressure vessel capable of operating in the 1.2-MW rf induction heater in future high-pressure tests has been designed, fabricated, and tested at pressures greater than 500 atm. It is recommended that thorough development and testing of in-reactor test models at power levels and operating conditions anticipated for in-reactor tests in the Nuclear Furnace be continued using these facilities.

RESULTS AND CONCLUSIONS

1. The Nuclear Furnace reactor, modified to accommodate a small-scale nuclear light bulb unit cell, could be operated such that the test assembly could be inserted and removed from the core at the reactor test site. The modifications to the Nuclear Furnace system for this mode of operation would be (1) alterations to the bell shield to provide a glory hole at the top through which the test assembly could be inserted and removed, (2) relocation of the nuclear instrument well from the top-centerline position in the bell shield, and (3) installation of an exhaust duct for the in-reactor test effluent which would penetrate the Nuclear Furnace scrubber elbow beneath the core. The in-reactor test effluent would flow to a separate scrubber. Remotely operated connect-disconnect couplings would be used to connect liquids, gases and wiring to the test assembly.

2. It is estimated that the Nuclear Furnace core lifetime could be extended to the order of 3 to 5 hr by increasing coolant flow, thereby reducing fuel element surface temperatures. With a core lifetime on the order of 3 to 5 hr, 10 or more tests of 10-to-15 min duration could be run using one core.

3. A basic test configuration with the following principal characteristics was selected: (1) test region diameter, 6.6 cm; (2) test region length, 17.8 cm; (3) argon used as the buffer gas to provide a radial inflow vortex flow; (3) U-235 fuel injected in the form of uranium hexafluoride during test start-up and in the form of a mixture of submicron particles and either uranium hexafluoride or gaseous argon during steady-state operation; (4) mass of U-235 contained in fuel region, 6.2 g; (5) average partial pressure of U-235 fuel within the fuel region, 125 atm; (6) test region total pressure, 500 atm; and (7) ratio of fuel region diameter to test region diameter, 0.6.

4. The basic test configuration would have the following calculated performance characteristics: (1) specific fission power level, 30.5 kW/g U-235, (2) total test region power, 190 kW; (3) net radiated heat flux, 0.71 kW/cm^2; (4) equivalent black-body radiating temperature, 3330°K; (5) outward radiating thermal heat flux of 4.84 kW/cm^2 and an inward reflected thermal heat flux of 4.13 kW/cm^2 (difference equals net radiated heat flux of 0.71 kW/cm^2); and (6) fuel surface radiating temperature, 5426°K.

5. It is feasible to place internally-cooled fused silica transparent walls between the fuel-containment test region and a propellant duct. This would permit propellant heating tests to be conducted, and would expose a transparent-wall structure to both the nuclear radiation and thermal environments of the test region. Addition of a propellant duct and transparent-wall structure would require a reduction in the test region diameter from 6.6 cm to approximately 5.08 cm. Seeded

hydrogen propellant would be exposed to an incident radiant heat flux of 4.63 kW/cm^2. The propellant would be heated to bulk exit temperatures in the range from 3300°K to 3700°K. Tests would be performed in which the total thermal radiation flux (incident plus reflected) passing through a transparent-wall structure would be 8.83 kW/cm^2, compared with 22.9 kW/cm^2 for the reference nuclear light bulb engine. The nuclear radiation dose rate in the transparent walls would be 3.0 Mrad/sec, compared with 5.0 Mrad/sec in the reference engine.

6. Measurements of in-reactor test performance could be made using thermocouples and flow-rate measuring instruments to determine the detailed heat balance in the test cell. Observation of the fissioning plasma and measurements of the emitted spectral flux could be performed using internally polished tubes which view the plasma region through the end walls and the peripheral liner.

7. RF plasma tests of models similar in geometry to those which would be used in in-reactor tests have been performed using the UARL 1.2-MW rf induction heater. Development and thorough testing of models and diagnostic equipment at power levels and operating conditions anticipated for in-reactor tests can be undertaken using this facility.

8. A self-critical cavity reactor employing a cold beryllium (40°K) inner reflector-moderator and a cold (40°K) outer deuterium-carbide reflector-moderator was analyzed. It has calculated critical masses of 1.15 kg of U-233 and 1.45 kg of U-235 for a spherical configuration with a cavity volume equal to the volume of one full-scale reference nuclear light bulb unit cell. At power levels which result in an outward-directed heat flux equal to that for the reference engine, the operating pressure would be approximately 250 atm. Consideration should be given this type of test reactor for future fissioning uranium plasma experiments.

INTRODUCTION

Major emphasis in the research on the nuclear light bulb engine concept (Ref. 1) conducted under Contract SNPC-70 has been placed on (1) simulation of the thermal environment in the fuel region and surrounding transparent-wall structure using small-scale models with rf-heated vortexes and (2) simulation of propellant heating in the nuclear light bulb engine by heating carbon- and tungsten-seeded streams of gas with thermal radiation from a dc arc discharge. A review of the work under this contract up to September 1972 is contained in Ref. 2. In the most recent fuel region simulation experiments gaseous UF_6 and tungsten particles in argon carrier gas have been successfully injected into rf plasmas operating at pressures up to 40 atm radiating up to 125 kW of power (see Ref. 3). Bulk exit temperatures of 4515°K have been measured in simulated propellant streams (argon seeded with submicron-sized tungsten particles) heated by dc arc discharges (see Ref. 4). The next major step in development of a nuclear light bulb engine, building on the results from the simulation experiments, is a series of demonstration tests in which the dc arc and rf-heated plasmas are replaced by a fissioning uranium plasma as the energy source for thermal radiation.

The Nuclear Furnace reactor, recently operated for the first time at the National Reactor Development Station (NRDS), is ideally suited for conducting in-reactor tests of models of the nuclear light bulb unit cell. This reactor is a solid-core nuclear rocket fuel element test reactor. It has been shown experimentally that four of its central fuel elements could be removed to provide an 8.4-cm-i.d. cylindrical test hole in which a test cell could be inserted. The power density would be sufficiently high to sustain a fissioning uranium plasma in the test cell at operating pressures of 500 atm.

The studies described herein are a continuation of the in-reactor test feasibility analyses of Refs. 5 and 6. Specific emphasis in the current study was placed on design of the basic unit test cell, detailed performance and heat transfer analyses of the contemplated tests, and further design and analyses of the methods for injecting various test gases and nuclear fuel into the test cell and for handling the effluent mixture exiting from the test. Test operations, instrumentation, and types of reactors for future tests are also discussed in the following sections of the report.

THE NUCLEAR FURNACE REACTOR

A detailed description of the Nuclear Furnace reactor and its effluent handling system are contained in Ref. 7. The reactor is a solid-core nuclear rocket fuel element test reactor designed by Los Alamos Scientific Laboratory (LASL). The core is approximately 32 cm in diameter and 134.5-cm long. Its 49 fuel elements are contained in a tube-bundle assembly along with light-water moderator. The core is self-contained in an aluminum vessel which can be removed through the top of the reactor reflector.

The nominal power level of the Nuclear Furnace is 44 MW, but can be extended to about 66 MW. The core lifetime, according to LASL personnel, might be extended to about 3 to 5 hr with additional coolant flow to reduce temperatures on the fuel element coolant hole surface.

The reactor can be altered to accommodate a small-scale nuclear light bulb test assembly by removing four of its central fuel elements, thus providing an 8.4-cm-i.d. cylindrical hole passing through the entire core. The specific fission power levels in the test region at the center of the core for the range of power levels from 44 to 66 MW would be from 25 to 40 kW per g of U-235.

The Nuclear Furnace is mounted on a rail car for transportation to the test cell. A crane and remote handling equipment mounted on an attached rail car can be transported with the Nuclear Furnace rail car such that the nuclear light bulb test assembly could be inserted and removed at the test cell without requiring the disconnecting and removal of the entire system to the Maintenance-Assembly-Disassembly (MAD) building.

A schematic diagram of the Nuclear Furnace reactor with the four central fuel elements replaced by an aluminum-cased test hole is shown in Fig. 1. A test assembly containing a small-scale model of a nuclear light bulb cell would be inserted through the top of the core lid. Plumbing and wiring would be passed through the top of the core assembly as shown in Fig. 2. Effluent from the test cell could be ducted into the Nuclear Furnace scrubber system or to a separate scrubber system connected directly to the test assembly. The ducting to handle the effluent in a separate scrubber system is shown in Fig. 1.

The Nuclear Furnace has a water-filled, bell-shaped, removable shield. The geometry of the shield is shown in Fig. 3. Access to remove a test assembly between runs could be provided by penetrating the bell shield with a glory hole at the top center. This would require the dislocation of the nuclear instrumentation well shown in Fig. 3. The removal of the nuclear instruments to another location in the shield was discussed with NRDS personnel and appears feasible. The glory hole

required for access to insert and remove the test assembly is shown in Fig. 3. The glory hole could be left open, which has been the practice for some NRDS reactor tests, or could be plugged by a water-filled shield segment dropped into place for the test run.

The mode of operation for nuclear light bulb in-reactor tests that appears most desirable is one in which test assemblies can be inserted and removed at the test cell site rather than at the MAD building. This would avoid reconnection check-out procedures requiring on the order of six weeks each time the reactor is removed from the cell and returned. If core lifetime can be extended to 3 to 5 hr, 10 or more test assemblies might be inserted in one Nuclear Furnace core, thus allowing tests of several configurations over a wide range of operating conditions.

DESCRIPTION OF TEST CELL CONFIGURATIONS

The small-scale unit cells used in the in-reactor tests are designed to simulate many of the conditions expected to exist in a full-scale nuclear light bulb engine unit cavity. Each of the test configurations described below would contain a gaseous nuclear fuel cloud suspended in a vortex flow field driven by tangentially injected argon buffer gas. The peripheral walls of the test regions would be highly reflective to the thermal radiation emitted from the fuel region. The various modifications to a basic configuration which are described below are concerned primarily with alternate component designs such as the pressure vessel, buffer-gas flow configurations, fuel-injector locations, and effluent handling options.

Basic Configuration

The test region of the basic test cell configuration is a cylindrical cavity with an inside diameter of 6.6 cm and a length of 17.8 cm. The cylindrical peripheral wall is made of aluminum with a highly-polished reflective inner surface. A revised design has been made of the basic configuration as described in Ref. 6. The cavity region is essentially unchanged; the major modification to the design is related to a simplification of the coolant flow circuits. In particular, the flow circuits have been configured to allow all connections of inlet gases and wiring to the test assembly to be connected at the top of the test cell. The bottom exhaust duct still exits through the bottom of the Nuclear Furnace core. An axial cross section of the new configuration is shown in Fig. 4 and a radial cross section at the cavity midplane is shown in Fig. 5.

Flow channels to provide for the injection of buffer gas, fuel, and required coolant for the various components are provided. The entire assembly is contained in an aluminum-lined fiberglass pressure vessel. The outside diameter of the pressure vessel is 8.13 cm so that the complete assembly can be inserted in an 8.38-cm-diam test hole available in the Nuclear Furnace. In this configuration, all of the coolant (liner coolant, end-wall coolant, and bypass coolant) enters the annulus between the liner and pressure vessel at the upper end of the test unit. When the flow reaches the upper end wall, part of it is used to cool the end wall and then is injected into the entrance to the exhaust port to cool the gases exiting the cavity. The remainder of the flow cools the liner and the pressure vessel adjacent to the cavity region. At the lower end wall, an additional quantity of coolant branches off to cool the lower end wall and lower exhaust duct. The buffer gas which drives the vortex is ducted through four tubes in the annulus between the pressure vessel and the liner as shown in Fig. 5. These tubes are fed from the upper end and terminate at the lower end of the cavity. The fuel is injected from the upper end in a single tube in the liner coolant annulus as shown in Fig. 4.

One branch line supplies the upper injector and a second continues past the cavity region to supply the lower injector. These fuel injectors would consist of a neutron-absorbing inner tube surrounded by an outer tube to form a coolant annulus. The outer tube would have a porous wall in the region where the injectors are exposed to the exhaust gases. This type of fuel injector configuration minimizes the length of the injector which is exposed to the hot exhaust duct gases. Dimensions and materials specifications for the components shown in Figs. 4 and 5 are given in Table I.

The total length of the in-reactor test assembly required to extend from the lid of the Nuclear Furnace core to the core bottom is approximately 188.0 cm, including about 30.5 cm of effluent duct between the outlet of the test cell pressure vessel and the core bottom.

The pressure vessel is a filament-wound fiberglass cylinder, approximately 157.5-cm long with an inside diameter of 7.36 cm and an outside diameter of 8.13 cm. The wall thickness of 0.385 cm is required for operation at an internal pressure of 500 atm. A design stress level of 52,000 N/cm^2 (75,000 psi) in the fiberglass was used. The maximum allowable uniaxial tensile stress for glass fibers is on the order of 207,000 N/cm^2 (300,000 psi). If it is assumed that the pressure vessel is wound so that it has similar tensile stress properties in both axial and hoop directions (alternate circumferential and axial fiber directions for 45^o angle winding), the maximum allowable stress would be 104,000 N/cm^2 (150,000 psi).

The pressure vessel is cooled on both sides so that the maximum allowable temperature of 390^oK will not be exceeded at the values of neutron and gamma ray heating anticipated at full-power operation of the Nuclear Furnace test reactor. Cooling on the outside surface of the pressure vessel would be provided by flowing hydrogen coolant between the annulus surrounding the pressure vessel and the aluminum test hole casing. Control of this coolant flow rate would be provided by orifices located at the inlet end of the annular passage.

Schematic diagrams of the pressure vessel end walls are included in the axial cross section shown in Fig. 4. The inlet end of the pressure vessel would be secured to the top of the reactor core lid as shown in Fig. 1. The capped (upper) end wall is similar in design to that currently employed in the UARL high-pressure simulation experiments described in Ref. 8. The capped end walls contain a winding ring and retainer flange as shown in Fig. 4. Several penetrations through the top of the pressure vessel are provided to supply the required buffer gas, fuel, and coolant flow. The outlet end of the pressure vessel is wound over a dome-shaped end wall to allow the test assembly to be inserted into the aluminum test hole casing. The fiberglass pressure vessel is wound on a 0.075-cm-thick aluminum pressure vessel liner. The liner is welded to the end-wall dome at the outlet end and to the upper end-wall plate on the inlet end. The filament-wound pressure vessel is bonded to the aluminum liner.

Modifications to Basic Configuration

Several modifications to a basic test cell configuration were considered in these studies. These modifications include (1) the use of an aluminum pressure vessel instead of a fiber wound pressure vessel, (2) the use of fuel injectors located other than on the axial centerline of the test cell, and (3) the use of axial buffer-gas bypass ports located at the periphery of the end walls. A schematic diagram of a test cell with an aluminum pressure vessel, off-axis fuel injectors and axial buffer-gas bypass ports is shown in Fig. 6.

The possible use of an aluminum pressure vessel was included because aluminum is not as susceptible to radiation damage effects as fiberglass. However, the use of aluminum would reduce the available inside diameter of the test region to 6.35 cm because the aluminum pressure vessel would have to be 0.584-cm thick to contain the 500-atm pressure within its stress limitations. It is also expected, that the use of an all aluminum pressure vessel would reduce the test performance levels due to greater absorption of thermal neutrons than occurs when the fiberglass pressure vessel is used.

The fuel injector location in the basic configuration was placed on the centerline to be consistent with the injector locations employed in the simulation experiments in the 1.2-MW rf induction heater (see Ref. 3). Fuel injectors located in the thru-flow exhaust ducts present sophisticated cooling requirements due to the flow of hot exhaust gases over the injectors. Additionally, two-component gas vortex tests have indicated superior simulated-fuel containment when fuel injectors were located near the periphery of the vortex cell (see Ref. 9 and 10). This was particularly true when axial buffer-gas bypass was included in the flow configuration. It was also demonstrated in the two-component gas vortex tests that simulated-fuel injection from one end wall resulted in good containment characteristics. Therefore, in Fig. 6, there is no fuel supply branch line leading to the lower end wall as shown in the basic configuration.

Radiant heat transfer calculations for the in-reactor test configurations which will be discussed later have indicated that the radial temperature distribution in the buffer-gas region between the edge-of-fuel location and the peripheral wall has very small gradients until a position about 1 cm from the edge of fuel is reached. Most of the buffer flow, therefore, is essentially at constant temperature. Two-component gas vortex experiments discussed in Refs. 9 and 10 have indicated that simulated-fuel containment increased as the simulated-fuel-to-buffer-gas weight flow ratio based on the flow through the thru-flow ducts increased. Some of the argon buffer-gas flow could be ducted through peripheral bypass ports on the end-wall peripheries instead of turning at the end wall and exiting through the thru-flow ducts. Since axial bypass has resulted in higher fuel containment concentrations in the two-component gas vortex tests (Ref. 10), the option of including peripheral bypass ports in the configuration was deemed desirable.

Propellant Heating Configuration

A modified unit cell for in-reactor tests of transparent walls and propellant heating is shown in Fig. 7. This configuration was described in Ref. 6. Briefly, provision is made for insertion of transparent walls across a segment of the test region liner. Behind the transparent-wall array is a propellant heating channel similar in dimensions and geometry to that employed in the UARL dc arc propellant heating experiments described in Ref. 4. Reflective aluminum liners are employed around the test region and around the propellant heating channel. The transparent-wall array is clamped into position by a split manifold as shown in Fig. 7. Transparent-wall coolant would be routed through the split manifolds. The inclusion of the transparent wall and propellant heating channel reduces the test region diameter to 5.08 cm. The propellant must be seeded with submicron particles to absorb the radiant energy. It is also necessary to use unseeded buffer flows at the edge of the propellant heating channels to keep the transparent walls and reflective liners clean. The porous foam and seeded hydrogen inlet used to control the propellant channel flow are also shown in Fig. 7. These techniques are under development in the propellant heating simulation experiments being performed with the UARL dc arc heater described in Ref. 4.

RADIANT HEAT TRANSFER ANALYSES

Calculations of the performance characteristics for in-reactor tests in Refs. 5 and 6 were based on an assumption that black-body spectral heat fluxes were emitted from the nuclear fuel cloud. Detailed radiant heat transfer calculations have been performed for the nuclear light bulb reference engine using neutron transport theory. These calculations reported in Refs. 12 and 13 include detailed analyses of the spectral heat fluxes emitted from the nuclear fuel cloud and the convection from the buffer-gas region of energy deposited in the buffer gas by conduction and thermal radiation absorption. The same analytical programs were used to calculate the spectral heat fluxes emitted from the nuclear fuel cloud for an in-reactor test, including the effect of convection by the buffer gas and the reflectivity of the aluminum liner on the spectral heat flux and on the temperature distribution in the fuel and buffer-gas regions. The results of the detailed radiant heat transfer analyses were used in calculations of the performance characteristics of in-reactor tests in the Nuclear Furnace.

Spectral Heat Fluxes

The flow pattern and geometry assumed for the radiant heat transfer analyses are shown in Fig. 8. An axial cross section of the unit cell is shown in Fig. 9(a). The argon buffer gas is injected tangentially through injection holes in the aluminum reflective liner. The argon flows radially inward with some of the flow turning axially along the streamlines shown to be extracted from the end of the configuration through axial bypass ports and/or through the thru-flow ports on the axial centerline. The only fluid dynamic constraint in the buffer-gas region is a requirement that the axial dynamic pressure be constant at every radial station. This constraint then defines the axial velocity of the flow at each radial station and as such is a function of local temperature, density, and the specified constant axial dynamic pressure.

The nuclear fuel cloud is assumed to have a radius equal to 0.6 times the cavity radius. The edge-of-fuel location is shown in Fig. 8. At this location, the nuclear fuel partial pressure is assumed equal to zero. The edge-of-fuel location is also designated as the radial stagnation surface. The radial stagnation surface is the radial station in the vortex flow field across which there is no net flow of buffer gas. This radial stagnation surface model was developed from many radial inflow fluid mechanics tests reported in Refs. 14 and 15.

The region of analysis for the radiant heat transfer calculations extends beyond the radial stagnation surface further into the fuel region so that at any wavelength, the optical depth, i.e., the number of radiation mean-free paths into

the fuel region, is greater than one. The innermost dashed line in Fig. 8(b) depicts the inner boundary of the radiant heat transfer region of analysis. The radial dimensions of these principal features of the radiant heat transfer region of analysis are shown in Fig. 8(b).

The spectral heat flux calculation is a temperature iteration procedure. A radial partial pressure distribution of nuclear fuel is assumed in the edge-of-fuel region. The analysis proceeds by varying local temperature until a desired constant heat flux across the region of analysis is calculated within a specified convergence criterion.

In order to calculate the spectral heat flux, detailed spectral absorption coefficients for the constituent gases are needed as functions of wavelength, temperature, and pressure. Typical spectral absorption coefficients for argon and uranium taken from Refs. 16 and 17 are shown in Fig. 9. Details of the procedures used in calculating these absorption coefficients are discussed in Refs. 16 and 17.

The reflective aluminum liner serves the purpose of trapping photons in the test region. The reflected thermal radiation is re-absorbed by the nuclear fuel in the edge-of-fuel region which causes the local temperature to rise there. For example, for a liner reflectivity of 0.9, the local temperature assumes a value such that for every ten units of thermal radiation directed outward, approximately nine units are returned to the nuclear fuel cloud in the steady-state condition. The aluminum reflectivities employed in these calculations are shown in Fig. 10. These reflectivities were calculated from measured data on the real and complex indices of refraction for aluminum. Description of the analysis in calculating these reflectivities is also reported in Ref. 17. The neutron transport theory calculations of the reflected heat flux indicate that the average angle of reflection from the cavity liner is on the order of 60°; therefore, the reflectivities at 60° were chosen as the representative values over all wave numbers for the subsequent spectral heat flux calculations.

The calculated temperature distribution for the in-reactor tests with argon buffer gas is shown in Fig. 13. The distribution in the edge-of-fuel and buffer-gas region was calculated using the spectral heat flux analysis described in Refs. 12 and 13. The distribution in the inner region of the fuel cloud was calculated using a radiation diffusion model. This latter calculation will be discussed in a subsequent section.

The variation of spectral heat flux at the aluminum wall for the temperature distribution shown in Fig. 11 are shown in Fig. 12. Since the energy released by fission in the test zone is a constant depending only on the contained nuclear fuel mass (which in this case is 6.2 g of U-235), the net radiation heat flux emitted from the nuclear fuel cloud is a constant 7.1×10^{9} erg/cm^{2}-sec. The

corresponding net heat flux at the wall with a 1/R reduction due to the cylindrical geometry is 4.26×10^9 erg/cm^2-sec. The interesting features of the spectral heat flux are that the black-body spectrum corresponding to the net heat flux shown in Fig. 12 is considerably different from the calculated spectrum which develops when a region such as the nuclear fuel cloud is surrounded by a reflective cavity wall. Thus, the shape of the emitted radiation spectrum seen by the reflective wall is more like a black-body spectrum corresponding to a radiating temperature of 5426°K. The effective black-body radiating temperature of 5426°K is the temperature corresponding to the outward directed heat flux from the edge-of-fuel location.

The corresponding variation of fractional heat fluxes for the spectral heat fluxes shown in Fig. 12 are shown in Fig. 13. The effect of the spectral detail can be seen in these fractional fluxes in that there is some enhancement of uv radiation above approximately 40,000 wave numbers. This short-wavelength radiation streams from inner, high-temperature zones of the fissioning plasma. This streaming of uv radiation through windows in the uranium spectral absorption coefficients is a feature which has been observed in radiant heat transfer calculations for the reference engine (see Ref. 13). However, the intensity of uv radiation in those cases is far greater than for the in-reactor test fissioning plasma because the temperatures in the interior of the fuel cloud are much higher in the reference engine.

The spectral heat flux incident on the aluminum liner was used to calculate a spectrum-weighted average reflectivity which at the liner surface was 0.908. Another factor to be considered in determining the effective reflectivity as seen by the fuel region is the subtended angle of the nuclear fuel cloud relative to the diffusely reflected radiation from the liner. The diffusely reflected radiation from the liner has a cosine distribution about the inward normal. Some of the reflected radiation therefore, does not intercept the fuel cloud but passes by the cloud and reflects off another portion of the liner. This subtended angle effect can be calculated for the case of an optically-thick cylindrical fissioning plasma surrounded by a reflecting surface by

$$\mathcal{R}_{EFF} = \mathcal{R} - \sum_{n=1}^{N} (1-\mathcal{R}) \left[\mathcal{R}\left(1 - \frac{R_F}{R_T}\right) \right]^n \qquad (1)$$

where $\mathcal{R}$ is the reflectivity, R_F is the fuel region radius, R_T is the test cavity radius, and n + 1 is the number of wall reflections, N is chosen sufficiently large to converge $\mathcal{R}_{EFF}$ in Eq. (1). The effect of fuel-to-cavity radius ratio on effective reflectivity for aluminum surface reflectivities of 0.9 and 0.908 is shown in Fig. 14. For the in-reactor test condition of $R_F/R_T = 0.6$ and $\mathcal{R} = 0.908$, the effective reflectivity as seen by the edge of fuel is 0.855. The effective

reflectivity is calculated by the neutron transport theory code (see Ref. 18) in the flux iteration procedures. The value of $\mathcal{R}_{EFF}$ from Eq. (1) and that from the neutron transport theory analysis corresponded exactly. One can conclude from Fig. 14 that it is desirable to expand the fuel radius to fill as much of the cavity as possible to take advantage of as much of the liner reflectivity as possible. The radius ratio of 0.6 was chosen on the basis of observed containment results from many two-component gas vortex containment measurements performed at UARL. It may be possible to expand the fuel-to-cavity radius ratio for the in-reactor test configuration by employing well chosen test configurations and appropriate ratios of buffer bypass-to-fuel weight flow.

Buffer-Gas Convection

The spectral absorption coefficients for argon shown in Fig. 9 indicate that at edge-of-fuel temperatures on the order of 5100°K, the spectral absorption coefficients for argon over the entire wave number range of interest are very small. Therefore it was expected that the heat transferred to the argon buffer gas from the fuel region would be essentially equal to that due to conduction. The results of calculation of the convection heat load in the buffer-gas flow shown in Fig. 15 verified this to be the case. It can be seen that the integrated convected energy is equal to the conducted energy; the radiation absorption by the argon buffer gas being so small that it was not of significant magnitude to plot on the curve in Fig. 15.

The temperature distribution shown in Fig. 11 indicates as does Fig. 15 that most of the convected energy is swept out of the buffer-gas region in the zone between the edge of fuel and a radial location approximately 0.4 cm outside the edge of fuel. Thus, a great deal of the buffer gas has no temperature rise and no convection heat load as it passes radially inward from the peripheral aluminum liner. The radial weight flow and axial velocity distributions in the argon buffer gas corresponding to the temperature distribution and integrated convected energy are shown in Fig. 16. It can be seen from Fig. 16(a) that a great deal of the required argon weight flow occurs in the zone where there is very little rise in the argon temperature. This results from the constraint that there be a constant axial dynamic pressure with radius requiring that a portion of the buffer flow turn and flow axially in each stream tube as the buffer flow proceeds inward.

As discussed in the section entitled DESCRIPTION OF TEST CELL CONFIGURATIONS, two-component gas vortex tests have indicated that simulated-fuel containment increases with an increase in fuel-to-buffer-gas weight flow through the axial thru-flow ducts. The 39.7 g/sec of argon flow required on the basis of the radiant heat transfer calculations results in a low fuel-to-buffer-gas flow rate ratio through the thru-flow ducts. The two-component gas vortex tests have also

indicated that containment can be improved by allowing axial buffer flow near the periphery of the cell to pass out through peripheral thru-flow ports in the end walls rather than flowing axially, then radially inward down the end walls, and finally through the thru-flow ducts. Thus, in the case of the radial weight flows shown in Fig. 16(a), if the buffer flow between the aluminum reflective liner and a radial location at 2.4 cm in from the liner were drawn off through axial thru-flow ports, the buffer weight flow which would then pass radially down the end walls and through the thru-flow ports would be on the order of 6 g/sec; a much lower flow rate of argon buffer gas through the thru-flow ports than when no axial bypass is used.

Calculations of the buffer-gas convection in the reference engine (Ref. 13) show that the total radial weight flow required to maintain the wall temperature at an acceptable limit is sensitive to the assumed position of the radial stagnation surface relative to the edge of fuel. If the stagnation surface is coincident with the edge of fuel, the radial buffer weight flow must go to zero at the edge-of-fuel location, leaving very little convection capacity in the last stream tube adjacent to the fuel region. By moving the stagnation surface inside the edge-of-fuel location, additional radial weight flow can pass across the buffer-gas fuel boundary and more radial weight flow can turn in the axial direction in the stream tubes which are absorbing the most heat by conduction from the fuel region. The actual position of the radial stagnation surface for the in-reactor test cell is not known; it will be inside the edge of fuel at a location determined by the detailed fluid mechanics associated with the balance between the outward diffusion of fuel and the inward flow of buffer gas, thus causing some reduction of the buffer-gas weight flow calculated for the case in which the radial stagnation surface location is coincident with the edge-of-fuel location.

The variation of axial velocity in the buffer region is shown in Fig. 16(b). The effect of the constraint of constant axial dynamic pressure can be seen by the relatively constant axial velocity in the region where the temperature distribution is constant, corresponding to a constant density buffer-gas region. Flow visualization measurements in various radial inflow vortex tests conducted at UARL have indicated that the axial velocity of the buffer-gas zone should be maximum approximately at the radial stagnation surface (Ref. 14). The model employed for these calculations exhibits this particular feature.

Consideration must also be given to the stability of vortex flows with superimposed axial velocities that are large, as in the edge-of-fuel region. Flow stability criteria for radial-inflow vortexes were discussed in Refs. 19 and 20. A Richardson number criterion for rotating flow derived in Ref. 19 is

$$Ri = \frac{V_{\phi_1}^2 \left(\frac{r}{r_1}\right)^{2n} \cdot \left(\frac{1}{r^2}\right) \left[\frac{r}{\rho}\frac{\partial \rho}{\partial r} + 2(n+1)\right]}{\left(\frac{\partial V_Z}{\partial r}\right)^2} \geq 0.25 \qquad (2)$$

In Eq. (2), V_{ϕ_1} is the average tangential velocity at the transparent peripheral wall, $\partial\rho/\partial r$ is the local radial gradient of total density, $\partial V_Z/\partial r$ is the axial shear (i.e., the local radial gradient of axial velocity), and the exponent n characterizes the tangential velocity profile (n = -1 is a free vortex; n = +1 is solid body rotation). Qualitatively, the numerator in Eq. (2) is the stabilizing term due to buoyancy or density stratification. The denominator represents the kinetic energy available to feed small perturbations and cause an instability. Stability occurs for $Ri \geq 0.25$.

Equation (2) can be applied using the temperature and velocity profiles shown in Figs. 11 and 16(b), respectively. By setting Ri = 0.25 in Eq. (2), one can calculate the minimum value of peripheral wall velocity for stability. For the range n = -1 to n = +1, this gives V_{ϕ_1} = 51 and 102 cm/sec, respectively, as limits. These limits are compatible with the calculated argon buffer-gas injection velocity of 107 cm/sec based on injection area criteria for radial-inflow vortex flow (see APPENDIX C of Ref. 21) for the basic in-reactor test configuration. The key point is that in general the large destabilizing axial shears which occur in the edge-of-fuel region (as in Fig. 16(b)) are balanced by the strong stabilizing effect of the very large temperature gradients (as in Fig. 11).

Density and Partial Pressure Distributions

Detailed calculations of thermal radiation spectral heat fluxes are required in the region at the edge of the fissioning plasma where in many of the wavelength ranges, the radiation mean-free path is of a dimension far greater than can be reasonably described by an average local temperature and density condition. Further into the fissioning plasma, the partial pressure of uranium and the onset of ionization of the various gaseous species results in high spectral absorption coefficients over most of the wavelength range of interest. In these regions, a radiation diffusion analysis can be employed.

There is coupling between the temperature distribution calculated for the fissioning plasma region and the containment characteristics in the fuel and buffer-gas mixture. A reasonable constraint for containment is to require that from the edge-of-fuel region inward, the local density at any station be less than or equal to the density of the buffer gas at the edge-of-fuel location. With this constraint, and for a total pressure of 500 atm, there exists an upper

limit on the amount of uranium (which has a higher mass number) that can be mixed with the argon at a given local temperature. A computer program was written which calculates the ratio of uranium to argon at local temperatures in the fuel region such that the total pressure of 500 atm is preserved and the total density of uranium plus argon equals that of argon at the edge-of-fuel temperature. The compositions of argon and uranium as functions of temperature and pressure, including the effects of ionization at high temperatures, were taken from Refs. 16 and 17. Calculations were made of uranium argon partial pressures over the temperature range expected in the region between the edge of fuel and the fissioning plasma centerline.

Rosseland mean opacities were calculated using the spectral absorption coefficients from Refs. 16 and 17 for the mixtures of uranium and argon. These opacities were used in a radiation diffusion analysis to determine the temperature distribution required to deliver a net heat flux at radial boundaries at 0.05-cm intervals from the centerline of the fuel zone equal to the total energy release due to the fissioning of the nuclear fuel within each boundary (local argon and uranium densities and partial pressures were calculated using the program discussed above). The program will converge only when the heat flux at the outer boundary of the problem corresponds to the net heat flux at the edge of fuel of 7.1×10^9 erg/cm^2-sec (i.e., 6.2 g of U-235 must be contained, based on the imposed density and total pressure constraints). The resulting temperature distribution, referred to earlier, is shown in Fig. 11. It can be seen that a slight discontinuity exists at the point where the Rosseland mean opacity analysis was coupled to the extrapolation of the neutron transport theory temperature distribution.

Using the temperature distribution which resulted in Fig. 11, the corresponding density and partial pressure distributions of the uranium and argon for the in-reactor test configuration were plotted and are shown in Fig. 17. The slight discontinuities mentioned earlier where the Rosseland mean analysis and the extrapolated transport theory analyses meet are also visible in the curves of Fig. 17. The integrated contained mass of uranium from these calculations was within 3 percent of the required uranium mass to deliver the heat flux required at the edge of fuel. This value of contained mass was considered to be close enough to the desired value such that no further iterations were performed. The curves shown in Fig. 17 were used to calculate average argon and uranium partial pressures and an average density of uranium in the fuel region. The resulting average uranium partial pressure was 125 atm and the average fuel density was 0.0284 g/cm^3. Comparison of these values to the previously estimated partial pressures and average densities will be discussed below in a comparison of the present results to the performance predicted in Refs. 5 and 6.

Further analysis employing density distributions based on more detailed containment criteria should be performed to establish a predicted upper limit for fuel containment for a configuration such as the one calculated in the present report. Variations of radiated energy, spectral heat fluxes, containment characteristics, and flow requirements should be calculated for different test cell diameters and for different fuel-to-cavity radius ratios. It is planned to pursue further work in these areas.

DETAILED THERMAL ANALYSIS

A computer program was written to calculate test cell temperatures and flow conditions required to maintain local temperatures below tolerable limits. Axial stepwise calculations are made of the heat generation rates and radiant heat loads, the temperature levels in the coolant and structural components, and the fractional pressure losses throughout the test assembly. The radial position in the pressure vessel at which the maximum temperature occurs is also calculated so that the distribution of heat from the pressure vessel to the liner coolant and the external pressure vessel coolant may be estimated. The program inputs consist of the component dimensions, coolant physical properties, coolant inlet temperatures and flow rates, and the physical properties of the structural materials. The required flow conditions to achieve the desired temperature levels throughout the system are varied until the desired temperature distributions for a fixed flow rate are determined.

The results of these calculations for the basic test cell configuration with hydrogen and argon liner coolants are given in Table II for key stations in the axial cross section of the test unit. (Station numbers in Table II are denoted on an axial cross-sectional view of the test configuration in Fig. 18.) For the case in which a fiberglass pressure vessel is employed and hydrogen coolant is used for both the liner and the end walls, the total hydrogen coolant weight flow was 300 g/sec with 100 g/sec branched off to cool each end wall. The calculated material temperatures are shown at locations in the configuration where the temperature is highest for the particular component. For example, the maximum temperature in the fiberglass pressure vessel was calculated to be 418°K at a point adjacent to the lower end wall and 0.24 cm from the inside surface of the fiberglass. The maximum temperature on the test cavity surface was calculated to be 556°K at the intersection of the reflective aluminum liner and the aluminum lower end wall. Local pressures throughout the system for these flow conditions are also shown in Table II.

Additional calculations were performed for configurations using an all-aluminum pressure vessel and for cases in which argon was used as the liner coolant fluid instead of hydrogen. Thus, four combinations of pressure vessel material and liner coolant are possible. The results for these four cases are summarized in Tables II and III. Temperatures throughout the test unit are quite similar for either hydrogen or argon coolant. However, the greater flow rates required with argon result in pressure drops through the system on the order of nearly 10 atm as compared to approximately 0.4 atm with hydrogen.

The increase in liner and end-wall coolant temperatures and other temperatures at various locations throughout the system as a result of adding nuclear fuel to

the test cell are of interest since they indicate the temperature rise anticipated when nuclear fuel is added. Therefore, the calculations for the four basic cases were supplemented by tare-temperature calculations in which the only gases flowing through the system were argon buffer gas and the two coolant fluids (i.e., injection of nuclear fuel was not included). The results of these cases are also shown in Tables II and III. It can be seen that with a fiberglass pressure vessel, the temperature rise in the upper end wall, liner, and lower end-wall coolants due to the addition of the 6.2 g of U-235 to the fuel containment region amount to 11, 58, and 62°K, respectively, for hydrogen coolant and 14, 38, and 53°K, respectively, for argon coolant. Similar temperature rises result when the aluminum pressure vessel is used.

One additional calculation was performed to determine the effect of deposition of nuclear fuel, should it occur, on various surfaces throughout the test cell. Separate calculations were performed to determine the coolant and exhaust port temperature rises associated with deposition of small amounts of uranium on the radial liner, the end walls, and on the walls of the thru-flow ducts. These results were translated in terms of a rate of temperature rise in various coolant fluids and system components relative to the rate of uranium deposition on the surfaces mentioned above. The results of these calculations are shown in Fig. 19. It can be seen that deposition on the end-wall surfaces results in the highest rate of temperature rise. Based on these results, and assuming that a typical test run with nuclear fuel flowing into the test cell would be on the order of 300 sec, and assuming that the maximum allowable temperature rise would be 100°K, the limit on the rate of nuclear fuel deposition on the end wall, radial liner, and thru-flow-duct surfaces is less than 3.17×10^{-5}, 1.24×10^{-4}, and 8.33×10^{-2} g/sec, respectively.

The results of the fuel handling experiments reported in Ref. 22, in which zinc vapor was transported through a simulated exhaust duct, indicate that injection of buffer flow through the manifold around the thru-flow duct, as depicted in Fig. 2, would serve to prevent the deposition of particles on the walls of the duct. The experiment did not include a simulated fuel injector on the centerline of the thru-flow duct, but it is expected that use of an injector designed such that its surface temperature is above the uranium melting point, i.e., above approximately 1450°K, would insure that no significant amount of fuel deposition would occur on the injector. Further investigations of fuel deposition on all the components of the system will become an integral part of the rf simulation experiments in which measurements of fuel containment will be made under thermal conditions and with vapor pressures similar to those anticipated for the nuclear light bulb in-reactor tests.

EVALUATION OF TEST PERFORMANCE

The results from the detailed radiant heat transfer analyses and the thermal analyses of the preceding sections were used to calculate the performance characteristics of an in-reactor test of a unit cell with the design characteristics and dimensions given in Figs. 4 and 5 and Table I. The two key factors which have resulted in minor changes to the performance characteristics relative to those reported in Refs. 5 and 6 are that the buffer-gas flow requirements to convect away the heat conducted to the buffer-gas region were increased from 25.3 g/sec to 39.7 g/sec and the effective reflectivity of the aluminum liner due to fuel-to-cavity radius ratio effects was reduced from an assumed value of 0.9 to an effective value of 0.855. The result of these two effects was to reduce the equivalent black-body radiating temperature for the outward directed radiant flux from 5940 to 5426°K. A comparison of the performance characteristics from Refs. 5 and 6 to the characteristics from the present analyses are shown in Table IV.

Calculations of density and partial pressure profiles for the inner zones of the fuel region discussed previously were used to calculate the ratio of average fuel density in the fuel region to the density of argon at the edge of the fissioning plasma. This ratio was 0.6 as compared to a value of 0.7 used in Refs. 5 and 6. Also, the average partial pressure of uranium in the fuel region was reduced from 195 atm to 125 atm. This latter reduction in fuel average partial pressure resulted from detailed calculations of the local fuel partial pressure throughout the fuel region based on a containment constraint that the total density of fuel and argon at all locations within the fuel region be equal to the density of the argon at the edge of fuel. Previous partial pressure estimates were based on extrapolations of earlier calculations of partial pressure related to the radiant heat flux per unit length emitted from the fuel cloud (Ref. 23).

A summary of the total heat balance in the cavity region for an in-reactor test of the basic test configuration is given in Table V. Included in the heat balance are (1) energy convected from the fuel region by the flow of nuclear fuel, carrier gas, and buffer gas entrained in the fuel region, (2) energy convected from the cell by the flow of argon buffer gas, and (3) thermal radiation heat flow to the cavity surfaces. The results of the heat balance calculations indicate that the ratio of thermal radiation heating (174.0 kW) to total power in the test cell (190 kW) is 0.915.

The fuel, carrier-gas, and buffer-gas flow conditions for the in-reactor test in the basic test cell are given in Table VI. The two forms of fuel injection, uranium particles in an argon carrier gas and a liquid UF_6-uranium particle slurry are considered in Table VI. Details of the fuel injection options were described in Ref. 6.

The variation of effective liner reflectivity with fuel-to-cavity radius ratio and a normalization factor for convection of energy by the buffer gas based on the results of the radiant heat transfer calculations were incorporated into the general performance analyses employed in Refs. 5 and 6. Updated performance curves which depict the variation of power level and radiating temperatures were calculated for the range of specific fission power from 0 to 100 kW/g of U-235. The results of these performance calculations are shown in Fig. 20.

The general performance analyses was also used to investigate the effect of varying fuel-to-cavity radius ratio and the related effective liner reflectivity shown in Fig. 14. The results of these calculations are shown in Fig. 21. It can be seen that the power radiated increases with fuel-to-cavity radius ratio but that there is only a small effect on the radiating temperatures. The relatively constant value for T* with increasing fuel-to-cavity radius ratio results from increasing proportions of energy convection from the fuel region as the fuel volume increases.

It may be desirable to obtain higher radiating temperatures by performing experiments at higher pressures than the reference pressure of 500 atm. The performance analyses modified to include reflectivity and convection heat load effects to the buffer-gas region was used to calculate the effect of increasing operating pressure on the performance of in-reactor tests. As reported in Ref. 6, with increased pressure the pressure vessel thickness must also increase and therefore the diameter of the fuel and buffer region must decrease. These effects were incorporated in the analyses. The results of those calculations are shown in Fig. 22. It can be seen that an increase in operating pressure over the range from 500 to 3000 atm results in extending the equivalent black-body radiating temperature of the outward directed flux to the order of 7200°K.

Detailed radiant heat transfer and containment calculations similar to those performed for the basic cell configuration should be carried out to verify the performance evaluations of the effects of fuel-to-cavity radius ratio and operating pressure to determine whether the containment parameters are consistent with the radial density profile constraints. Based on the results for the basic cell, it is anticipated that the performance evaluations in these two cases are adequate for predicting ranges of performance with the variation of the parameters used.

Total Flow Requirements

The total flow requirements to conduct an in-reactor test are based on the coolant, buffer, and fuel flows during the test and the duration of the various phases of the test. The sequence of events for a reference in-reactor test are shown in Table VII of Ref. 6 and is repeated in Table VII of this report. Descriptions of the phases of operation in the sequence of test events is contained in

detail in Ref. 6. Using this sequence of events, the total volumes of fuel, buffer gas, and coolant required to conduct a test were calculated. These total flows are summarized in Table VIII. As can be seen, the total flow requirements were included for cases with argon or hydrogen liner coolant and with the two fuel injection options described above and in Ref. 6. These total weights indicate both the total requirements for material and gas supplies to perform the tests and total masses of materials which must be handled in either the Nuclear Furnace scrubber or a separate effluent handling system.

Performance Levels for Propellant Heating Configuration

Since propellant heating demonstration tests and tests to demonstrate the feasibility of using the transparent-wall structure in the radiation and thermal environments of a nuclear reactor are of importance, analyses were also performed to determine the range of radiating temperatures and power levels for in-reactor tests of a cell having a propellant heating channel as shown in the sketches in Fig. 7. The results of these analyses are summarized in Table IX. For the reference specific fission power level of 30.5 kW/g of U-235, a propellant heating configuration would have a radiating power of 120 kW. The corresponding equivalent fuel region black-body radiating temperature and equivalent fuel region surface radiating temperature would be 3330°K and 4611°K, respectively. These temperatures were calculated by assuming that the effective surface reflectivity of the aluminum liner was reduced from $\mathcal{R}_{EFF} = 0.855$ to $\mathcal{R}_{EFF} = 0.728$ due to the presence of absorbing propellant. On the basis of propellant heating results in the UARL dc arc heater facility (see Refs. 4 and 24), this power and radiating temperature should result in demonstration tests which would deliver a bulk propellant temperature in the range of 3300 to 3700°K.

Transparent-wall tests could also be performed with no seeded propellant flowing through the propellant heating channel. The total thermal radiation flux (incident plus reflected) passing through the transparent-wall structure would be 8.83 kW/cm^2, compared with 22.9 kW/cm^2 for the reference nuclear light bulb engine. These radiation fluxes were calculated assuming the combined effective reflectivity of the aluminum liner was $\mathcal{R}_{EFF} = 0.855$. The nuclear radiation dose rate in the transparent structure would be dominated by the dose rate from the driver reactor which has been calculated for the Nuclear Furnace to be on the order of 30 W/g. This corresponds to a nuclear radiation dose rate of 3.0 Mrad/sec. Thus, the ionizing dose rate delivered to the silica in a transparent-wall test would be approximately 60 percent of that anticipated for the reference engine (see Refs. 25 and 26). At these dose rates, significant tests of the coloration of fused silica could be performed in a combined nuclear and thermal radiation environment.

EFFLUENT HANDLING

Total flow requirements for an in-reactor test were discussed previously and the materials expended per test are given in Table VIII. Discussions on adding the effluent of an in-reactor test into the Nuclear Furnace scrubber system were held with LASL and NRDS representatives. It was concluded that the Nuclear Furnace scrubber had more than enough capacity to handle the in-reactor test total exhaust materials. However, it would be preferable to collect the uranium metal or uranium compounds (390 g of U-235 per test run) in a smaller separator system to avoid adding nuclear fuel materials to the large underground storage tanks which collect the Nuclear Furnace scrubber water.

Therefore, the possibility of connecting a separate scrubber system to the Nuclear Furnace which could be remotely disconnected such that the test assembly could be inserted and extracted at the test site was explored. Figure 1 contains a sketch of the Nuclear Furnace with the test assembly inserted and connected to a separate effluent handling system. The ducting to the separate scrubber system through the bottom of the core would pass through a water-cooled jacket connected directly beneath the Nuclear Furnace scrubber elbow under the core. Since the environment around the cooling jacket is hot hydrogen exiting from the core, some of the cooling jacket water would be exhausted radially into the hydrogen exhaust. This flow would supplement the water injection from the peripheral walls of the Nuclear Furnace exhaust chamber. A remote connection coupling underneath the exhaust elbow is shown in Fig. 1.

An expanded cross-sectional view of the location where the water cooling jacket nearly meets the bottom of the reactor core is shown in Fig. 2. The outer annulus of the cooling jacket would be permanently attached to the exhaust elbow. The Nuclear Furnace core, when dropped into place, would be positioned such that a small clearance would exist between the cooling jacket outer annulus and the core bottom. The in-reactor test assembly exhaust duct would fit down through the cooling jacket. The orifice plate at the base of the reactor core would serve as a positioning disc as the test assembly was dropped into place. A reflective shield and coolant baffle attached to the base of the orifice plate would protect the region of intersection of the orifice plate and the cooling jacket from intense heat fluxes emitted by the hot hydrogen exhaust gases. This baffle would also serve to duct cooling water flow exiting the top of the jacket downward along the jacket periphery. The test assembly exhaust duct would extend down through the Nuclear Furnace exhaust elbow to the remotely operated connect-disconnect fitting.

Further design analyses must be performed to determine the jacket cooling flow required and to determine the effect of the presence of the effluent duct in the Nuclear Furnace exhaust chamber on the hydrogen and scrubber water flow. Also, the

position of the remotely operated connect-disconnect coupling will need to be established relative to its accessibility to the remote handling equipment. It is planned to hold further discussions with NRDS representatives with regard to the design and operation of the system for handling the in-reactor test effluent.

INSTRUMENTATION FOR IN-REACTOR TESTS

The principal method of determining the performance of an in-reactor test will be through measurement of the heat balance in the test assembly. Test components will be heated by neutron and gamma-rays from the driving reactor before nuclear fuel is introduced into the vortex. Temperatures in the system before introduction of the nuclear fuel will serve as tare measurements for subsequent measurements of test performance. The temperature levels throughout the system are given in Tables II and III for the test operation before nuclear fuel is introduced. Once the test is operating at full-power, steady-state conditions, temperature measurements at stations in the reflective liner and end-wall coolant passages will indicate the total amount of energy incident on the test region periphery. If these temperatures remain steady, it will be an indication that there is no deposition of nuclear fuel occurring on these surfaces. Control of the flow rate through the test cell will be accomplished by orificing the various coolant, buffer gas, and fuel injection supply lines as described in Ref. 6. The positions of the various thermocouples required to determine the heat balance in the test assembly are shown in Fig. 23. Additional thermocouples would be located throughout the system at positions expected to exhibit the highest temperatures during test operation, such as the end-wall surfaces at the periphery of the cavity. Thermocouples at these locations are also shown in Fig. 23.

Pressure measurements would also be desirable. Pressure transducers are shown in Fig. 23 near the exhaust duct entrances and in the end walls near the periphery of the cavity. Pressure measurements from these locations will indicate the pressure drop across the radial-inflow vortex and will indicate whether there is pressure and flow balance between the two exhaust ducts.

It will be necessary to constrict the thru-flow ducts near the exit locations of the test assembly to reduce the pressure from 500 atm to the working pressure of the effluent cleanup system. This might be accomplished with one orifice or a series of orifices. It would be desirable to make differential pressure measurements across this orifice or series of orifices to insure that appropriate pressure drops and flow conditions are maintained.

The instrumentation used would be of the type currently used to measure coolant and surface temperatures and pressures in Nuclear Furnace tests. The leads from the thermocouples would pass through the top of the test assembly as shown in Fig. 2. Further connections would then be made to the multi-connector plug through which the instrumentation leads of the Nuclear Furnace reactor are connected.

Direct measurements of spectral emission from the fissioning plasma in the test cell during a test are desired. Methods for observing the spectral emission from the test region are under development in the UARL rf plasma simulation tests. An internally polished optical tube can be inserted into the test configuration through the annular region between the liner and exhaust duct to the end wall of the test cavity. Several of these viewing tubes can be used at different radial stations across the end wall so that the size of the fissioning plasma and the variation in spectral emission with radius can be observed. A similar optical tube can be inserted through the liner coolant passage to observe the spectral flux emitted radially. These tubes would have a low flow of neon bled through them, thus allowing them to be transparent to the radiation emitted from the nuclear fuel cloud. Corner mirrors would be employed to reflect the emitted light to a detector system packaged within a cooled shield just beneath the bell shield which covers the Nuclear Furnace reactor (this system was sketched in Fig. 14 of Ref. 6). A straight viewing port and one with corner mirrors to view the peripheral surface of the fissioning plasma are shown in Fig. 23.

Tests to verify that such an instrumentation package could be housed under the bell shield, cooled, and shielded to prevent a high level of background noise should be performed in an early Nuclear Furnace test. In addition, bench tests using controlled light sources should be performed to determine the calibration factors required for the internally polished neon filled tubes. In particular, the efficiency of the corner mirrors should be calibrated to determine the number of corners and reflections which could be allowed in such an optical path without seriously depleting the signal strength.

The Nuclear Furnace system has on the order of 150 channels for recording instrumentation signals. If the Nuclear Furnace were operated for the purpose of testing nuclear light bulb configurations, many of these channels would be available for the unit cell test assembly. For example, the number of thermocouples currently used to measure the outlet temperature from each fuel element would be cut back considerably. LASL and NRDS representatives have indicated that there is no shortage of instrumentation channels which could be used to record the nuclear light bulb test measurements. It is estimated that approximately 30 instrumentation channels will be needed. The precise number of temperature, pressure, and flow measuring instruments required will be determined as more experience is gained in the in-reactor test simulation experiments conducted in the UARL 1.2-MW rf induction heater facility.

COMPARISON OF SIMULATION EXPERIMENTS TO IN-REACTOR TESTS

For the past three years, experiments directed toward simulating the conditions of an in-reactor test have been conducted at UARL. These experiments have included (1) injection of simulated nuclear fuel into an rf plasma, (2) heating of a simulated propellant stream to high bulk exit temperatures using a dc arc radiant energy source, (3) design, fabrication, and testing of a filament-wound pressure vessel suitable for use in future rf plasma experiments up to pressures of 500 atm, and (4) tests of thru-flow port flow geometries designed to minimize deposition of simulated fuel on the duct walls.

Fuel-Containment Experiments

The 1.2-MW rf induction heater facility at UARL has been employed to conduct experiments related to the in-reactor test fissioning plasma experiments. These plasmas are operated with argon buffer gas injected from the end walls and with various forms of simulated fuel injected through probe injectors on the axial centerline (see Refs. 3 and 27). To date, simulated fuels in the form of gaseous UF_6 and tungsten particles added to argon carrier gas have been successfully injected into the rf plasma operating at pressures up to 40 atm and power levels up to approximately 125 kW. The development of particle seeder technology required to inject tungsten seeds and the design of systems to inject liquid UF_6 into the rf plasma have progressed substantially. Experiments employing these injection systems will be continued in the coming year.

Propellant Heating Experiments

Experiments have been conducted to simulate radiant heating of the propellant stream of a nuclear light bulb engine (see Refs. 4 and 24). The primary objective was to obtain high bulk exit temperatures in the flowing simulated propellant stream by absorption of large fractions of the incident thermal radiation.

A high-power, vortex-stabilized dc arc within an uncooled fused silica tube was used as the radiant energy source. It was surrounded by a mirror system to increase the radiation incident on the simulated propellant. The 12.7-cm-long by 2.3-cm-wide, diverging-duct test section had a transparent front wall and a reflecting rear wall. The geometry of this test section was quite similar to the propellant heating configuration shown in Fig. 7. The central stream of seeded gas, a tungsten-particle/argon aerosol, had unseeded argon buffer layers on both sides to prevent coating of the duct walls. Arc operating times were approximately 0.5 sec with power levels up to 780 kW. Bulk exit temperatures were measured using a calorimeter downstream of the duct.

The maximum simulated propellant bulk exit temperature obtained was 4515°K, compared with 3300 to 3700°K expected in in-reactor tests in the Nuclear Furnace. The maximum temperature in these tests was limited primarily by the amount of radiation incident on the test section (determined by the arc operating characteristics and the effectiveness of the mirror cavity).

Fuel-Handling Experiments

Experiments in which zinc metal is vaporized and added to argon flow in a duct which simulated the thru-flow port of the in-reactor test configuration have been conducted employing a plasma torch facility. These experiments are described in Refs. 22 and 28. A swirling flow of argon was heated using a dc arc plasma torch, passed through a vaporizer section where zinc vapor was entrained and entered a bypass inlet section and then a 2.54-cm-diam by 60-cm-long pyrex exhaust duct. Cold bypass argon was injected with swirl through four different bypass inlet section geometries. Radial distributions of temperature were measured in some tests and observations were made of the deposition of zinc on the duct walls. These experiments led to the development of a bypass inlet geometry which appears capable of achieving condensation of the vapor in the flow, with very little deposition on the wall for long distances. In this inlet, bypass flow was injected with swirl from 188 ports in the 2.54-cm-i.d., 13.5-cm-long wall (47 ports in each of four rows spaced 90° apart around the circumference). In one test, only 0.15 percent of the 9.5 g of zinc vapor passing through the inlet in a 2-min test was deposited on the wall. The mixture flow rate in this test was 3.9 g/sec and the bypass flow rate was 36.3 g/sec; hence, the bypass ratio was 9.3.

To make further progress on the design of exhaust system components, it is recommended that further tests be conducted using models which more closely mock-up the entire lengths of the exhaust ducts developed in the conceptual design studies. These tests should employ uranium-vapor/argon-gas mixtures for closer simulation of the properties of the mixtures in the engine and in-reactor test model.

Pressure Vessel Development

In the present contract year, development of a filament-wound fiberglass pressure vessel for use in the 1.2-MW rf facility was undertaken (see Ref. 8). With minor exceptions, this pressure vessel is similar in design and dimensions to the proposed in-reactor geometry for tests with fissioning uranium plasmas in the Nuclear Furnace. The pressure vessel and associated equipment were designed for use with the UARL 1.2-MW rf induction heater in tests with rf plasmas at pressures up to 500 atm.

The fiberglass filament-wound pressure vessel, which was designed for an operating pressure of 500 atm, has an inside diameter of 7.76 cm, a length of 28.1 cm, and a maximum wall thickness of approximately 5 mm. Alternate axial and hoop layers (a total of 28 layers) are used to provide the required strength. Immediately inside the filament-wound pressure vessel is a silicone rubber sealing liner. Cooling water flows in the annulus between the liner and the fused silica tube. This cooling water will contain dye in tests with plasmas to protect the liner and pressure vessel from the intense thermal radiation.

Initially, tests were conducted to verify the strength and reliability of the filament-wound pressure vessel design. One vessel was hydrostatically tested to 680 atm before it failed. Another was cycled more than 60 times between 0 and at least 540 atm before it developed a crack in the outer fiber layers.

A series of cold-flow tests of the model was then conducted at pressures up to about 510 atm. At 510 atm, the flow rates of argon and cooling water were 3.35 liter/sec (STP) and 26 gal/min, respectively. It was demonstrated that the model is capable of being operated for extended periods at the 500-atm pressure level and is, therefore, ready for use in initial high-pressure rf plasma experiments.

ALTERNATE TEST REACTORS

The in-reactor tests in the Nuclear Furnace are viewed as preliminary tests to demonstrate the operation of a fissioning uranium plasma in a small-scale test cell. Future tests of the gas core concepts should follow Nuclear Furnace tests. The role of future tests would be to attempt to scale up the size and/or the performance level of in-reactor tests (i.e., the total power radiated and the black-body radiating temperature at the edge of the fissioning plasma). A review of possible high-power-density nuclear reactors which might be available in the 1975-1980 time period was conducted to identify possible candidate test reactors for future nuclear light bulb in-reactor tests. Estimates were then made of the performance level of tests in these reactors. Also, an assessment was made of their availability and adaptability for use as fissioning plasma test reactors.

Candidate Test Reactors

In addition to the Nuclear Furnace, there are four other candidate test reactors which might be used for uranium fissioning plasma in-reactor tests. These reactors are the High Flux Isotope Reactor (HFIR) described in Ref. 29, the Kinetic Intense Neutron Generator (KING) described in Ref. 20, the NASA-Lewis Fission Uranium Plasma Facility (FUPF) test reactor which is in preliminary design stages and has been described in private communications with the NASA-Lewis representatives, and a self-critical cavity reactor concept which is under investigation at UARL. The features of these reactors are discussed below. Detailed discussions of the criticality requirements and size of the self-critical cavity are discussed in a subsequent section.

HFIR is operated at Oak Ridge National Laboratory to produce transuranium elements. It has a high power density and a thermal neutron flux on the order of $3\text{-}5 \times 10^{15}$ neutrons/cm^2-sec in a test zone approximately 10-cm in diameter and 60 cm long. The core lifetime in HFIR is approximately 23 days. It is conceivable that a HFIR-type reactor could be designed and constructed for use as a driver reactor for nuclear light bulb tests of small models.

The KING reactor is a circulating fuel reactor with a flux trap and test zone located on the axial centerline. Because the fuel is a solution with a high thermal capacity, the thermal neutron fluxes in the KING reactor can be extremely high, on the order of 10^{16} neutrons/cm^2-sec. The NASA-Lewis FUPF is in the early stages of design. The objectives of that design exercise are to provide a test facility which would accommodate spherical or cylindrical configurations on the order of 60-cm-in.-diameter and 90 cm in length. The thermal neutron fluxes are yet to be determined in the final configuration for the test-bed reactor, but the design will be such that the flux levels will be as high as possible so that fissioning uranium plasmas can be sustained in the test cells.

The principal characteristics of the candidate test reactors, as well as the Nuclear Furnace, are summarized in Table X. The principal characteristics which are included in Table X are the flux trap diameter available, the specific fission rate in the flux trap test region in kW/g of U-235, the estimated turn-around time per test, and the core lifetime of these particular test-bed reactors. The flux trap diameter indicates the size of cell which can be tested in the various reactors, the specific fission rate is related to the potential of these test reactors to sustain uranium plasmas with high radiating temperatures, the test turn-around time is an indication of the frequency of testing, and the test core lifetime indicates the frequency with which replacement of core fuel elements would be required. However, the test-core lifetime in a case such as the Nuclear Furnace or HFIR is a different parameter than normally considered. For example, the HFIR core is regularly changed every 23 days; the time required to replace the core in HFIR is on the order of one day. The Nuclear Furnace core can be replaced in a few months. Core lifetime for the KING reactor or a self-critical cavity reactor is not a fuel-element-related factor (the KING reactor is fueled by an aqueous uranyl sulfate solution and the self-critical cavity reactor would be fueled by flowing UF_6 or a particle-carrier gas system). Here, core lifetimes are established by constraints on other components of the system.

The in-reactor test performance levels for the various candidate reactors were calculated using the general performance analyses of Ref. 6. These results are summarized on Fig. 24. It can be seen that the important parameter is the specific fission power. The KING reactor, with its very high power density, appears to be a very attractive test reactor for small-sized tests. The pressure level of these tests can be reduced to the order of 100-200 atm and still produce radiating temperatures which approach those of the nuclear light bulb reference engine.

Design and Operational Status of Candidate Test Reactors

In evaluating the potential test reactors for nuclear light bulb in-reactor tests, one must consider the status of the design and operation of these reactors and whether a site for testing has been developed or not. Other factors to be considered are the possible period of operation, access to insert nuclear light bulb test cells, availability of a scrubber system to handle the effluent, and capacity for the test system to handle a full-scale test. A summary of these particular features for the candidate test reactors is shown in Table XI.

The only two candidate reactors with completed designs are the Nuclear Furnace and HFIR, both of which are operational reactors. The operation of the other candidate test reactors is estimated to be in the 1975-1980 period, should they be developed. The question of access for insertion of the test cell is considered good for all of the test reactors with the exception of HFIR. The HFIR reactor would require alterations to insert a system such as the nuclear light bulb in-reactor

test cell through the top of the reactor. The HFIR reactor would have to be redesigned as a separate facility to accommodate fissioning plasma tests. An effluent scrubber is available for the Nuclear Furnace and would be designed for any of the other candidate test reactors should they be available for gas-core tests. The site development would depend upon the location of the test reactor. Test sites are developed for the Nuclear Furnace and the HFIR reactor. The other candidate test reactors could be located and operated at NRDS.

The investment for initial tests can only be estimated on a relative scale. The point in entering this column in Table XI was to show that because the Nuclear Furnace is available and because its core, scrubber system, and site are already developed, the investment for initial tests should be considered relatively low. Design work has been completed on HFIR and has begun on the KING reactor and therefore, the investment to develop these reactors to accommodate fissioning plasma tests is medium on a relative scale. The FUPF and the self-critical cavity reactors which are yet to be thoroughly designed would require a relatively higher investment. However, it is expected that the self-critical cavity may not cost as much as a facility requiring fabrication and testing of driver-reactor fuel elements.

The final column in Table XI relates to the capacity to handle full-scale tests. None of these test reactors can handle a full-scale nuclear light bulb cell with the exception of the self-critical cavity which would be designed to accommodate a nuclear light bulb reference engine unit cell.

The conclusion from these discussions and evaluations of the candidate test reactors is that the most realistic near-term facility for testing a small nuclear light bulb unit is the Nuclear Furnace. Such a test, depending upon funding level, could be designed and performed in the time period from 1975 through 1978. The investment for such tests would be relatively lower than the investment required for the development of a new test reactor facility.

For future tests, a test configuration capable of testing larger cells at higher powers is desirable. The KING reactor appears to be a very attractive facility for testing small cells operating at high radiating temperatures. Ultimately, a self-critical cavity must be tested. The feasibility of a self-critical test-bed reactor requires further serious consideration. In particular, if a self-critical test facility is feasible and if the cost of developing that facility is of the same order of magnitude as the development of a driver reactor test facility, it seems that the self-critical cavity would yield more basic and useful experimental information than would a system relying on external driver fuel elements. The question of future test facilities should remain open until thorough evaluations of the various candidate test reactors are completed.

Self-Critical Cavity Test Reactors

Gaseous core nuclear rocket engines have tended to be large, high-pressure devices for two primary reasons: (1) there is a requirement for enough critical nuclear fuel density to make the system self-critical and (2) the temperature in the fissioning plasma must be high enough to radiate the required heat fluxes to the hydrogen propellant. The critical fuel density in externally moderated cavity reactors is governed by the efficiency of the moderator material in slowing down fission neutrons to thermal energies and then in allowing the thermal neutrons to diffuse back into the cavity. Thus, thermal neutrons moderated in the external reflector-moderator must diffuse back through several scattering mean-free paths to re-enter the cavity and cause more fissions in the gaseous nuclear plasma. In a gaseous nuclear rocket engine, hot hydrogen surrounding the fission plasma creates an additional thermal neutron diffusion barrier due to the high scattering cross section of hydrogen. This scattering rate is further enhanced by the thermal motion of the very hot hydrogen (see Ref. 31). The self-critical cavity described here indicates a method by which critical fuel density and cavity reactor size can be reduced by improving the flow of neutrons into the cavity by (1) embedding segmented propellant channels along portions of the cavity surface and (2) by choosing a reflector-moderator which has a very low thermal neutron scattering cross section.

Beryllium, cooled to temperatures below 100°K, has a very low scattering cross section for thermal neutrons below 0.006 eV. It is estimated that clean cavities employing a cold beryllium reflector could have critical fuel density requirements about an order of magnitude less than those for cavities reflected by room temperature beryllium. A sketch of a test reactor configuration is shown in Fig. 25. A refrigeration cycle or low-temperature heat exchanger would be required to keep the beryllium very cold. The liner of the cavity would be constructed of a reflective material (aluminum, for example) such that less than ten percent of the incident radiant flux would be absorbed by the liner. For tests to demonstrate the heating of propellant, the cavity surface would be interrupted at discrete locations by axial propellant channels which might cover 10 to 25 percent of the cavity surface. The reflecting liners would serve to focus the radiant heat flux onto the propellant channels. The propellant channels would be isolated from the fuel region by segments of internally-cooled transparent walls such as those employed in the nuclear light bulb test configuration with the propellant heating option shown in Fig. 7. For initial experiments, the propellant heating channels could be omitted and the entire vortex region could be surrounded by the reflective aluminum liner. The major components of the system are shown in Fig. 25, including the low-temperature heat exchanger or refrigeration system for the cold beryllium reflector.

A figure of merit for the performance of a reflector-moderator material used for cavity reactors is the ratio of the square root of the age of fission neutrons

divided by the thermal neutron mean-free-path, $\sqrt{\tau} / \lambda_{tr}$ (see Ref. 32). Table XII contains a comparison of this fighre of merit for several moderator materials. It can be seen that cold beryllium with large transport mean-free-paths at low thermal neutron energies would be an excellent reflector-moderator for reducing critical fuel density. The leakage of thermal neutrons from the outside of such a reflector would be very large unless the reflector material is backed by a good thermal neutron scattering material. Deuterium compounds such as frozen heavy water or deuterium-carbide would be a good choice for the outer reflector material depicted in Fig. 25.

Preliminary Multigroup Criticality Calculations

Multigroup neutron transport theory calculations were performed for a spherical cavity reactor with a combined beryllium and deuterium-carbide reflector surrounding spherical cavity equal in volume to the cavity size of a nuclear light bulb reference engine unit cell. The neutron energy group structure employed for these calculations is shown in Table XIII. The cold beryllium scattering cross sections were taken from Ref. 38. For purposes of determining scattering cross sections below 0.006 at temperatures other than those presented in Ref. 33 it was assumed the inelastic scattering cross section varied as T^2. This temperature dependent variation in the inelastic scattering cross section was taken from the analyses of Ref. 34.

The critical mass requirements for the spherical cavity configuration, were 1.15 kg of U-233 and 1.44 kg for U-235. The temperatures of the beryllium and deuterium carbide reflector zones were 40°K. It was assumed that the operating pressure in the cavity was 250 atm. Argon buffer gas at 250 atm was in the zone between the reflective liner and the fuel cloud. The coolant for the cold beryllium and the deuterium carbide region was deuterium gas occupying 10 percent of the reflector moderator volume. The deuterium gas can be cooled externally in a refrigeration system or, as an alternative in a cryogenic heat exchanger. Using a reflectivity of 0.9 for the liner material, and requiring that the outward-directed radiant flux be equal to that of the nuclear light bulb engine, the curves of Ref. 23 were used to determine the uranium partial pressure corresponding to the critical fuel density necessary to produce the outward-directed thermal radiation flux. The pressure was 60 atm. Assuming that the uranium is approximately singly ionized in the fuel region, that would correspond to a pressure of 30 atm of uranium nuclei. If the injection fuel form were UF_6, the pressure due to fluorine nuclei would be on the order of 180 atm, thereby requiring a combined uranium, uranium electrons, and fluorine carrier gas pressure on the order of 240 atm. Thus, it appears feasible that a self-critical cavity reactor test bed could be fabricated in the geometry and configuration discussed above and operated at approximately 250 atm.

Further calculations should be performed at temperatures lower than 40°K to increase the fraction of thermal neutrons below the 0.006 scattering cutoff for the beryllium. Operating the reflector at an even colder temperature should result in further reductions in critical mass. An additional calculation was performed with the beryllium and deuterium carbide at room temperature. The critical mass increased by a factor of approximately 4. Thus, the cavity assembly described above has very large negative temperature reactivity coefficient, indicating a relatively stable and safe configuration for damping out possible power excursions.

REFERENCES

1. McLafferty, G. H. and H. E. Bauer: Studies of Specific Nuclear Light Bulb and Open-Cycle Gaseous Nuclear Rocket Engines. United Aircraft Research Laboratories Report G-910093-37, prepared under Contract NASw-847, September, 1967. Also issued as NASA CR-1030.

2. Kendall, J. S.: Investigation of Gaseous Nuclear Rocket Technology--Summary Technical Report. United Aircraft Research Laboratories Report L-910905-13, prepared under Contract SNPC-70, September, 1972.

3. Roman, W. C. and J. F. Jaminet: Development of RF Plasma Simulations of In-Reactor Tests of Small Models of the Nuclear Light Bulb Fuel Region. United Aircraft Research Laboratories Report L-910900-12, prepared under Contract SNPC-70, September, 1972.

4. Klein, J. F.: Nuclear Light Bulb Propellant Heating Simulation Using a Tungsten-Particle/Argon Aerosol and Radiation from a DC Arc Surrounded by a Segmented Mirror Cavity. United Aircraft Research Laboratories Report L-910900-13, prepared under Contract SNPC-70, September, 1972.

5. Latham, T. S. and H. E. Bauer: Analytical Studies of In-Reactor Tests of a Nuclear Light Bulb Unit Cell. United Aircraft Research Laboratories Report J-910900-6, prepared under Contract SNPC-70, September, 1970. Also issued as NASA CR-111098.

6. Latham, T. S. and H. E. Bauer: Analytical Design Studies of In-Reactor Tests of a Nuclear Light Bulb Unit Cell. United Aircraft Research Laboratories Report K-910900-11, prepared under Contract SNPC-70, September, 1971.

7. Anon.: Nuclear Safety Analysis Report, Part II, Testing Operation. Los Alamos Scientific Laboratory Report N-DOT-063-71, November, 1971.

8. Jaminet, J. F.: Development of a Model and Test Equipment for Cold-Flow Tests at 500 Atm of Small Nuclear Light Bulb Configurations. United Aircraft Research Laboratories Report L-910900-14, prepared under Contract SNPC-70, September, 1972.

9. Mensing, A. E. and J. F. Jaminet: Experimental Investigations of Heavy-Gas Containment in R-F Heated and Unheated Two-Component Vortexes. United Aircraft Research Laboratories Report H-910091-20, prepared under Contract NASw-847, September 1969.

REFERENCES (Continued)

10. Jaminet, J. F. and A. E. Mensing: Experimental Investigation of Simulated-Fuel Containment in R-F Heated and Unheated Two-Component Vortexes. United Aircraft Research Laboratories Report J-910900-2, September, 1970. Also issued as NASA CR-111101.

11. Kendall, J. S.: Experimental Investigation of Containment in Constant-Temperature Radial-Inflow Vortexes. United Aircraft Research Laboratories Report F-910091-15, prepared under Contract NASw-847, September, 1967. Also issued as NASA CR-1029.

12. Rodgers, R. J., T. S. Latham and H. E. Bauer: Analytical Studies of Nuclear Light Bulb Engine Radiant Heat Transfer and Performance Characteristics. United Aircraft Research Laboratories Report K-910900-10, prepared under Contract SNPC-70, September, 1971.

13. Rodgers, R. J. and T. S. Latham: Analytical Design and Performance Studies of the Nuclear Light Bulb Engine. United Aircraft Research Laboratories Report L-910900-16, prepared under Contract SNPC-70, September, 1972.

14. Travers, A.: Experimental Investigation of Radial-Inflow Vortexes in Jet-Injection and Rotating-Peripheral-Wall Water Vortex Tubes. United Aircraft Research Laboratories Report F-910091-14, prepared under Contract NASw-847, September, 1967.

15. Anderson, O.: Theoretical Effect of Mach Number and Temperature Gradient on Primary and Secondary Flows in a Jet-Driven Vortex. Air Force Systems Command Report RTD-TDR-63-1098, prepared by United Aircraft Research Laboratories under Contract AF 04(611)-8189, November 1963.

16. Krascella, N. L.: Theoretical Investigation of the Spectral Opacities of Hydrogen and Nuclear Fuel. Air Force Systems Command Report RTD-TDR-63-1101 prepared by UARL, November, 1963.

17. Krascella, N. L.: Spectral Absorption Coefficients of Argon and Silicon and Spectral Reflectivity of Aluminum. United Aircraft Research Laboratories Report L-910904-3, prepared under Contract SNPC-70, September, 1972.

18. Engle, W. W.: A Users Manual for ANISN, A One-Dimensional Discrete Ordinates Transport Code with Anisotropic Scattering. Union Carbide Nuclear Corporation Division Report K-1693, March 30, 1967.

REFERENCES (Continued)

19. Kinney, R. B.: Theoretical Effect of Seed Opacity and Turbulence on Temperature Distributions in the Propellant Region of a Vortex-Stabilized Gaseous Nuclear Rocket. United Aircraft Research Laboratories Report E-910092-8, prepared under Contract NASw-847, September, 1966. Also issued as NASA CR-694.

20. Clark, J.W., B.V. Johnson, J.S. Kendall, A.E. Mensing and A. Travers: Open-Cycle and Light-Bulb Types of Vortex-Stabilized Gaseous Nuclear Rockets. J. Spacecraft Rockets, vol.5, no.8, August 1968, pp. 941-947.

21. Vogt, P. G.: Development and Tests of Small Fused Silica Models of Transparent Walls for the Nuclear Light Bulb Engine. United Aircraft Research Laboratories Report J-910900-3, prepared under Contract SNPC-70, September, 1970. Also issued as NASA CR-111100.

22. Kendall, J. S. and R. C. Stoeffler: Conceptual Design Studies and Experiments Related to Cavity Exhaust Systems for Nuclear Light Bulb Configurations. United Aircraft Research Laboratories Report L-910900-15, prepared under Contract SNPC-70, September, 1972.

23. Kesten, A. S. and N. L. Krascella: Theoretical Investigation of Radiant Heat Transfer in the Fuel Region of a Gaseous Nuclear Rocket Engine. United Aircraft Research Laboratories Report E-910092-9, prepared under Contract NASw-847, September, 1966. Also issued as NASA CR-695.

24. Klein, J. F.: Experiments to Simulate Heating of Propellant by Thermal Radiation in a Nuclear Light Bulb Engine. United Aircraft Research Laboratories Report K-910900-8, prepared under Contract SNPC-70, September, 1971.

25. Latham, T. S.: Nuclear Studies of the Nuclear Light Bulb Rocket Engine. United Aircraft Research Laboratories Report G-910375-3, prepared under Contract NASw-847, September, 1968. Also issued as NASA CR-1315.

26. Palma, G. E.: Measurements of the UV and VUV Transmission of Optical Materials During High-Energy Electron Irradiation. United Aircraft Research Laboratories Report L-990929-3, prepared under Contract SNPC-70, September, 1972.

27. Roman, W. C. and J. F. Jaminet: Experimental Investigations to Simulate the Thermal Environment and Fuel Region in Nuclear Light Bulb Reactors Using an R-F Radiant Energy Source. United Aircraft Research Laboratories Report K-910900-7, prepared under Contract SNPC-70, September, 1971.

REFERENCES (Continued)

28. Bauer, H. E.: Initial Experiments to Investigate the Condensation of Flowing Metal Vapor/Heated-Gas Mixtures in a Duct. United Aircraft Research Laboratories Report K-910900-9, prepared under Contract SNPC-70, September, 1971.

29. Cheverton, R. D. and T. M. Sims: HFIR Core Nuclear Design. Oak Ridge National Laboratory Report ORNL-4621, July, 1971.

30. King, L. D. P.: Status of Work Related to the King Reactor as of March, 1972. Los Alamos Scientific Laboratory Report LA-492C-MS, August, 1972.

31. Latham, T. S.: Nuclear Criticality of a Specific Vortex-Stabilized Gaseous Nuclear Rocket Engine. United Aircraft Research Laboratories Report E-910375-1, prepared under Contract SNPC-70, October, 1966. Also issued as NASA CR-697.

32. Safonov, G.: Externally Moderated Reactors. Rand Corporation Report R-316, July, 1957.

33. Hughes, D. J. and R. B. Schwartz: Neutron Cross Sections. Second Edition, Brookhaven National Laboratory Report BNL-325, July, 1960.

34. Weinstock, R.: Inelastic Scattering of Slow Neutrons. Physical Review, Second Series, vol. 65, nos. 1 and 2, January, 1944, pp. 1-20.

LIST OF SYMBOLS

C_τ	Ratio of fuel to buffer-gas residence times, dimensionless
$\dot{D}$	Dose rate of nuclear radiation in transparent wall, Mrad/sec
K_F	Density containment factor, dimensionless
M_F	Fuel loading, g
P	Operating pressure, atm
P_A	Argon partial pressure, atm
P_U	Uranium partial pressure, atm
Q_{COND}	Energy conducted in buffer region, kW
Q_{CONV}	Energy convected by buffer gas, kW
Q'''_{CONV}	Volumetric convection energy in buffer region, kW/cm^3
Q_F	Specific fission power, kW/g of U-235
Q_R	Power radiated, kW
q_L	Net heat flux at reflective aluminum wall, erg/cm^2-sec
q_L^+	Heat flux directed radially outward at reflective aluminum wall, erg/cm^2-sec
q_L^-	Heat flux directed radially inward at reflective aluminum wall, erg/cm^2-sec
q_{TW}	Total heat flux through transparent wall, kW/cm^2
q_6	Net heat flux at nominal edge-of-fuel location, erg/cm^2-sec
q_6^+	Heat flux directed radially outward at nominal edge-of-fuel location, erg/cm^2-sec
q_6^-	Heat flux directed radially inward at nominal edge-of-fuel location, erg/cm^2-sec
q_ω	Spectral heat flux at reflective aluminum wall, erg/cm^2-sec

LIST OF SYMBOLS (Continued)

$\mathcal{R}$	Aluminum spectral-heat-flux-weighted reflectivity, dimensionless
$\mathcal{R}_{EFF}$	Effective reflectivity at edge of fuel, dimensionless
$\mathcal{R}_{\omega}$	Aluminum spectral reflectivity, dimensionless
R	Radius, cm
R_F	Radius of edge-of-fuel location, cm
R_T	Radius of reflective aluminum wall, cm
R_1	Radius of inside boundary of region of analysis, cm
Ri	Richardson number, dimensionless
T	Temperature, °K
T*	Equivalent blackbody radiating temperature, °K
T_P	Propellant bulk exit temperature, °K
T_6^*	Equivalent blackbody radiating temperature corresponding to q_6^+, °K
t	Time, sec
t_A	Time after Nuclear Furnace reaches steady-state power level, min
V(R)	Volume within radius R, cm^3
$V(R_{AL})$	Volume within reflective aluminum wall, cm^3
V_Z	Buffer gas axial velocity, cm/sec
V_{ϕ_1}	Average tangential velocity at aluminum reflecting wall, cm/sec
W_{BR}	Buffer gas radial weight flow rate, g/sec
W_F	Fuel weight flow rate, g/sec
α_{ω}	Spectral absorption coefficient, cm^{-1}
λ	Wavelength, μ

LIST OF SYMBOLS (Continued)

λ_{tr}	Transport mean free path, cm
ρ	Density, gm/cm^3
ρ_A	Argon density, g/cm^3
ρ_{B6}	Buffer-gas density at edge-of-fuel location, g/cm^3
$\bar{\rho}_{F6}$	Average fuel density based on volume within edge-of-fuel location, g/cm^3
ρ_U	Uranium density, g/cm^3
τ	Neutron age, cm^2
τ_B	Buffer-gas residence time in cavity, sec
τ_F	Average fuel residence time in cavity, sec
ϕ	Angle of incident radiation to vector normal to reflecting surface, degrees
ω	Wave number, cm^{-1}

TABLE I

UNIT CELL DIMENSIONS AND MATERIAL SPECIFICATIONS FOR
FIBERGLASS AND ALUMINUM PRESSURE VESSEL

Schematic Diagram of Unit Cell Shown in Figs. 4 and 5

Region	Material	i.d., cm	o.d., cm	Thickness, cm
Midplane Cross Section for Fiberglass Pressure Vessel				
Fuel	U-235 or Pu-239 and Argon	--	3.96	--
Buffer Gas	Argon	3.96	6.60	1.32
Reflective Aluminum Liner	Aluminum	6.60	6.85	0.125
Liner Coolant	Argon or Hydrogen	6.85	7.21	0.18
Pressure Vessel Liner	Aluminum	7.21	7.36	0.075
Fiberglass Pressure Vessel	Fiberglass Composite	7.36	8.13	0.385
Midplane Cross Section for Aluminum Pressure Vessel				
Fuel	U-235 or Pu-239 and Argon	--	3.80	--
Buffer Gas	Argon	3.80	6.35	1.28
Reflective Aluminum Liner	Aluminum	6.35	6.60	0.125
Liner Coolant	Argon or Hydrogen	6.60	6.96	0.18
Aluminum Pressure Vessel	Aluminum	6.96	8.13	0.584
Cross Section at Inlet End of Fuel Injection Plane for Both Pressure Vessel Configurations				
Fuel Injector	Boral	0.031	0.092	0.030
Thru-Flow Duct	Fuel and Argon	0.092	1.00	0.454
Thru-Flow Duct Wall	Stainless Steel	1.000	1.27	0.135
Bypass and End-Wall Coolant	Argon or Hydrogen	1.27	2.05	0.39
Bypass Duct Wall	Stainless Steel	2.05	2.25	0.10

Note: Remaining dimensions from reflective aluminum liner out to pressure vessel o.d. same as in midplane cross section.

TABLE II

TEMPERATURES AND PRESSURES IN NUCLEAR FURNACE IN-REACTOR TEST CELL

Fiberglass Pressure Vessel

See Fig.18 for Locations of Station Numbers and Coolant Flow Rates

Location of Temperature and Pressure	Station Number	Temperature, °K				Pressure Relative to 500 atm, atm			
		Argon Liner Coolant		Hydrogen Liner Coolant		Argon Liner Coolant		Hydrogen Liner Coolant	
		Fuel	No Fuel	Fuel	No Fuel	Fuel	No Fuel	Fuel	No Fuel
Fuel Inlet	1	555	-	555	-				
Coolant Inlet and Buffer Gas Inlet	2	278	278	278	278	0.0	0.0	+0.0	+0.0
Upper End-Wall and Liner Coolant Inlet	3	288	287	284	284	-5.64	-5.64	-0.138	-0.138
Upper End-Wall Max. Surface Temp.	4	537	298	503	293				
Upper End-Wall Coolant Outlet	5	302	288	295	284				
Liner Max. Surface Temp. (Fuel)	6	519		553					
Liner Max. Surface Temp. (No Fuel)	7		307		304				
Lower End-Wall Coolant Outlet	8	332	293	339	288	-6.72	-6.65	-0.159	-0.157
Lower End-Wall Max. Surface Temp.	9	588	304	556	293				
Lower End-Wall Coolant Outlet	10	347	294	350	288				
Liner Coolant Outlet	11	341	303	348	290	-7.70	-7.51	-0.169	-0.165
Pressure Vessel Outside Coolant Outlet	12	281	281	281	280				

TABLE II (Continued)

TEMPERATURES AND PRESSURES IN NUCLEAR FURNACE IN-REACTOR TEST CELL

Fiberglass Pressure Vessel

See Fig.18 for Locations of Station Numbers and Coolant Flow Rates

Location of Temperature and Pressure	Station Number	Temperature, °K				Pressure Relative to 500 atm, atm			
		Argon Liner Coolant		Hydrogen Liner Coolant		Argon Liner Coolant		Hydrogen Liner Coolant	
		Fuel	No Fuel	Fuel	No Fuel	Fuel	No Fuel	Fuel	No Fuel
Pressure Vessel Max. Temp.	13	412	390	418	390				
Mixed-Mean, Entrance Upper Exhaust Duct*	14	349	314	330	304	-7.10	-7.05	-0.211	-0.209
Mixed-Mean, Entrance Lower Exhaust Duct*	15	392	319	383	308	-8.41	-8.08	-0.253	-0.229
Mixed-Mean, Outlet Upper Exhaust Duct	16	354	319	331	305	-9.72	-9.25	-0.395	-0.371
Mixed-Mean, Outlet Lower Exhaust Duct	17	395	322	384	308	-9.54	-9.01	-0.342	-0.293
Upper Exhaust Duct Max. Surface Temp.	18	367	331	342	315				
Lower Exhaust Duct Max. Surface Temp.	19	411	337	395	319				

* After addition of end-wall coolant flow to exhaust duct.

TABLE III

TEMPERATURES AND PRESSURES IN NUCLEAR FURNACE IN-REACTOR TEST CELL

Aluminum Pressure Vessel

See Fig. 18 for Locations of Station Numbers and Coolant Flow Rates

Location of Temperature and Pressure	Station Number	Temperature, °K				Pressure Relative to 500 atm, atm			
		Argon Liner Coolant		Hydrogen Liner Coolant		Argon Liner Coolant		Hydrogen Liner Coolant	
		Fuel	No Fuel	Fuel	No Fuel	Fuel	No Fuel	Fuel	No Fuel
Fuel Inlet	1	555		555					
Coolant Inlet and Buffer Gas Inlet	2	278	278	278	278	0.0	0.0	+0.0	+0.0
Upper End-Wall and Liner Coolant Inlet	3	286	286	283	283	-6.01	-6.01	-0.147	-0.147
Upper End-Wall Max. Surface Temp	4	532	297	499	293				
Upper End-Wall Coolant Outlet	5	300	287	293	284				
Liner Max Surface Temp (Fuel)	6	501		534					
Liner Max. Surface Temp (No Fuel)	7		301		299				
Lower End-Wall Coolant Inlet	8	326	290	332	286	-7.15	-7.08	-0.169	-0.167
Lower End-Wall Max Surface Temp	9	577	301	546	296				
Lower End-Wall Coolant Outlet	10	340	291	342	287				
Liner Coolant Outlet	11	332	297	336	292	-8.17	-7.99	-0.180	-0.176
Pressure Vessel Outside Coolant Outlet	12	290	290	290	289				
Pressure Vessel Max. Temp.	20	336	292	332	297				
Mixed-Mean, Entrance Upper Exhaust Duct *	14	343	312	326	302	-7.76	-7.69	-0.235	-0.232

TABLE III (Continued)

Location of Temperature and Pressure	Station Number	Temperature, °K				Pressure Relative to 500 atm, atm			
		Argon Liner Coolant		Hydrogen Liner Coolant		Argon Liner Coolant		Hydrogen Liner Coolant	
		Fuel	No Fuel	Fuel	No Fuel	Fuel	No Fuel	Fuel	No Fuel
Mixed-Mean, Entrance									
Lower Exhaust Duct *	15	382	316	373	306	-9.14	-8.79	-0.268	-0.253
Mixed-Mean, Outlet Upper Exhaust Duct	16	348	317	327	303	-10.33	-10.02	-0.411	-0.315
Mixed Mean, Outlet Lower Exhaust Duct	17	385	319	374	306	-10.24	-9.67	-0.351	-0.315
Upper Exhaust Duct Max. Surface Temp	18	361	329	337	314				
Lower Exhaust Duct Max. Surface Temp	19	400	333	384	317				

* After addition of end-wall coolant flow to exhaust duct.

TABLE IV

PERFORMANCE LEVELS FOR IN-REACTOR TEST

Specifications for Unit Cell Given in Table I and Figs. 4 and 5

Operating Pressure, P = 500 atm

Argon Buffer Gas, U-235 Fuel

$R_F/R_T = 0.6$, $\tau_F/\tau_B = 1.0$

	Results From Reference 3	Results From Present Study
Specific Fission Power, Q_F - kW/g of U-235	30.5	30.5
Fuel Loading, M_F - g	6.22	6.22
Total Power, Q_T - kW	190	190
Power Radiated, Q_R - kW	173.4	174
Aluminum Liner Spectral-Heat-Flux-Weighted Reflectivity, $\mathcal{R}$	0.9	0.908
Aluminum Liner Effective Reflectivity, $\mathcal{R}_{EFF}$	0.9	0.855
Equivalent Fuel Region Surface Radiation Temperature, T_6^* - °K	5940	5426
Outward Directed Fuel Region Surface Heat Flux, q_6^+ - kW/CM^2	7.1	4.84
Equivalent Fuel Region Black-Body Radiation Temperature, T^* - °K	3330	3330

(Continued)

TABLE IV (Concluded)

	Results From Reference 3	Results From Present Study
Net Fuel Region Surface Heat Flux, q_6 - kW/cm^2	0.71	0.71
Edge-Of-Fuel Temperature, T_6 - °K	5940	5130
Average Fuel Density for Volume Inside R_F, $\bar{\rho}_{F6}$ - g/cm^3	0.0284	0.0284
Density Containment Factor, $K_F = \bar{\rho}_{F6}/\rho_{B6}$	0.7	0.6
Average Fuel Partial Pressure for Volume Inside R_F, $\bar{P}_{F6}$ - atm	195	125
Fuel Partial Pressure Ratio, $\bar{P}_{F6}/P$	0.39	0.25

TABLE V

SUMMARY OF HEAT BALANCE IN CAVITY REGION OF IN-REACTOR TEST UNIT CELL

Specifications For Unit Cell Given in Table I and Figs. 4 and 5

Fuel Flow Rate, g/sec	1.6
Fuel Injection Temperature, °K	555
Average Fuel Temperature Rise, °K	9886
Net Energy Deposition Rate in Fuel, kW	6.6
Carrier and Buffer Gas Flow Rate in Fuel Region, g/sec	0.44
Carrier and Buffer Gas Injection Temperature, °K	555
Average Carrier and Buffer Gas Temperature Rise, °K	8591
Net Energy Deposition Rate in Carrier and Buffer Gas in Fuel Region, kW	2.0
Argon Buffer Gas Flow Rate, g/sec	39.7
Argon Buffer Gas Injection Temperature, °K	555
Energy Deposition Rate in Buffer Gas by Heat Conduction and Thermal Radiation from Fuel Region, kW	5.7
Energy Deposition Rate in Buffer Gas by Neutrons and Gamma Rays from Nuclear Furnace, kW	4.3
Average Buffer Gas Temperature Rise, °K	482
Net Energy Deposition Rate in Buffer Gas, kW	10.0
Thermal Radiation Heat Flow to End wall, kW	26.4
Thermal Radiation Heat Flow to Liner, kW	147
Total Rate of Energy Deposition in Test Cell, kW	190.0
Rate of Energy Deposition by Thermal Radiation, kW	174.0
Ratio of Thermal Radiation Energy Deposition Rate to Total Rate of Energy Deposition	0.915

TABLE VI

FUEL AND BUFFER-GAS FLOW CONDITIONS FOR IN-REACTOR TESTS

Specifications for Unit Cell Given in Table I and Figs. 4 and 5

Mass of Fuel in Cavity, g	6.22
Fuel Flow Rate Per Injector Tube, g/sec	0.80
Argon Carrier Gas Flow Rate Per Injector Tube, g/sec	0.133
Fluorine Carrier Gas Flow Rate Per Injector Tube, g/sec	0.182
Fission Heating Rate in Fuel, kW/g	30.5
Fission Heating Rate in Fuel In Poison Shrouded Injectors, kW/g	2.0
Fuel Inlet Temperature, Argon Carrier Gas, °K	350
Fuel Inlet Temperature, UF_6 - Particle Slurry, °K	350
Fuel Injection Temperature, Argon Carrier Gas, °K	555
Fuel Injection Temperature, UF_6 - Particle Slurry, °K	555
Argon Buffer - Gas Flow Rate, g/sec	39.7
Argon Buffer - Gas Injection Temperature, °K	555
Argon Buffer - Gas Manifold Injection Area, cm^2	0.782
Argon Buffer - Gas Injection Velocity, cm/sec	107
Mixed-Mean Temperature of Fuel and Buffer - Gas Mixture Exiting Cavity, °K	1432

TABLE VII

SEQUENCE OF EVENTS FOR REFERENCE IN-REACTOR TEST

t_A = Time in Minutes After Nuclear Furnace Reaches Steady-State Power Level

t_A = 0 to t_A = 1 min
1. Flow hydrogen from Nuclear Furnace supply system through test region to bring components to thermal equilibrium.
t_A = 1 min to t_A = 2.5 min
1. Pressurize test region to operating level (500 atm).
2. Start high-pressure buffer-gas and coolant flow.
t_A = 2.5 min to t_A = 3.5 min
1. Start injection of liquid UF_6.
t_A = 3.5 min to t_A = 4 min
1. Add particles of uranium to UF_6 to increase uranium partial pressure or commence uranium particle-argon carrier gas fuel injection.
t_A = 4 min to t_A = 7 min
1. Full-power, steady-state operation.
2. Measure flows, temperatures and record spectral emission data.
t_A = 7 min to t_A = 8 min
1. Shut off fuel injection flow.
2. Purge fuel injection lines with argon.
t_A = 8 min to t_A = 9 min
1. Depressurize unit to Nuclear Furnace level.
2. Switch over to cooling with hydrogen from Nuclear Furnace supply system.
t_A = 9 min to t_A = 10 min
1. Shut down Nuclear Furnace.

TABLE VIII

TOTAL WEIGHT OF MATERIAL EXPENDED DURING EACH TEST RUN

Test Time = 10 min

Test Sequence Described in Table VII

Material Flow Rates Given in Tables V and VI

Flow Circuit	Total Weight - g
Nuclear Furnace Hydrogen	3.00×10^5
Argon Buffer Gas	1.91×10^4
Liner and End-Wall Coolant, Argon	4.36×10^6
Liner and End-Wall Coolant, Hydrogen	1.44×10^5
U-235 Fuel (Uranium in UF_6 and Particles)	3.90×10^2
Argon Carrier Gas for UF_6-Argon System	5.71×10^2
Fluorine Contained in UF_6 doe UF_6-Argon System	2.60×10^1
Fluorine Contained in UF_6 for All-UF_6 System	2.98×10^2

TABLE IX

PERFORMANCE LEVELS FOR PROPELLANT HEATING AND TRANSPARENT-WALL IN-REACTOR TEST

Geometry and Dimensions of Unit Cell With Propellant Heating Channel Shown in Fig. 7

Operating Pressure = 500 atm

Argon Buffer Gas, U-235 Fuel

$R_F/R_T = 0.6$, $\tau_F/\tau_B = 1.0$, $K_F = 0.6$

Specific Fission Power, Q_F-kW/g of U-235	30.5
Fuel Loading, M_F-g	3.7
Total Power, Q_T-kW	131
Power Radiated, Q_R-kW	120
Aluminum Liner Spectral-Heat-Flux-Weighted Reflectivity, $\mathcal{R}$	0.908
Effective Reflectivity, $\mathcal{R}_{EFF}$	0.728
Equivalent Fuel Region Surface Radiating Temperature, T_6^*-°K	4611
Outward Directed Fuel Region Surface Heat Flux, q_6^+-kW/cm^2	2.61
Equivalent Fuel Region Black-Body Radiating Temperature, T*-°K	3330
Net Fuel Region Surface Heat Flux, q_6-kW/cm^2	0.71
Total Heat Flux Through Transparent Wall (No Seeded Propellant in Duct), Outward Directed Plus Reflected, q_{TW}-kW/cm^2	8.83*
Nuclear Radiation Dose Rate in Transparent Wall, $\dot{D}$-MR/sec	3.0
Range of Propellant Bulk Exit Temperatures, T_P-°K	3300-3700

*In this case, $\mathcal{R}_{EFF}$ is increased to 0.855 and $q_6^+ = 4.9$ kW/cm^2 because there is no seeded propellant in the duct.

TABLE X

PRINCIPAL CHARACTERISTICS OF CANDIDATE TEST REACTORS FOR NUCLEAR LIGHT BULB IN-REACTOR TESTS

Nuclear Furnace (NF)
Fissioning Uranium Plasma Facility (FUPF)
High Flux Isotope Reactor (HFIR)
Kinetic Intense Neutron Generator (KING)
Self-Critical Cavity (SCC)

Principal Characteristics

Reactor	Flux Trap Diameter, cm	Specific Fission Rate, kW/g U-235	Turn-Around Time Per Test	Test Time Per Core
NF	8.4	26-40	~30 da	3-5 hr
FUPF	28.2	7-15	~30 da	mo.-yr
HFIR	8.4	70	1-5 da	23 da
KING	8.4	130-390	1-5 da	mo.-yr
SCC	24.4-48.8	---	~30 da	mo.-yr

TABLE XI

DESIGN AND OPERATIONAL STATUS OF CANDIDATE TEST REACTORS

Reactor	Design Completed	Period of Operation	Access for GNR Tests	Scrubber Available	Site Developed	Investment for Initial Tests	Capacity for Full-Scale Tests
Nuclear Furnace	Yes	1972	Good	Yes	Yes	Low	No
Lewis Test Reactor	No	1976	Good	Yes	No*	High	No
High Flux Isotope Reactor	Yes	1965	Fair	No	Yes	Medium	No
Kinetic Intense Neutron Generator	No	1976	Good	Yes	No*	Medium	No
Self-Critical Cavity	No	1978	Good	Yes	No*	High	Yes

*Could be operated at NRDS.

TABLE XII

VARIATION OF CAVITY REACTOR CRITICAL FUEL DENSITY
WITH REFLECTOR-MODERATOR FIGURE-OF-MERIT

Data Taken From Ref. 32

Figure-of-Merit = $(\tau)^{\frac{1}{2}}/\lambda_{tr}$

Cavity Diameter = 1 m

Moderator Material	$(\tau)^{\frac{1}{2}}/\lambda_{tr}$, Dimensionless	U-235 Critical Density, Atoms/cm^3
Graphite (300°K)	7.25	1×10^{19}
Beryllium (300°K)	6.75	3.5×10^{18}
Heavy Water (300°K)	4.08	1.2×10^{18}
Beryllium (100°K)	0.47	$2.0\text{-}4.0 \times 10^{17}$*

*Extrapolated range of values.

TABLE XIII

NEUTRON ENERGY GROUP STRUCTURE USED FOR SELF-CRITICAL CAVITY TEST REACTOR CRITICAL MASS CALCULATIONS

Group Number	Upper Energy - ev	Lower Energy - ev
1	1.0×10^7	2.865×10^6
2	2.865×10^6	1.35×10^6
3	1.35×10^6	8.21×10^5
4	8.21×10^5	3.88×10^5
5	3.88×10^5	1.11×10^5
6	1.11×10^5	1.5×10^4
7	1.5×10^4	3.35×10^3
8	3.35×10^3	5.83×10^2
9	5.83×10^2	1.01×10^2
10	1.01×10^2	29.0
11	29.0	8.32
12	8.32	1.125
13	1.125	0.414
14	0.414	0.025
15	0.025	0.006
16	0.006	0.00175
17	0.00175	0.0

TABLE XIV

DIMENSIONS, TEMPERATURES AND COMPOSITIONS IN SPHERICAL CRITICALITY CALCULATIONS FOR SELF-CRITICAL CAVITY REACTOR WITH COLD BERYLLIUM REFLECTOR

Operating Pressure = 250 atm

Cavity Volume Equal to Volume of One Nuclear Light Bulb Unit Cell Cavity

See Fig. 25 For Sketch Reactor Configuration

U-233 Critical Mass = 1.15 kg

U-235 Critical Mass = 1.44 kg

Region	Inner Radius, cm	Outer Radius, cm	Temperature, °K	Material	Density, g/cm^3	Volume Fraction
Fuel	0.0	38.98	35,000	U-233 U-235 Argon	4.64×10^{-5} 5.80×10^{-5} 3.3×10^{-4}	-- -- --
Argon Buffer Gas	38.98	43.45	2,000	Argon	6.31×10^{-2}	1.0
Reflective Aluminum Liner	43.45	43.55	600	Aluminum	2.70	1.0
Argon Liner Coolant	43.44	45.49	600	Argon	0.210	1.0
Graphite Insulating Layer	45.49	45.99	300	Carbon	1.90	1.0
Cold Beryllium and D_2 Coolant	45.99	57.99	40	Beryllium Deuterium(D_2)	1.84 1.42	0.9 0.1
Cold Deuterium-Carbide and D_2 Coolant	57.99	105.99	40	Deuterium(D_2) Deuterium Carbide(C_xD_{2x})	1.42 0.97	0.1 0.9
D_2 Coolant Plenum	105.99	111.07	40	Deuterium(D_2)	1.42	1.0
Steel Pressure Vessel	111.07	116.15	300	Iron	7.70	1.0

FIG. 1

NUCLEAR FURNACE AXIAL VIEW

SKETCH TAKEN FROM REF. 7
POWER LEVEL = 44 - 66 MW

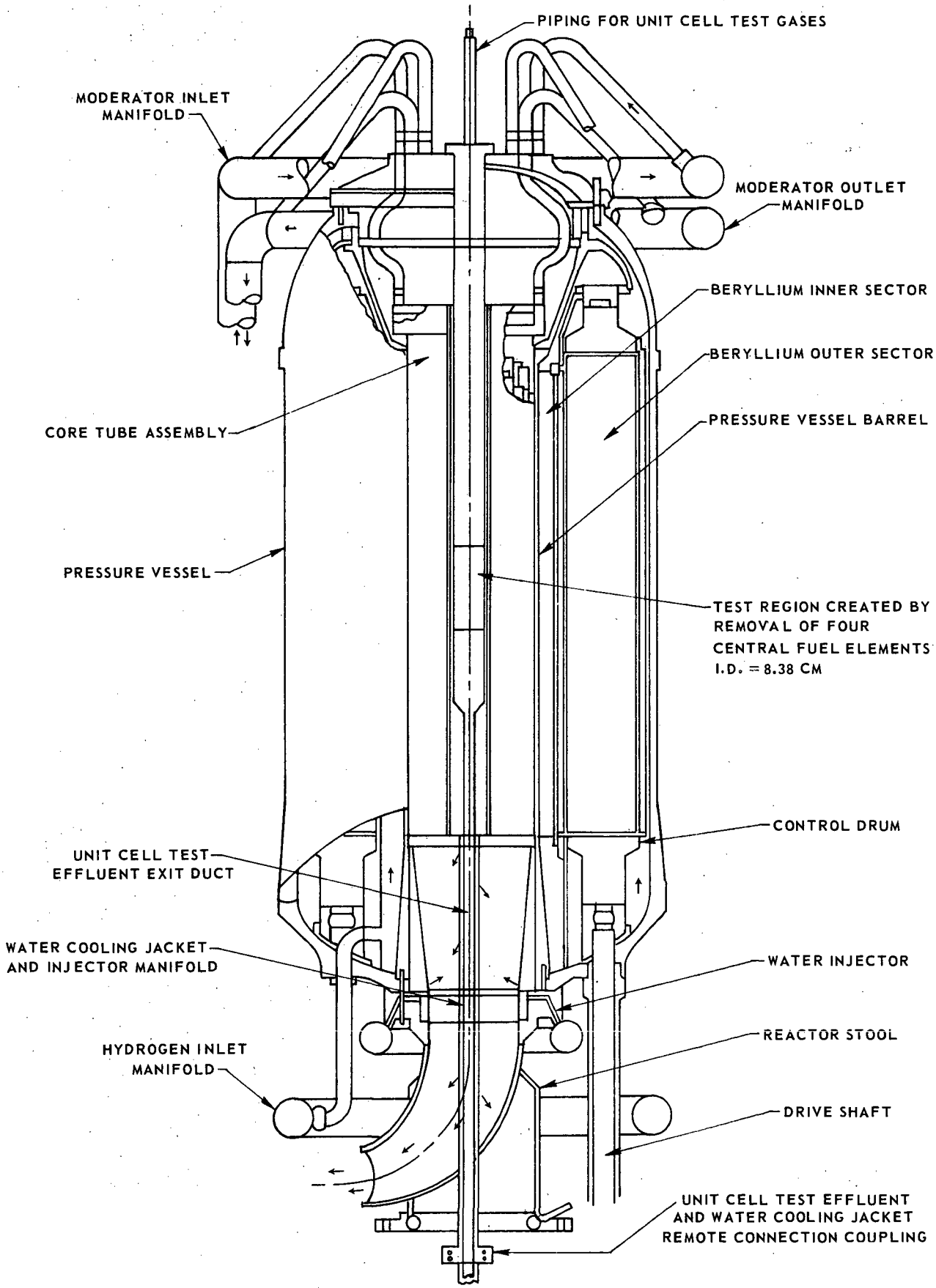

SCHEMATIC DIAGRAM OF PIPING AND ELECTRICAL CONNECTIONS TO TEST CELL

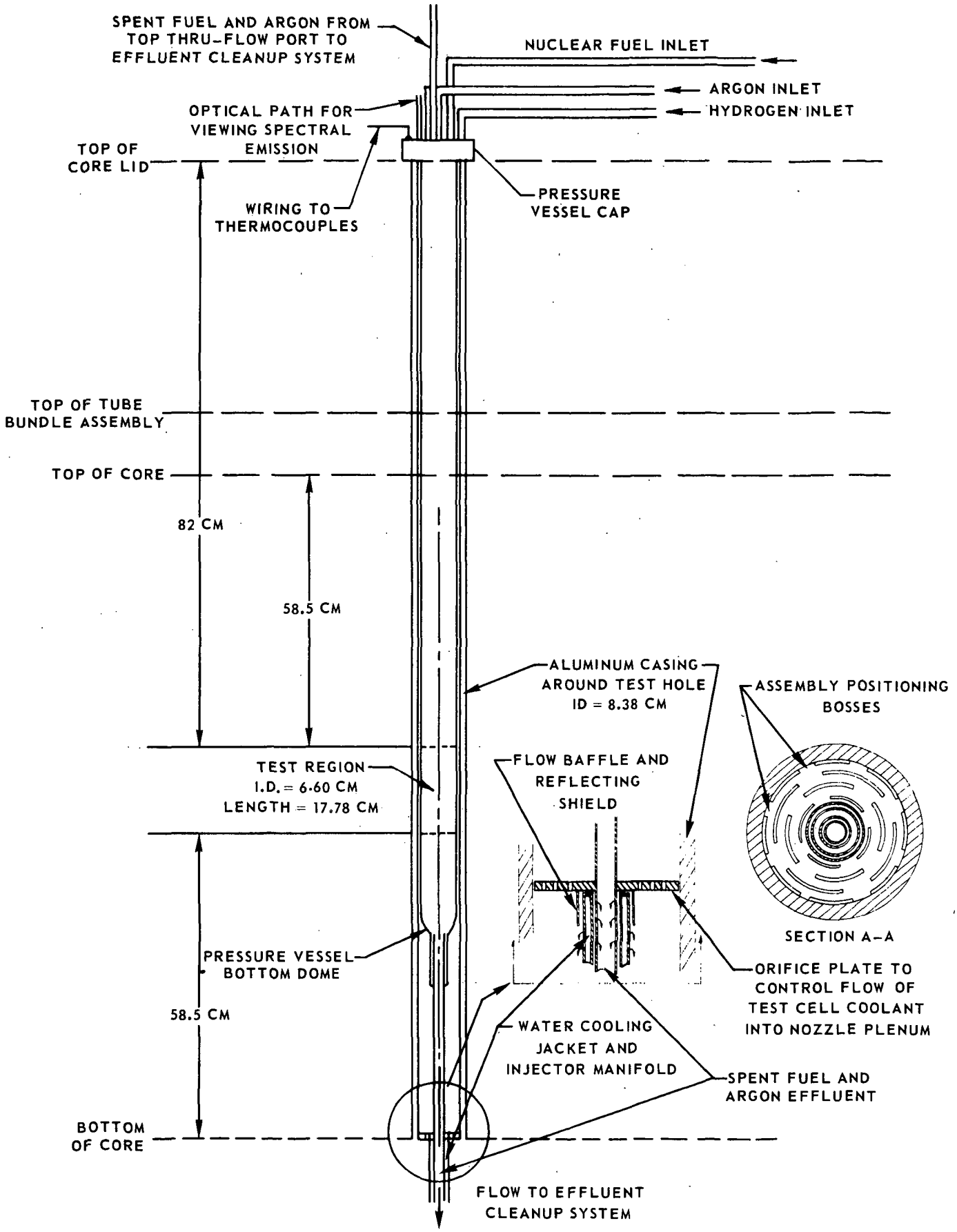

NUCLEAR FURNACE SHIELD

SKETCH TAKEN FROM REF. 7

CRANE CLEARANCE ABOVE SHIELD REQUIRED FOR INSERTION-EXTRACTION OF TEST ASSEMBLY = 3.0 M (TEST ASSEMBLY LENGTH OVERALL = 2.7M)

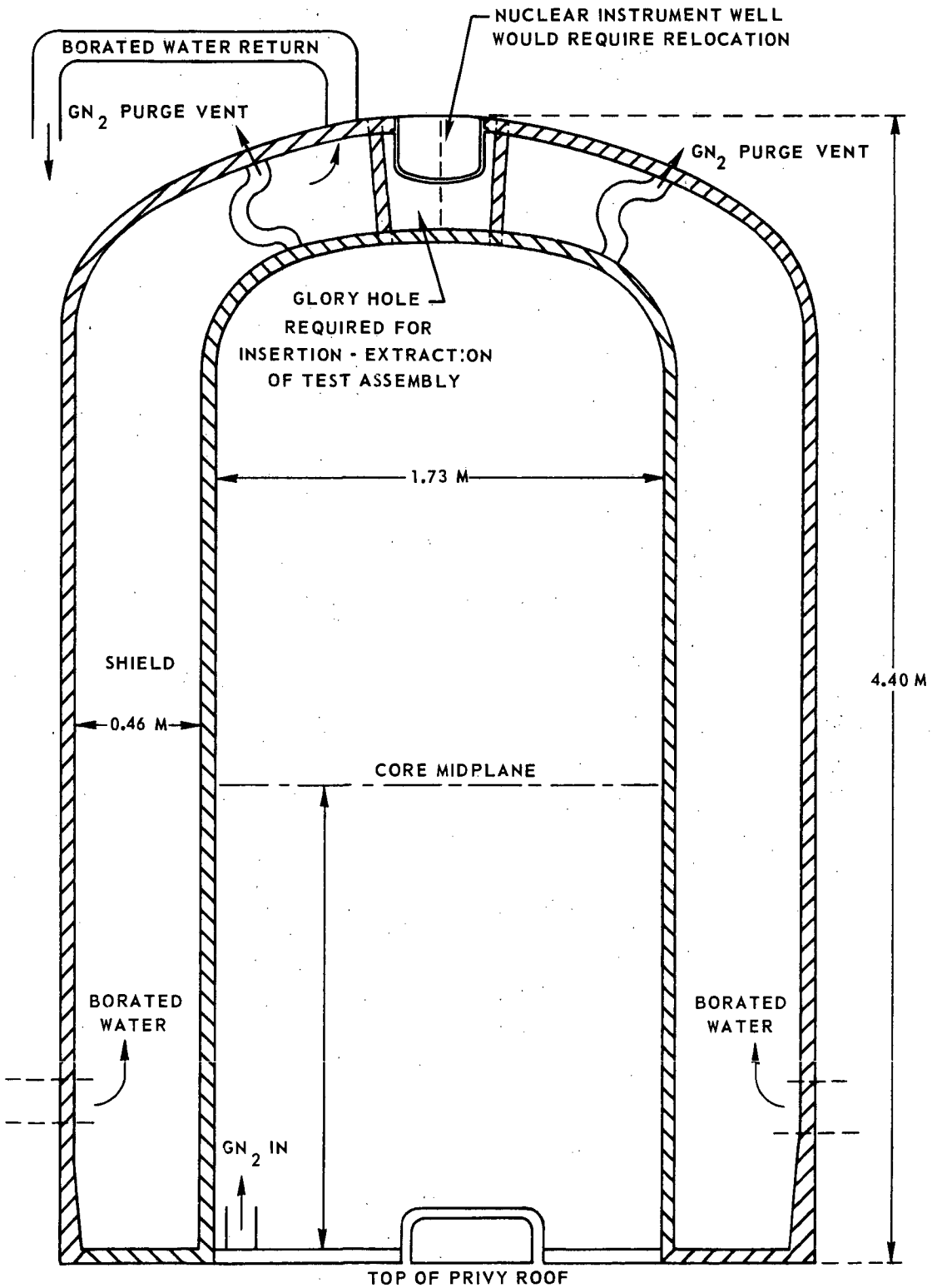

FIG. 4

PRELIMINARY LAYOUT OF IN-REACTOR TEST CELL

I.D. OF TEST HOLE CASING = 8.4 CM

DIMENSIONS OF CYLINDRICAL CAVITY REGION: 6.6-CM I.D. X 17.8-CM LONG

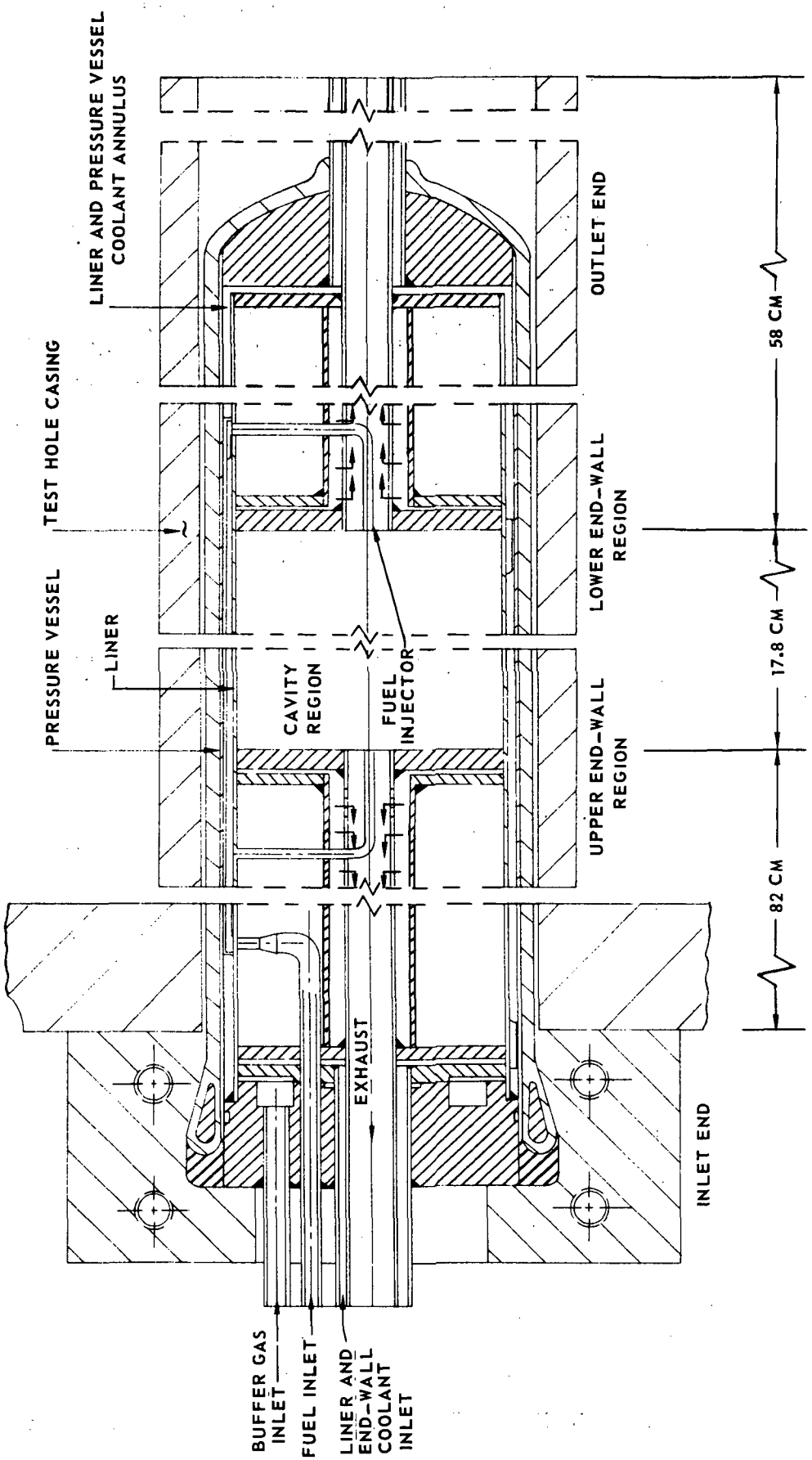

FIG. 5

CROSS-SECTION OF IN-REACTOR TEST CELL AT AXIAL MIDPLANE

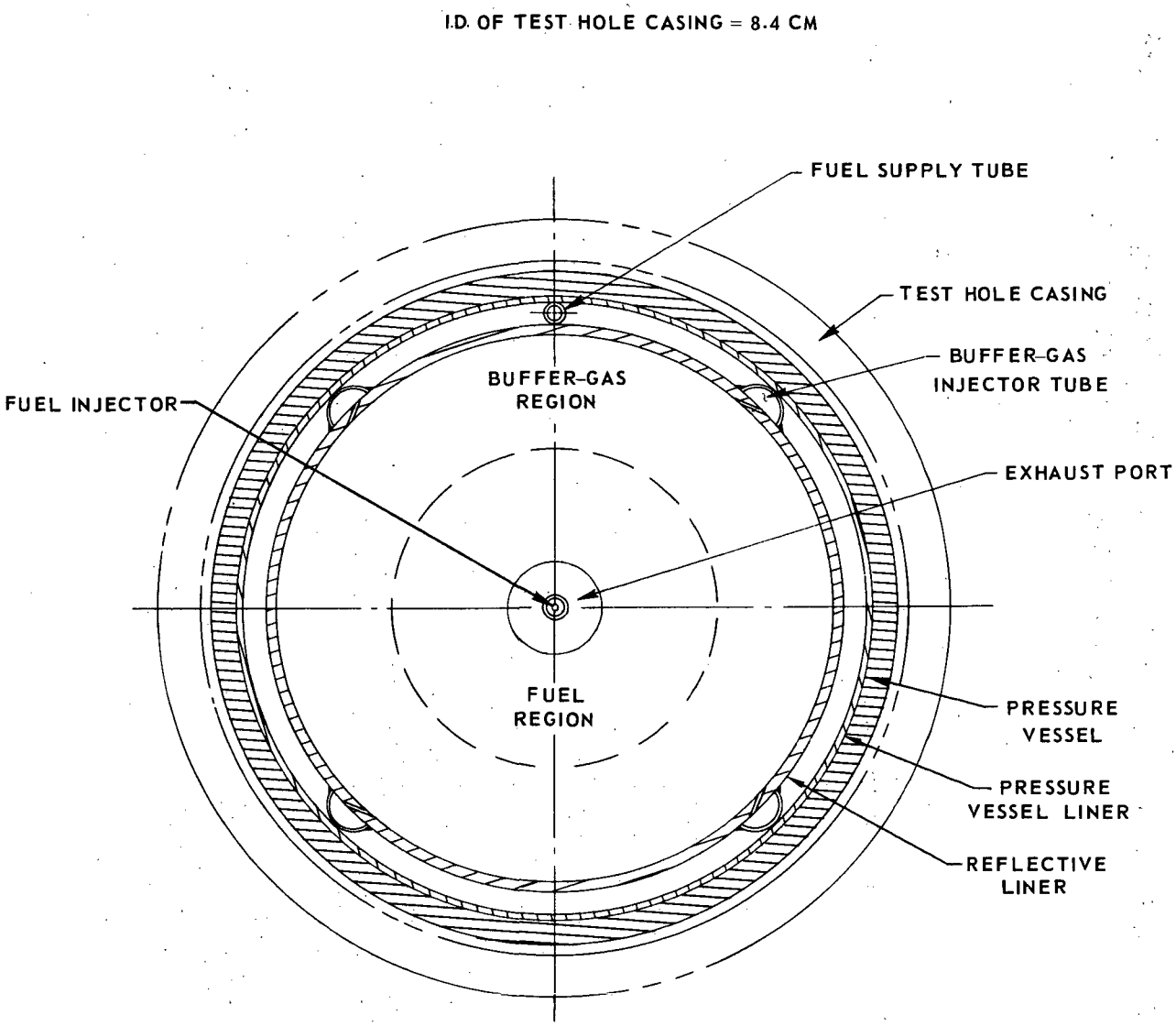

L-910900-17

SCHEMATIC DIAGRAM OF UNIT CELL WITH ALUMINUM PRESSURE VESSEL, OFF-AXIS FUEL INJECTORS AND BUFFER-GAS AXIAL BYPASS PORTS

USE OF ALUMINUM PRESSURE VESSEL REDUCES LINER I.D. TO 6.35 CM

FLOW ANNULI AND WALL THICKNESS SAME AS SHOWN FOR UNIT CELL IN FIG. 4

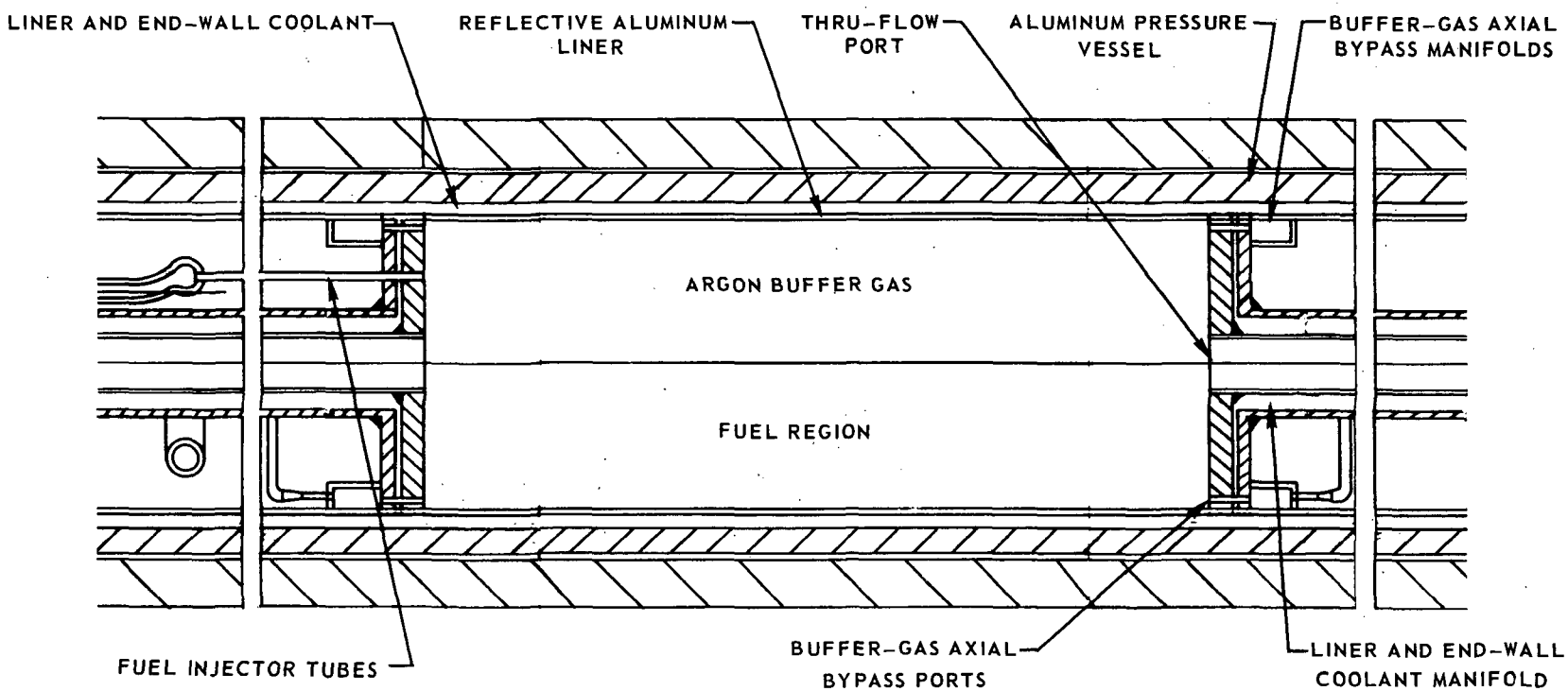

FIG. 6

UNIT CELL FOR IN-REACTOR TESTS OF TRANSPARENT WALLS AND PROPELLANT HEATING

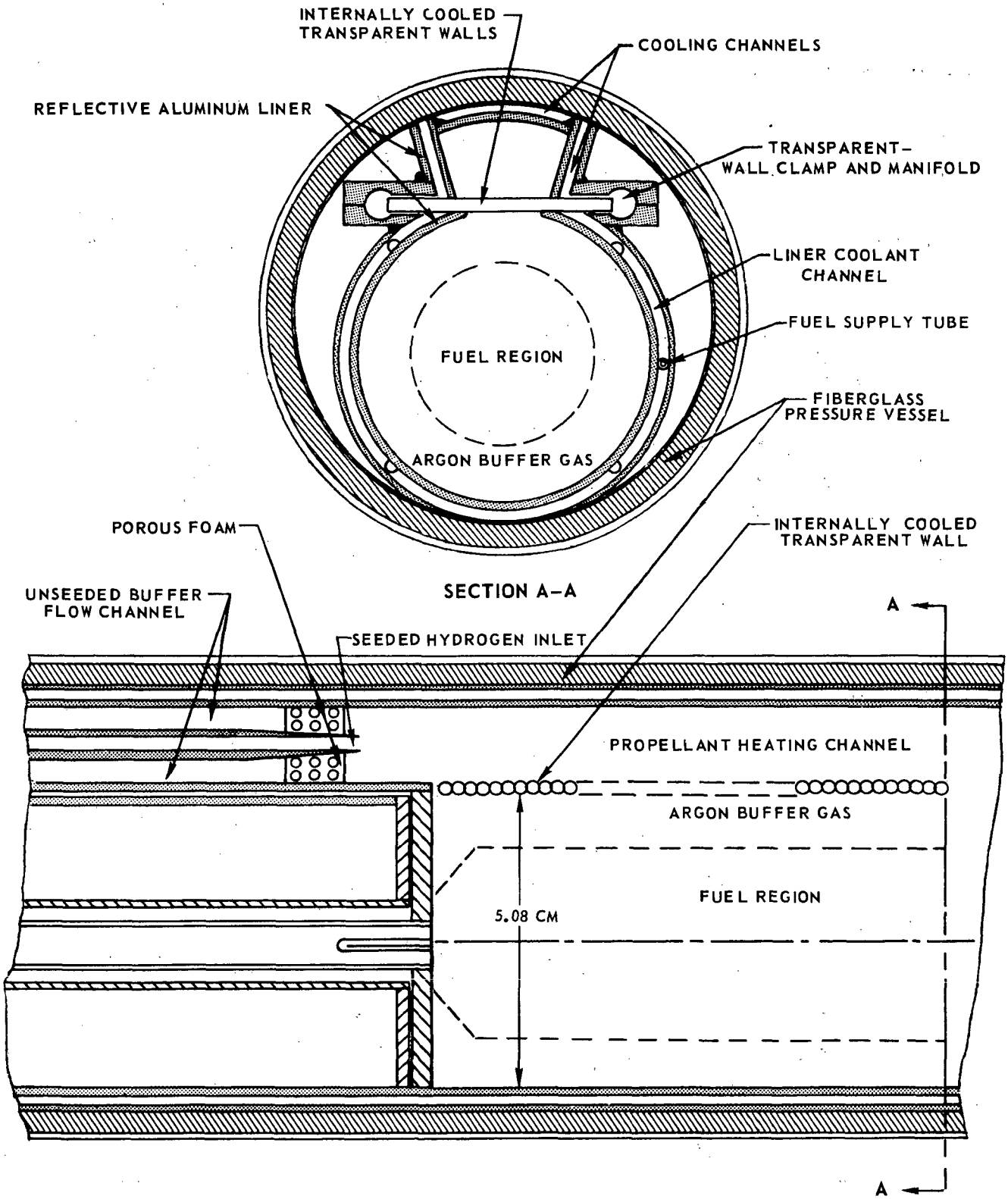

BUFFER-GAS FLOW PATTERN ASSUMED IN CONVECTION AND CONDUCTION ANALYSIS IN BUFFER REGION

(a) AXIAL CROSS-SECTION

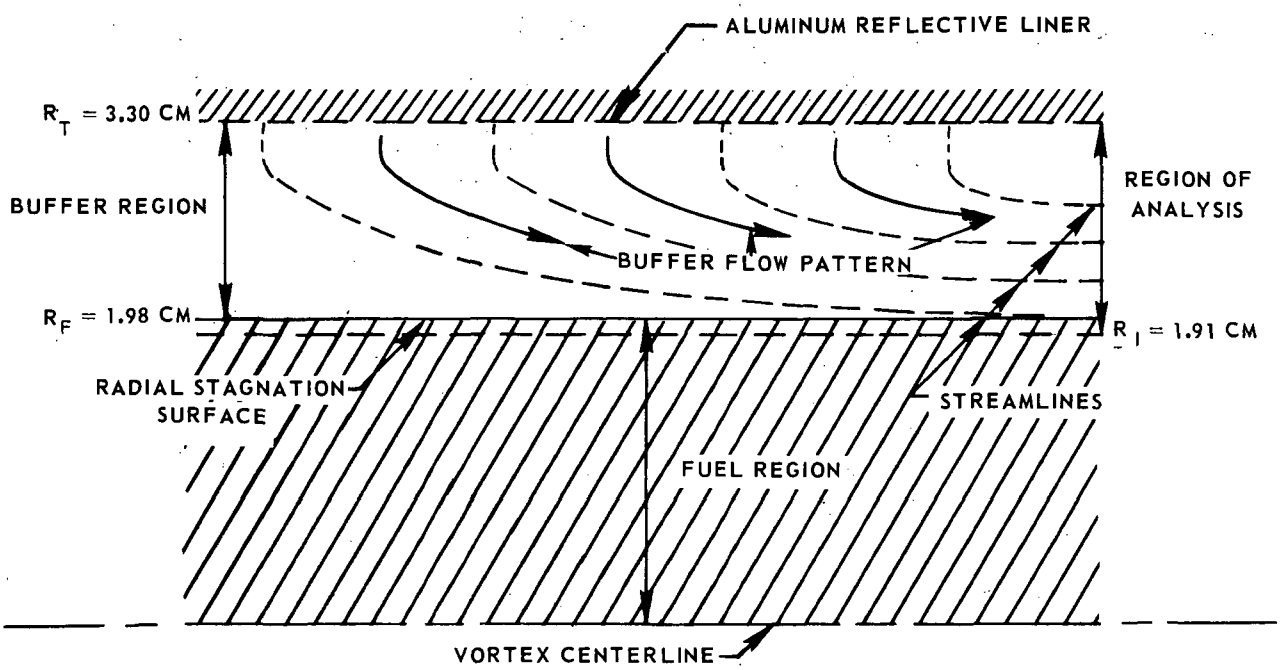

(b) CYLINDRICAL CROSS-SECTION

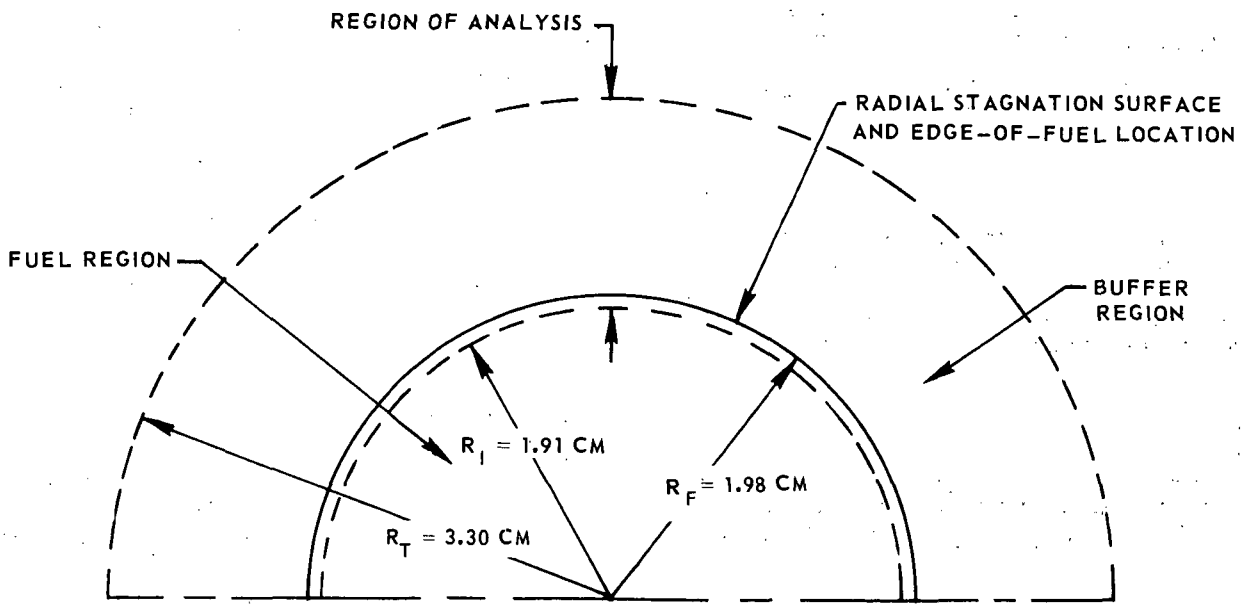

FIG.9

SPECTRAL ABSORPTION COEFFICIENT OF ARGON AT VARIOUS TEMPERATURES FOR A TOTAL PRESSURE OF 500 ATM

DATA TAKEN FROM REF. 17

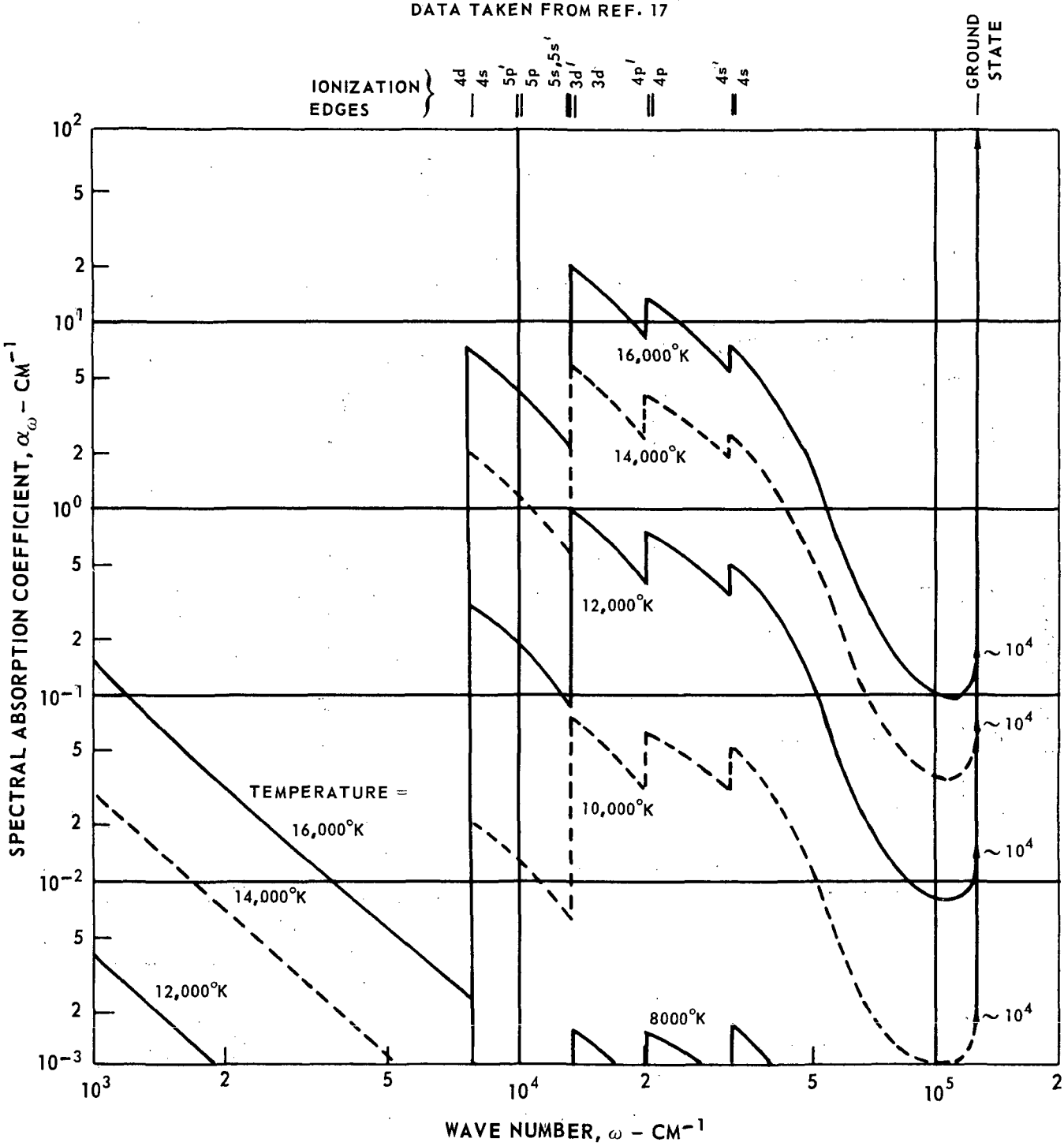

CALCULATED VARIATION OF ALUMINUM REFLECTIVITY WITH WAVE NUMBER FOR SEVERAL ANGLES OF INCIDENCE

DATA TAKEN FROM REF. 17

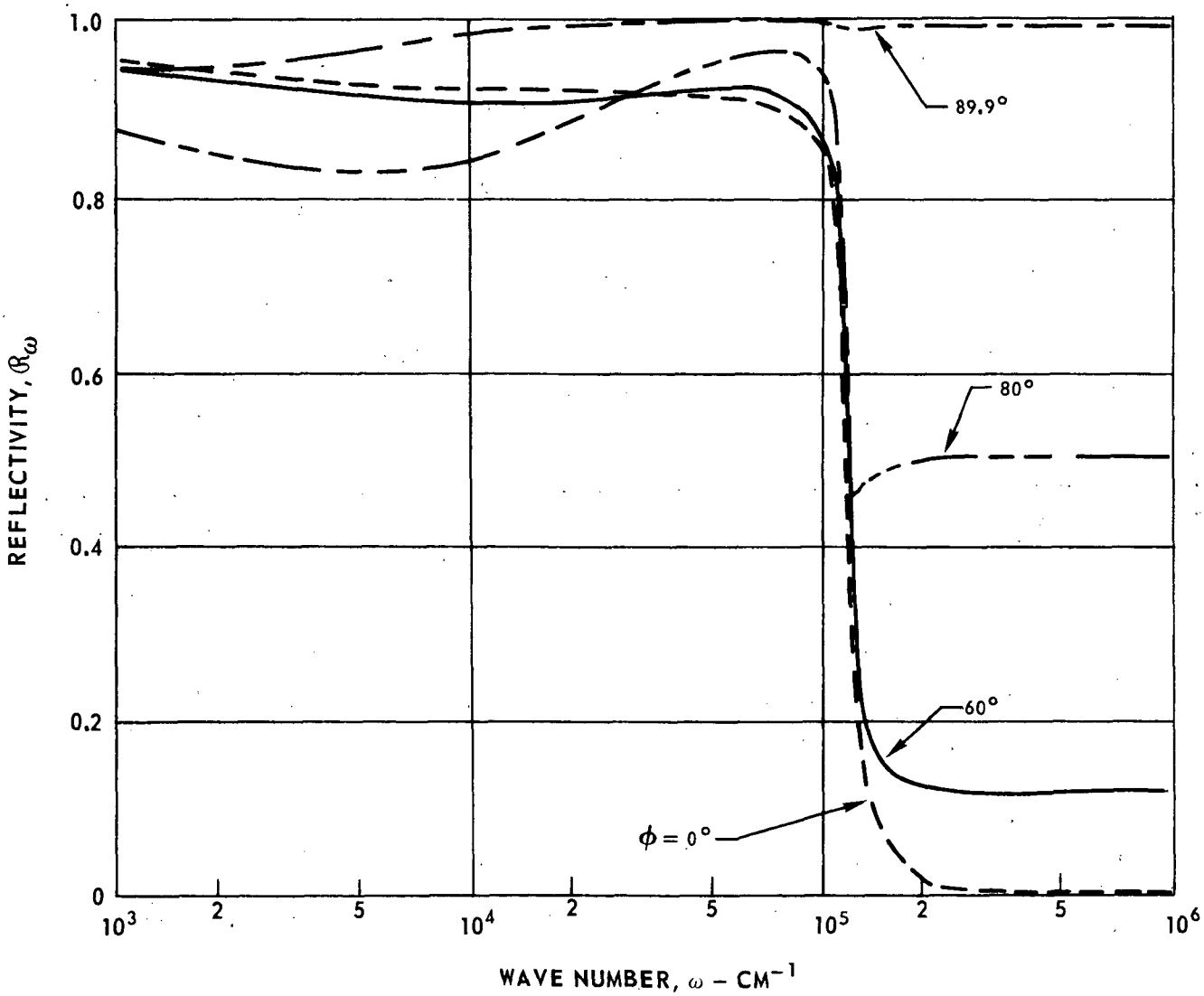

FIG. 11

TEMPERATURE DISTRIBUTION FOR IN-REACTOR TEST CONFIGURATION WITH ARGON BUFFER GAS

SEE FIG. 8 FOR GEOMETRY AND DIMENSIONS OF REGION OF ANALYSIS

SEE FIG. 17 FOR FUEL AND ARGON RADIAL PARTIAL PRESSURE DISTRIBUTIONS IN REGION OF ANALYSIS

NET RADIATION HEAT FLUX AT EDGE-OF-FUEL LOCATION, $q_6 = 0.71 \times 10^{10}$ ERG/CM^2 - SEC

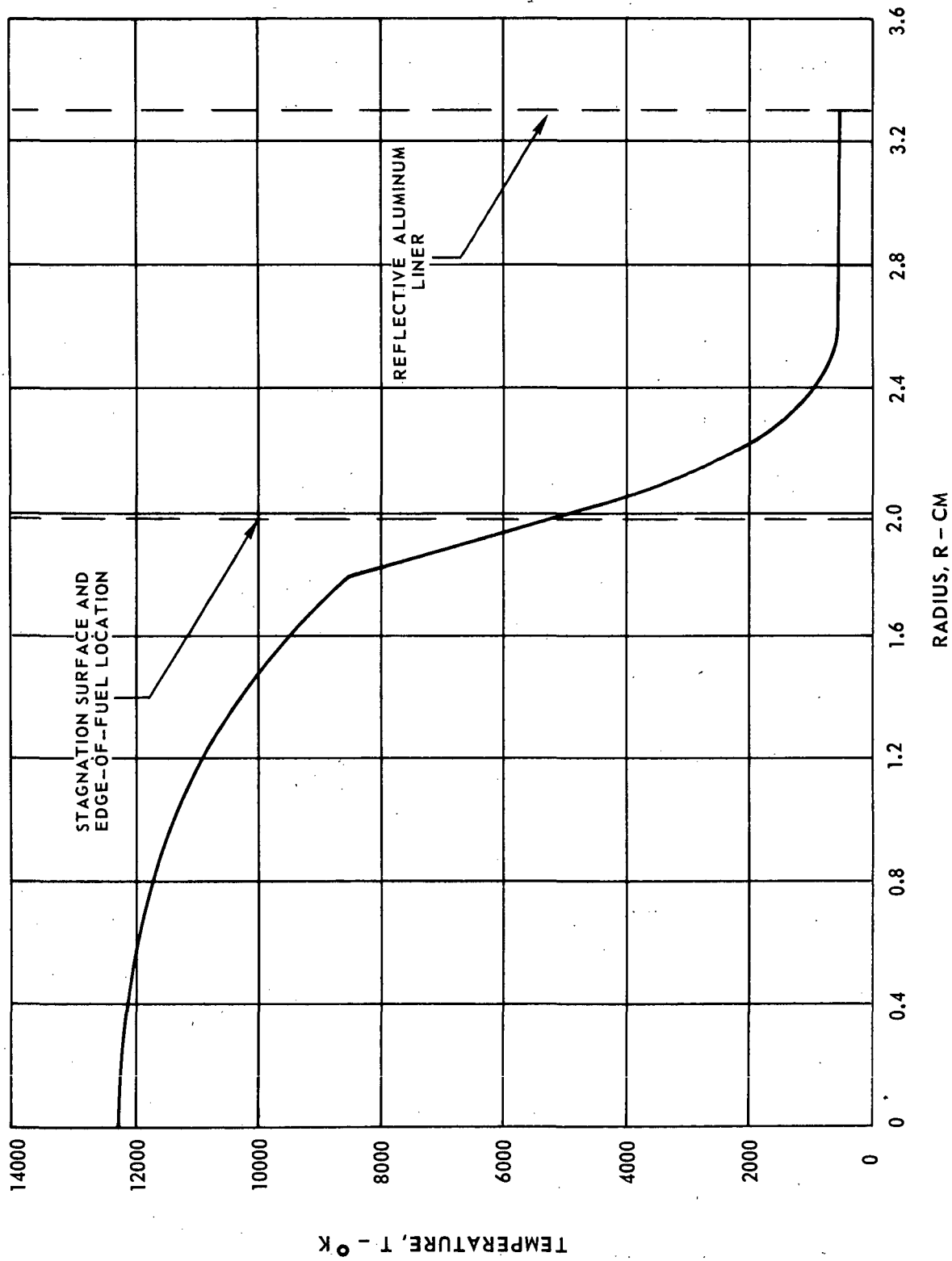

VARIATION OF SPECTRAL HEAT FLUX AT ALUMINUM WALL WITH WAVE NUMBER FOR IN-REACTOR TEST CONFIGURATION

SEE FIG. 8 FOR GEOMETRY DESCRIPTION AND DIMENSIONS OF REGION OF ANALYSIS

NET HEAT FLUX AT AL WALL, $q_L = \int_{10^3}^{10^6} q_\omega d\omega = 0.426\times10^{10}$ ERG/CM^2 – SEC

NET HEAT FLUX AT NOMINAL EDGE-OF-FUEL LOCATION, $q_6 = 0.71\times10^{10}$ ERG/CM^2 – SEC

CALCULATED OUTWARD DIRECTED HEAT FLUX AT NOMINAL EDGE-OF-FUEL LOCATION, $q_6^+ = 4.838\times10^{10}$ ERG/CM^2 – SEC

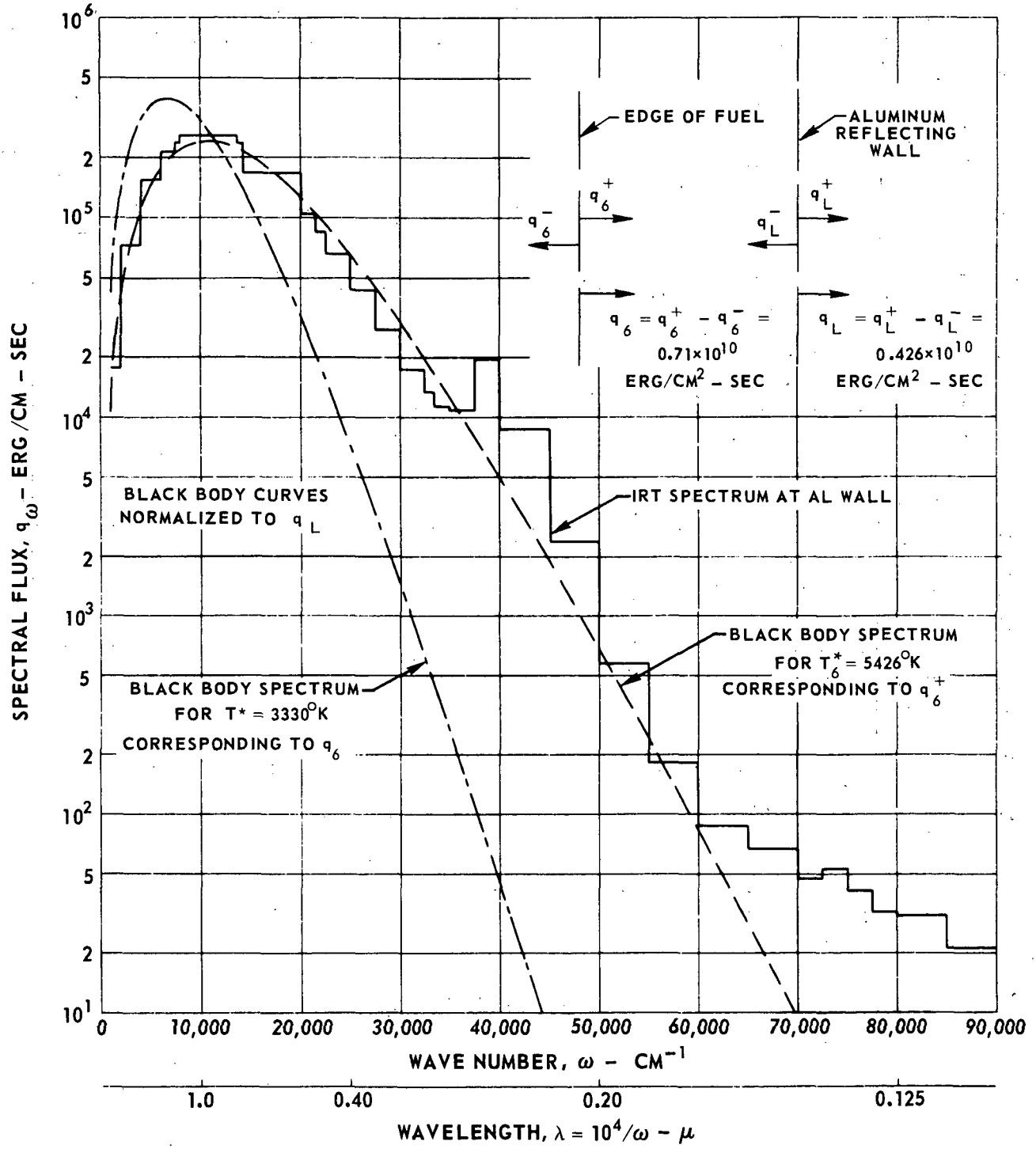

VARIATION OF FRACTIONAL HEAT FLUX AT ALUMINUM WALL WITH WAVE NUMBER FOR IN-REACTOR TEST CONFIGURATION

SEE FIG.8 FOR GEOMETRY AND DIMENSIONS OF REGION OF ANALYSIS

SEE FIG.12 FOR CORRESPONDING SPECTRAL HEAT FLUX

NET HEAT FLUX AT AL WALL, $q_L = \int_{10^3}^{10^6} q_\omega \, d\omega = 0.426 \times 10^{10}$ ERG/CM^2 – SEC

NET HEAT FLUX AT NOMINAL EDGE-OF-FUEL LOCATION, $q_6 = 0.71 \times 10^{10}$ ERG/CM^2 – SEC

CALCULATED OUTWARD DIRECTED HEAT FLUX AT NOMINAL EDGE-OF-FUEL LOCATION,

$q_6^+ = 4.838 \times 10^{10}$ ERG/CM^2 – SEC

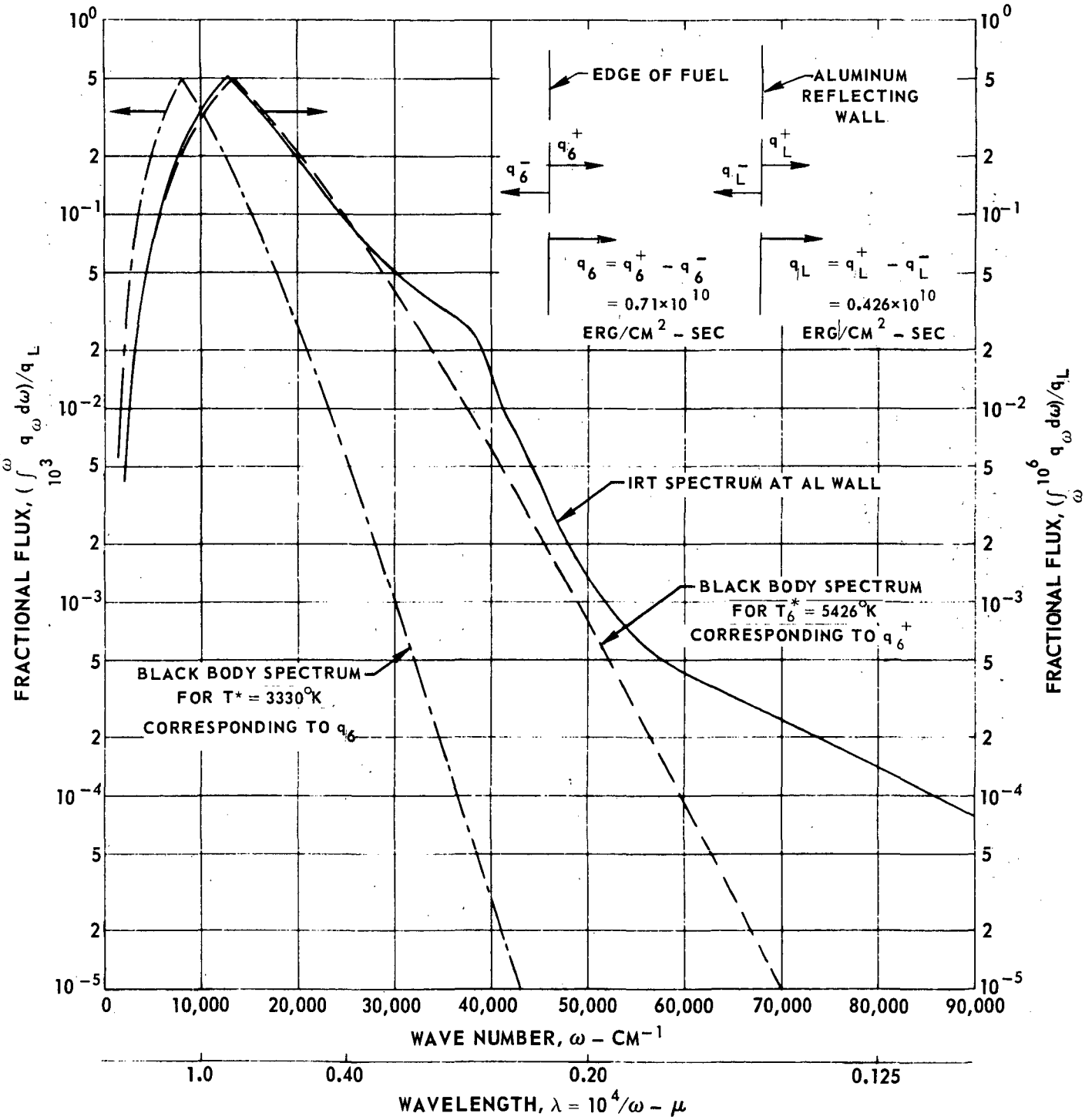

L-910900-17

VARIATION OF EFFECTIVE REFLECTIVITY AT EDGE OF FUEL WITH FUEL-TO-CAVITY RADIUS RATIO FOR SEVERAL ALUMINUM WALL REFLECTIVITIES

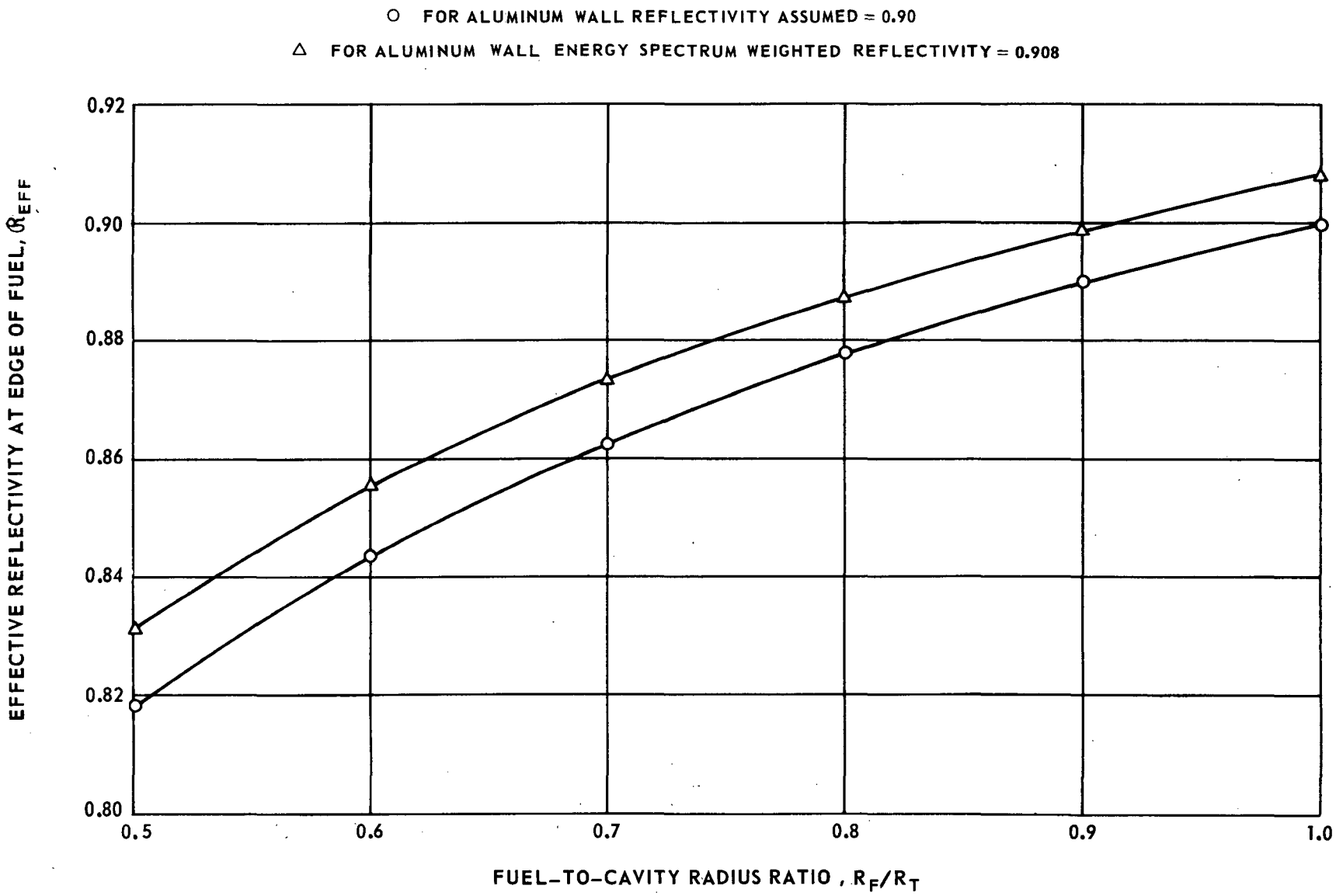

FIG. 14

VARIATION OF INTEGRATED CONVECTED ENERGY WITH RADIUS FOR IN-REACTOR TEST CONFIGURATION WITH ARGON BUFFER GAS

SEE FIG. 8 FOR GEOMETRY AND DIMENSIONS OF REGION OF ANALYSIS

CONDUCTED AND CONVECTED ENERGY VARIATION WITH RADIUS IDENTICAL DUE TO NEGLIGIBLE RADIATION ABSORPTION BY BUFFER GAS

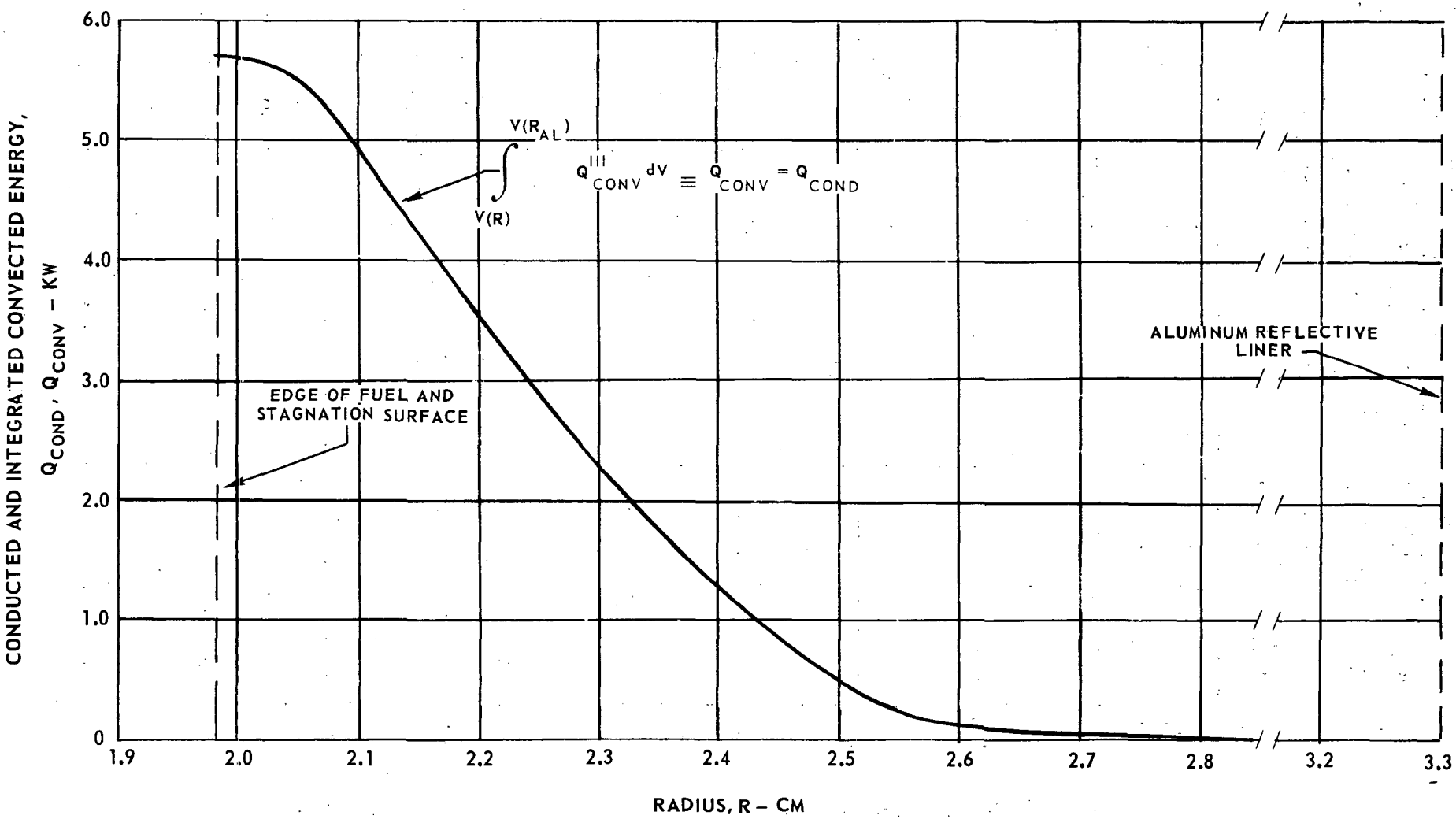

L-61090-17

FIG. 15

FIG. 16

RADIAL WEIGHT FLOW AND AXIAL VELOCITY DISTRIBUTIONS BETWEEN ASSUMED RADIAL STAGNATION SURFACE AND ALUMINUM REFLECTIVE LINER FOR IN-REACTOR TEST CONFIGURATION WITH ARGON BUFFER GAS

SEE FIG. 8 FOR GEOMETRY AND DIMENSIONS OF REGION OF ANALYSIS

(a) RADIAL WEIGHT FLOW

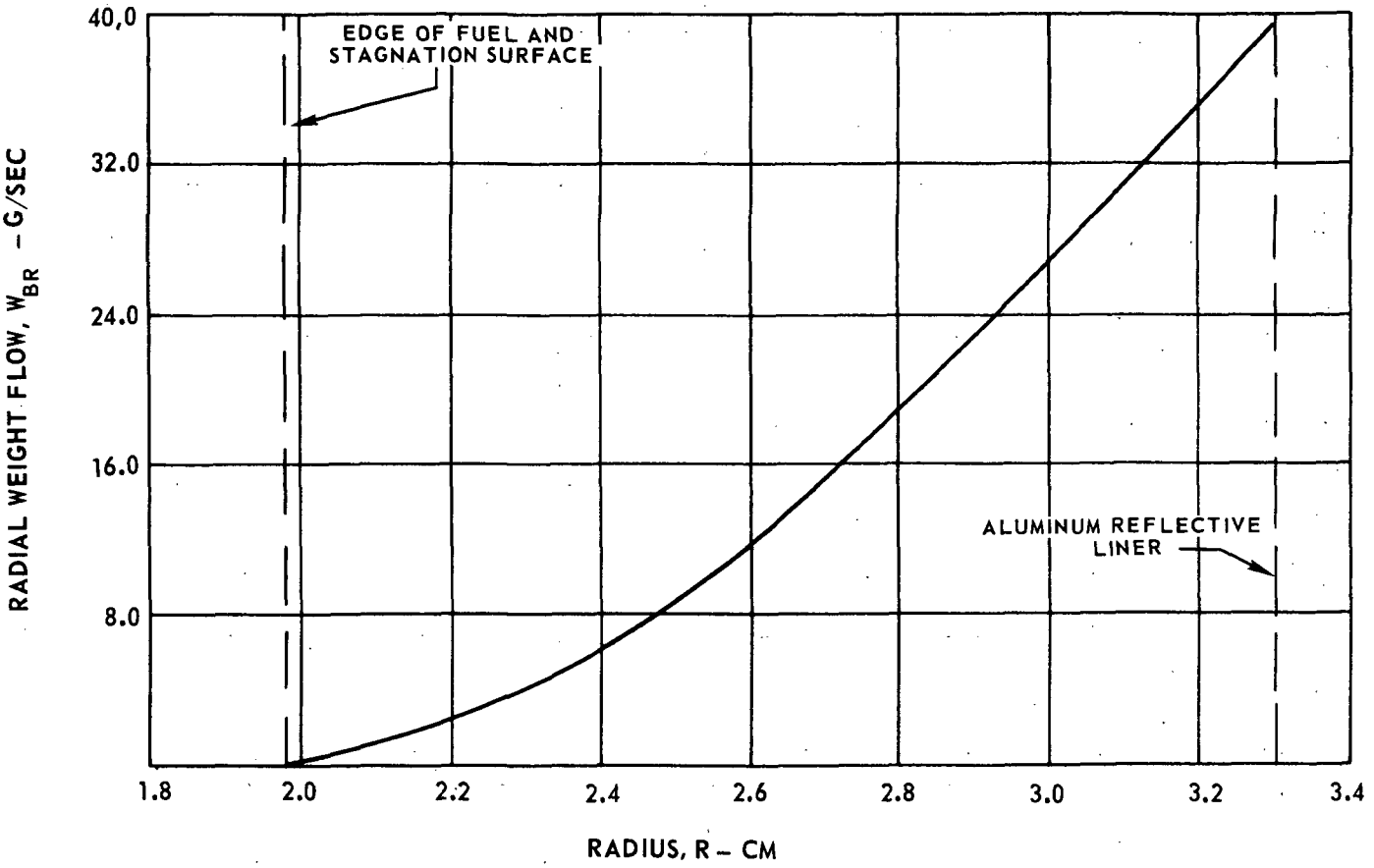

(b) AXIAL VELOCITY

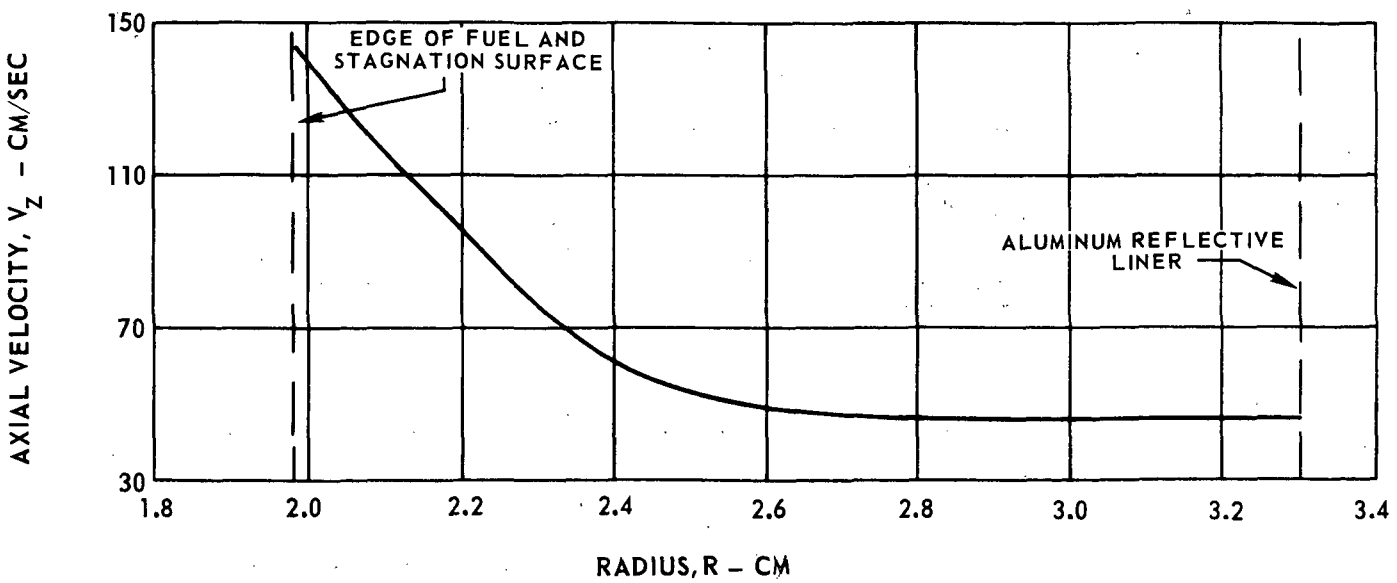

CALCULATED DENSITY AND PARTIAL PRESSURE DISTRIBUTIONS OF URANIUM AND ARGON FOR IN-REACTOR TEST CONFIGURATION

SEE FIG. 8 FOR GEOMETRY AND DIMENSIONS OF REGION OF ANALYSIS

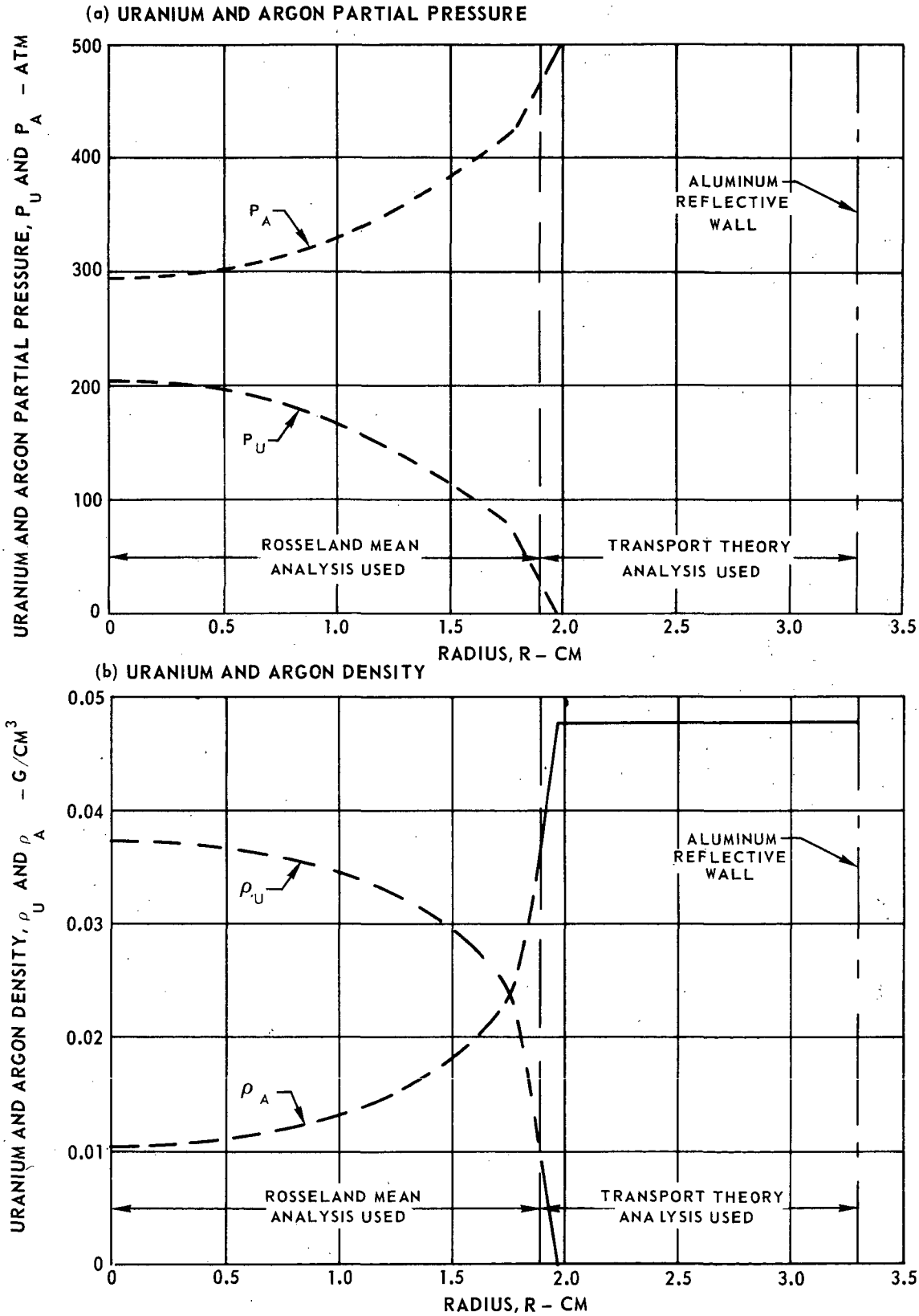

STATION NUMBERS FOR IN-REACTOR TEST CELL KEY TEMPERATURES AND PRESSURES

○ DENOTES STATION NUMBER FOR LOCAL TEMPERATURES AND PRESSURES GIVEN IN TABLES II AND III

COOLANT FLOW (G/SEC)	HYDROGEN	ARGON
TOTAL FOR LINER AND END WALLS	300	9000
UPPER-END-WALL BRANCH	100	6000
LOWER-END-WALL BRANCH	100	2000

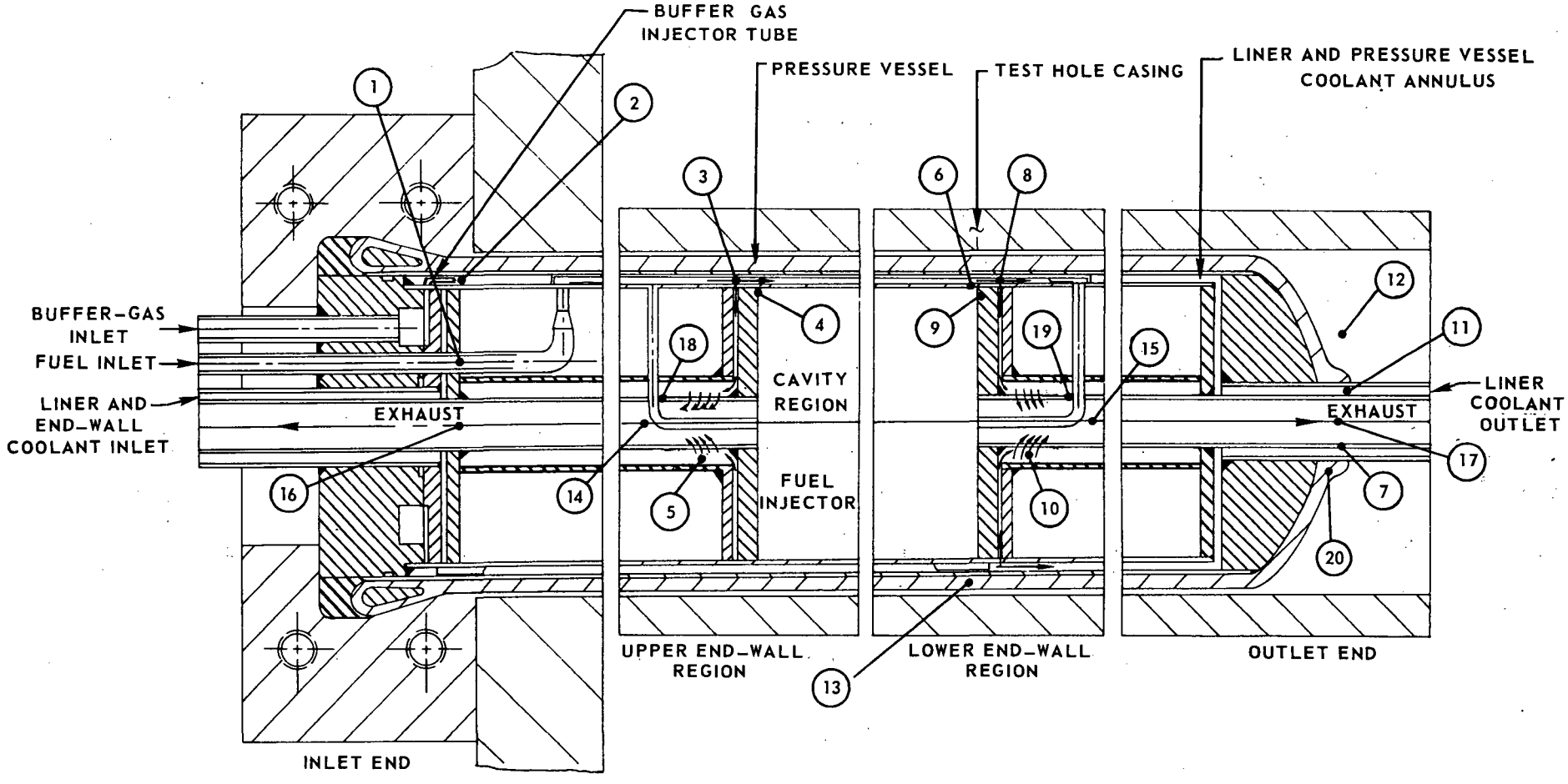

L-910900-17

FIG. 18

TEMPERATURE VARIATIONS DUE TO POSSIBLE DEPOSITION OF NUCLEAR FUEL ON END WALLS, REFLECTIVE ALUMINUM LINER AND THRU-FLOW DUCT WALLS

TOTAL FUEL FLOW RATE, W_F = 1.6 G/SEC
RATES OF CHANGE OF TEMPERATURE SHOWN DUE TO FISSIONING OF DEPOSITED FUEL ONLY

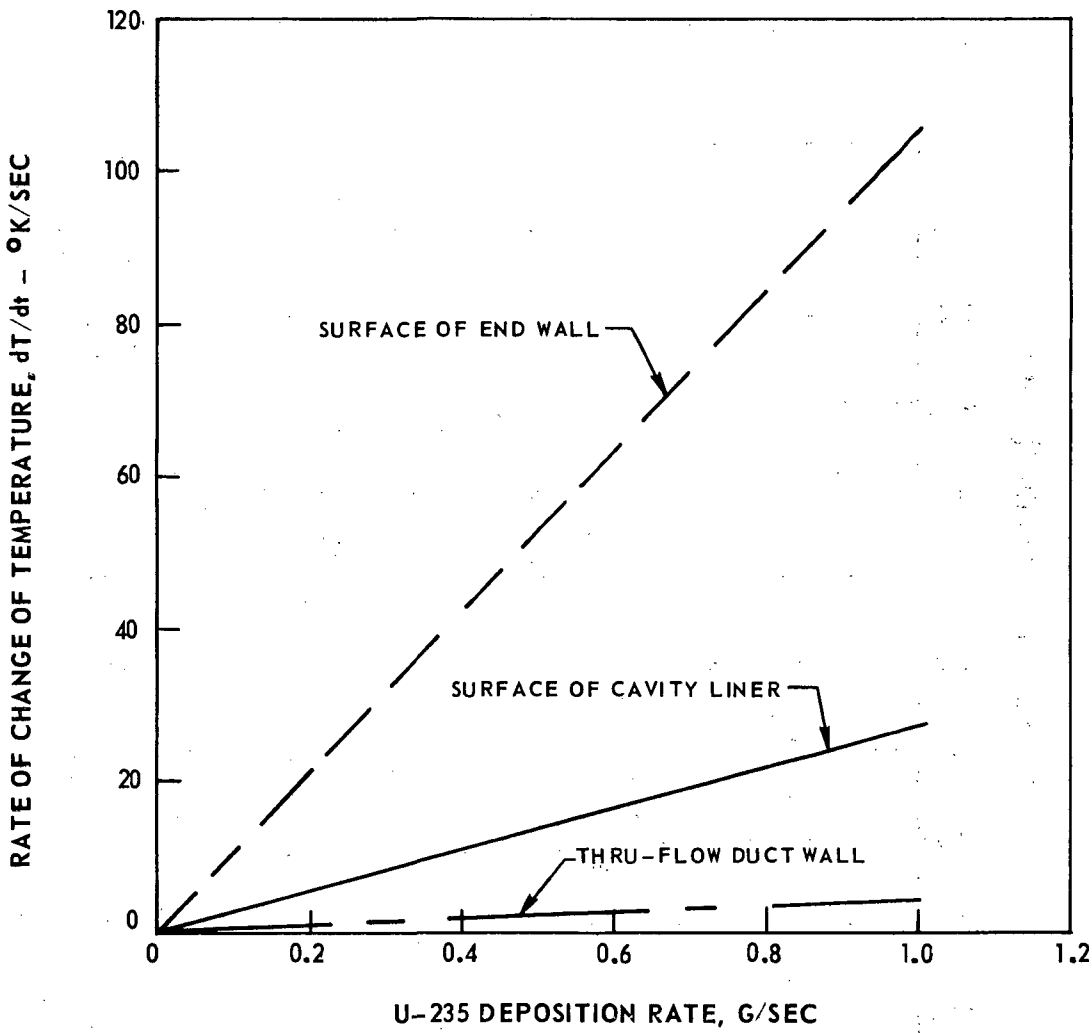

RANGE OF RADIATING TEMPERATURES AND POWER LEVELS FOR IN-REACTOR TESTS OF UNIT CELL

SPECIFICATIONS FOR UNIT CELL GIVEN IN TABLE I AND FIGS. 4 AND 5

VALUES OF REFERENCE DESIGN PARAMETERS

$P = 500$ ATM

$C_T = 1.0$

$\mathcal{R}_{EFF} = 0.855$

$R_F / R_T = 0.6$

$K_F = 0.6$

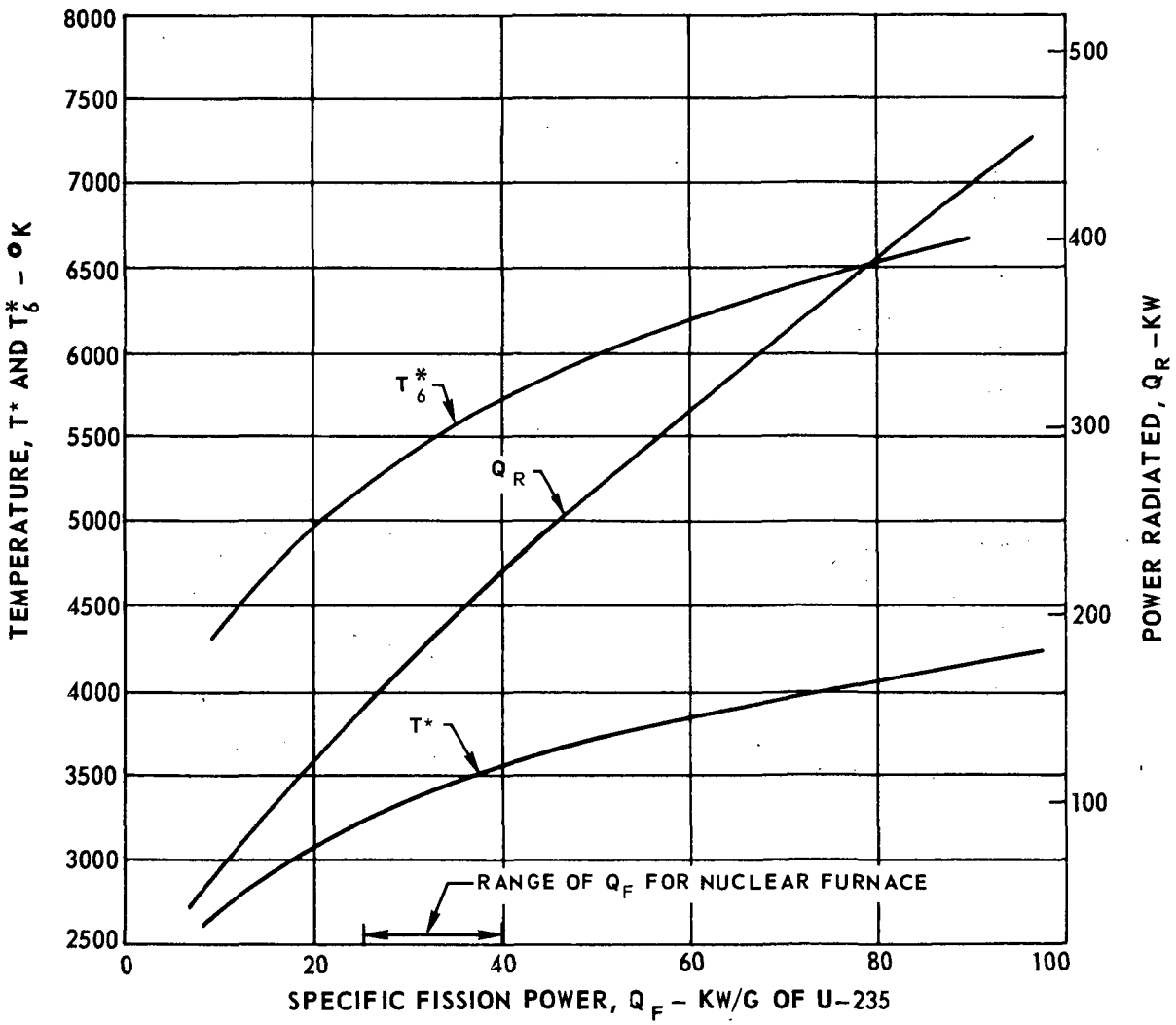

EFFECT OF VARIATION OF FUEL-TO CAVITY RADIUS RATIO ON RADIATING TEMPERATURES AND POWER LEVELS FOR IN-REACTOR TEST

SPECIFICATIONS FOR UNIT CELL GIVEN IN TABLE I AND FIGS. 4 AND 5

OPERATING PRESSURE = 500 ATM

U-235 NUCLEAR FUEL

$\bar{\rho}_{F_6}/\rho_{B_6} = 0.6$, $Q_F = 30.5$ KW/G, $\tau_F/\tau_B = 1.0$

SEE FIG.14 FOR VARIATION OF EFFECTIVE ALUMINUM LINER REFLECTIVITY WITH FUEL-TO- CAVITY RADIUS RATIO

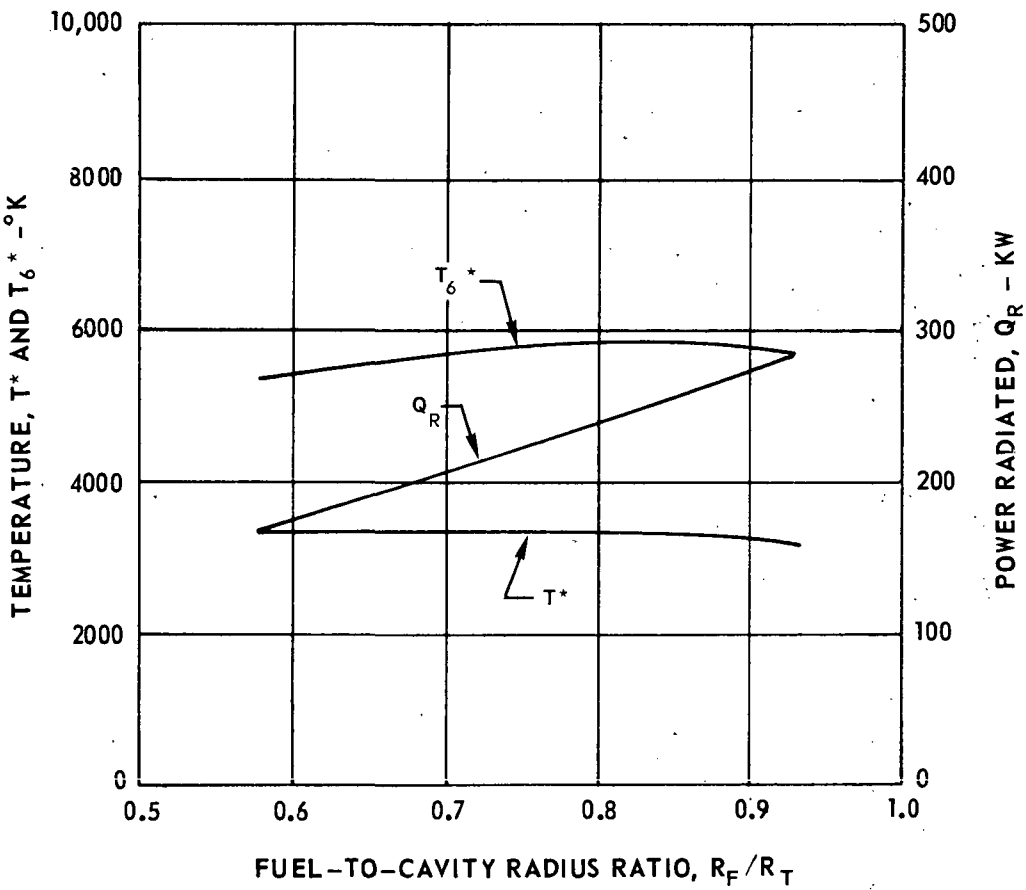

RANGES OF RADIATING TEMPERATURES AND POWER LEVELS FOR IN-REACTOR TESTS OF A UNIT CELL AT DIFFERENT OPERATING PRESSURES

SPECIFICATIONS FOR UNIT CELL GIVEN IN TABLE I AND FIGS. 4 AND 5

$\mathcal{R}_{EFF} = 0.855$ $C_T = 1.0$ $K_F = 0.6$ $R_F/R_T = 0.6$

U-235 NUCLEAR FUEL

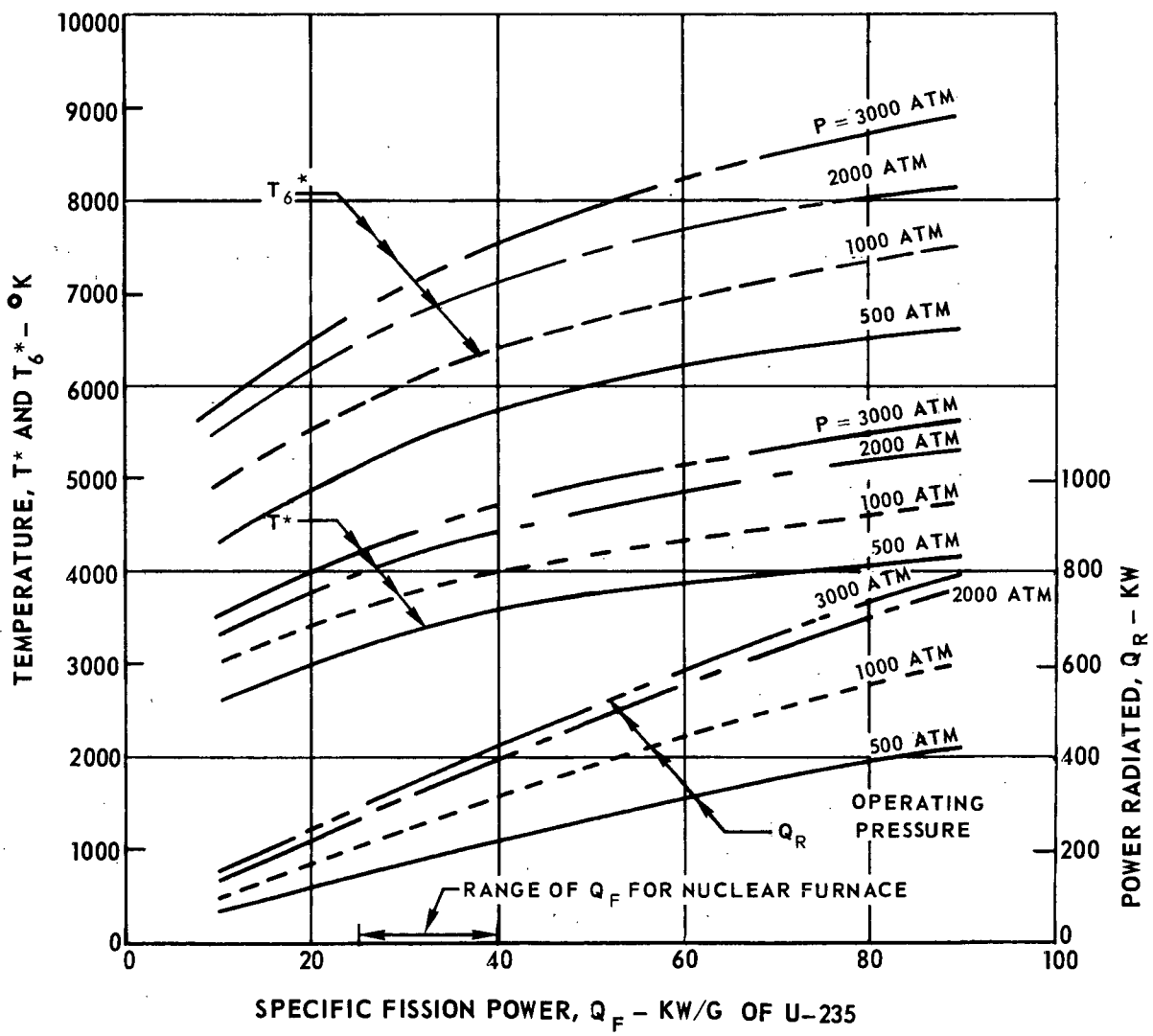

FIG. 23

INSTRUMENTATION LOCATIONS FOR IN-REACTOR TESTS OF A UNIT CELL

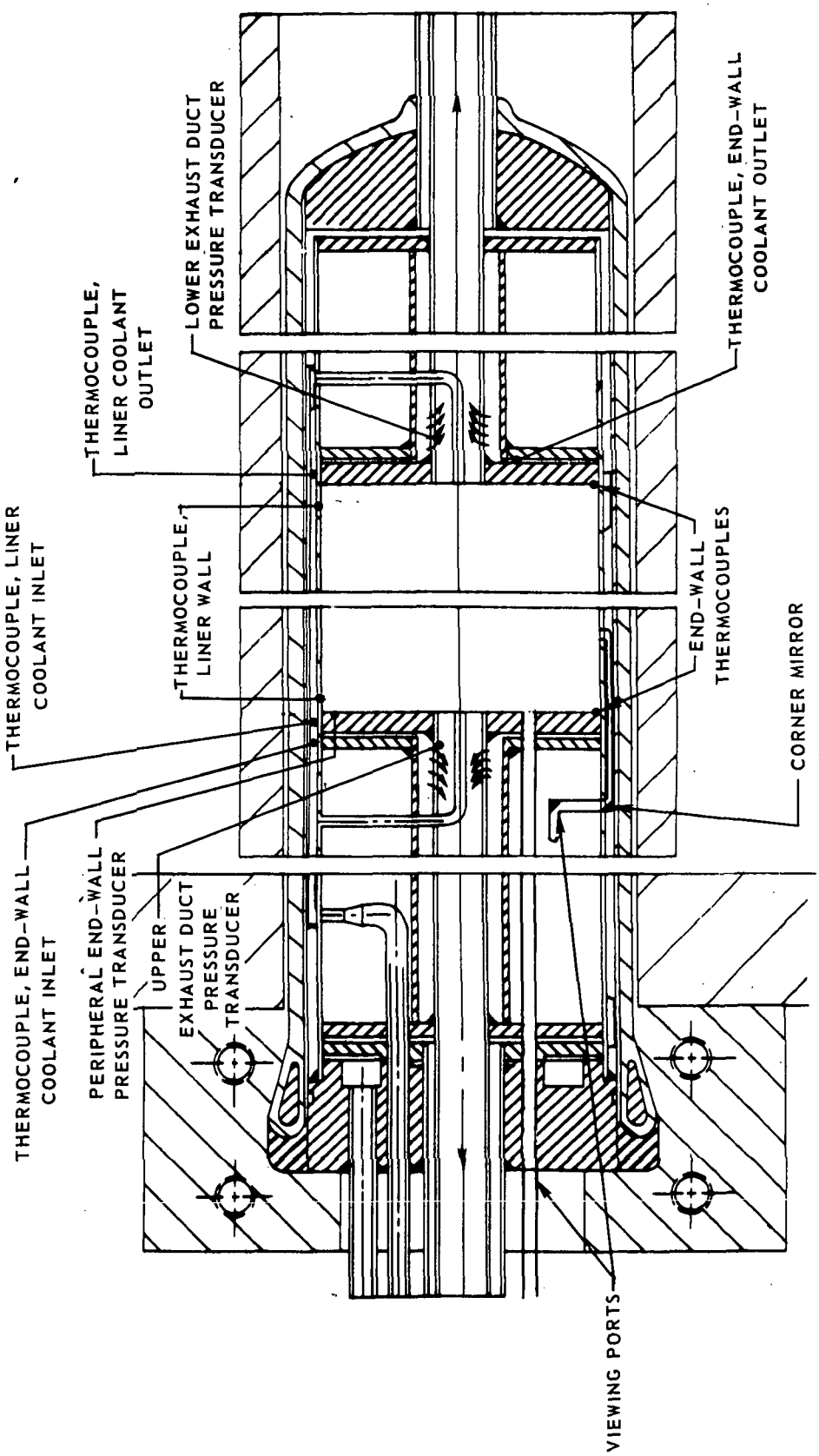

FIG. 24

CALCULATED IN-REACTOR TEST PERFORMANCE

FISSIONING URANIUM PLASMA FACILITY (FUPF)
NUCLEAR FURNACE (NF)
HIGH-FLUX ISOTOPE REACTOR (HFIR)
KINETIC INTENSE NEUTRON GENERATOR (KING)

SEE FIGS. 4 AND 5 FOR TEST CONFIGURATION DETAILS

REFLECTIVITY, $\mathcal{R}$ = 0.855

CONTAINMENT DENSITY RATIO, $\bar{\rho}_{F_6} / \rho_{B_6} = 0.6$

● DENOTES PERFORMANCE AT REFERENCE TEST CONDITION; SEE TABLE IV

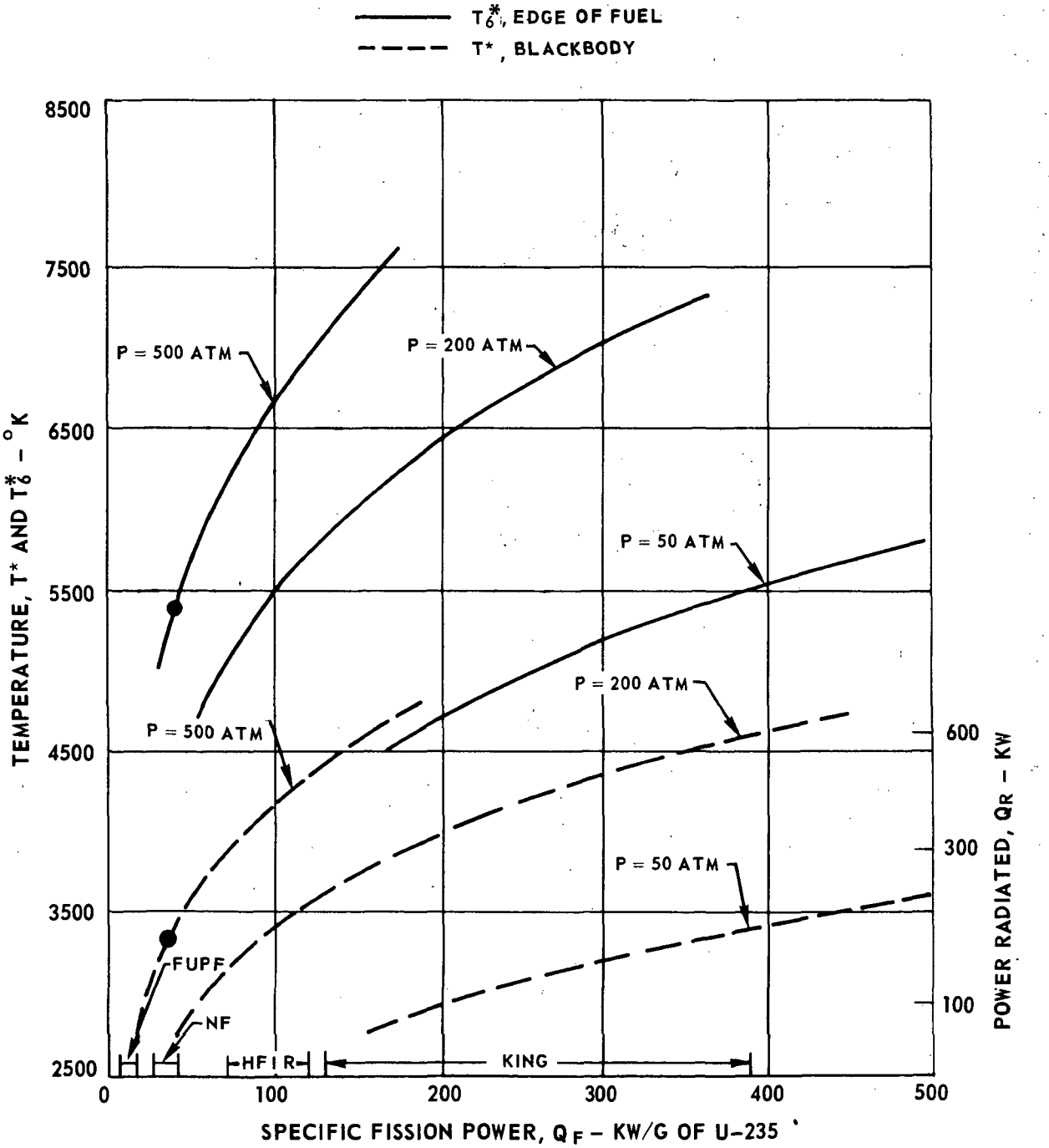

FIG. 25

NUCLEAR LIGHT BULB TEST REACTOR WITH COLD BERYLLIUM REFLECTOR

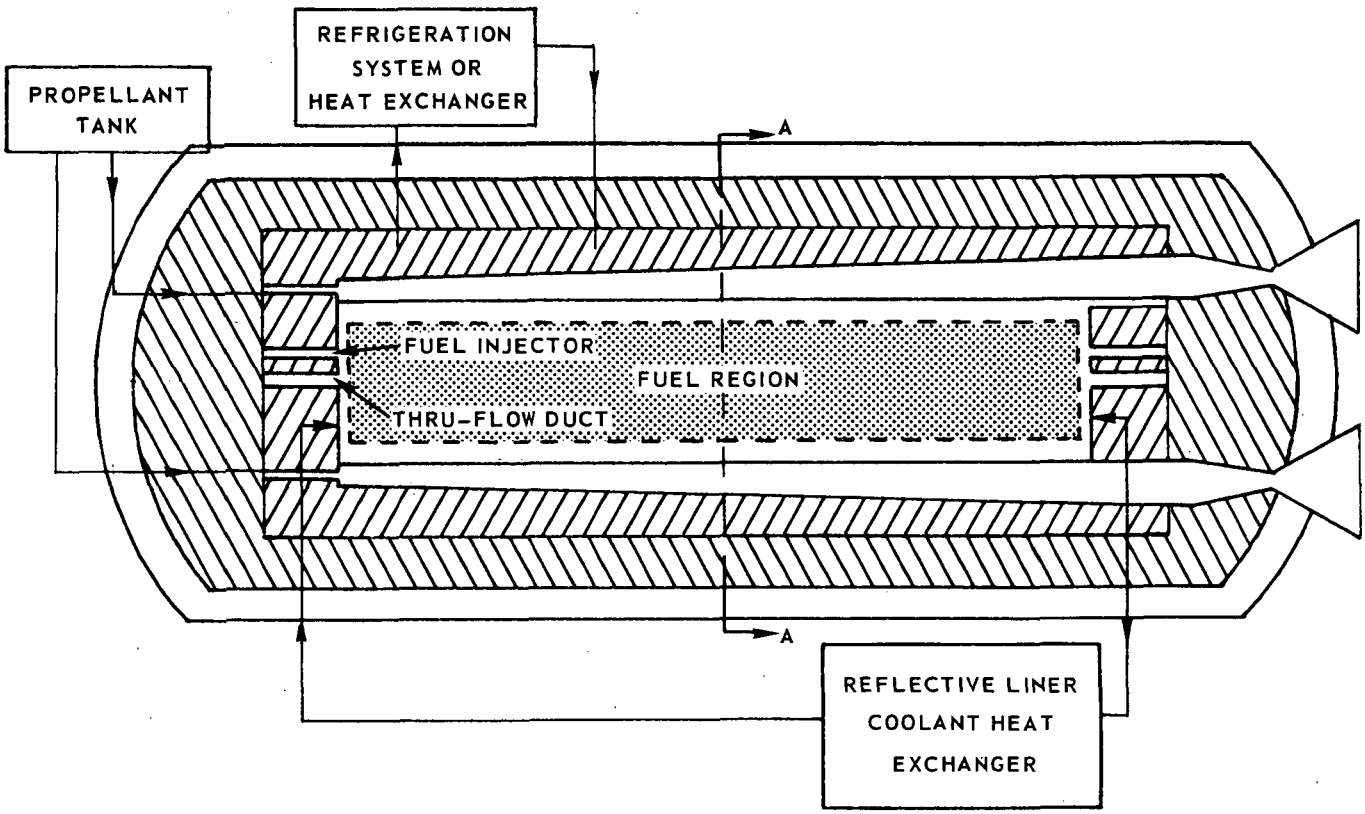

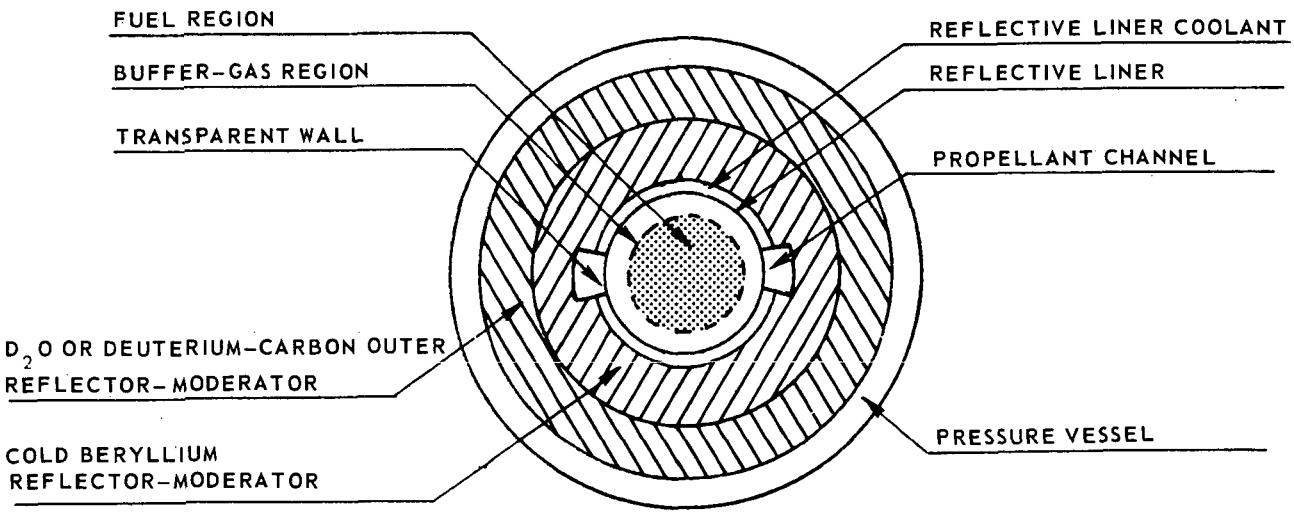

SECTION A-A

United
Aircraft
Research
Laboratories

UNITED AIRCRAFT CORPORATION

EAST HARTFORD, CONNECTICUT 06108